Examination of Vascular Remodelling in Resistance Arteries using Laser Scanning Confocal Microscopy

by

Simon Peter McGrory

A thesis presented for the degree of Master of Science (Med Sci) in the Faculty of Medicine, University of Glasgow.

December 2003

Lab 440
West Medical Building
University of Glasgow
Glasgow
G12-8QQ

Contents

Chapter 3:
Analysis of the Tunica Adventitia of Resistance Arteries using Laser Scanning Confocal Microscopy and the Quantification of Collagen within the Adventitial Layer of Carotid Arteries in a Rabbit Model of Heart Failure

Chapter 4:
Analysis of the Tunica Media of Resistance Arteries using Laser Scanning Confocal Microscopy and the Quantification of Collagen within the Medial Layer of Carotid Arteries in a Rabbit Model of Heart Failure

Chapter 5:
Analysis of the Tunica Intima of Resistance Arteries using Laser Scanning Confocal Microscopy

Chapter 6:
General Analysis of the Morphological Characteristics of Resistance Arteries revealed by Laser Scanning Confocal Microscopy

Chapter 7 :
General Discussion

Appendix

Acknowledgements

Firstly I would like to thank Professor J C McGrath for the opportunity to work and study within his lab. I came to work with him as a young trainee technician with little experience now 10 years later I have had great opportunities not normally available to technical staff, thanks Ian I couldn't ask for a better boss and supervisor.

To the unsung heroes of laboratory life- thanks Joyce for you support and gentle pushes every now and then. Well Angela- it's done! A big thank you to you for your support both while writing this and also around the lab, between us I think the lab just about survives. Mrs K- a true friend or is that "work colleague"? Thank you for constantly being there, your just like a second mother always ready to praise or nagg! To Monty for your varied and informative insights into science and also John for you expert knowledge of microscopy and help with image analysis. To Di and Jean and other members of the West Medical breakfast club, the day would not be the same without our little conversations about this and that! – a time to switch off from science.

A big thanks to my friends and the rising stars of lab 440: Jude for her help with a few figures and also for proof reading and also Laura, Darren and Majid. I also have to mention Melissa, the jet setter- you bring something special to the lab, one day we'll find out what. Zeeshan, a good mate who evens the score when it comes to female control in the lab. A big thanks to Craig, Clare and Janet for their support with the confocal, each of you is a great friend. Others who deserve a mention include; Silvia, Jillian, Craig L, Alison W, Leanne, Clare, Sr Brigid and Fr John. Thanks.

To my family, my sisters and brother; Catherine, Kevin and Patricia thank you for everything over the years also Jane and Andy, I could not have asked for better friends in you all. To

Kieran who makes us realize that life is for fun and my parents, words can't express how much I have to thank you for your constant love and support over the years in whatever I have chosen to do, thank you.

Lastly I wish to acknowledge Ann McGee a great friend who will always be missed. The car and the lab are very quiet but I always know that you are watching over us- our own confocal guardian angel. May you find the same happiness where you are now as you did among your friends here.

List of Figures

Chapter 1
General Introduction

Chapter 2
Materials and Methods

Chapter 3
Analysis of the Tunica Adventitia of Resistance Arteries using Laser Scanning Confocal Microscopy and the Quantification of Collagen within the Adventitial Layer of Carotid Arteries in a Rabbit Model of Heart Failure

Chapter 4
Analysis of the Tunica Media of Resistance Arteries using Laser Scanning Confocal Microscopy and the Quantification of Collagen within the Medial Layer of Carotid Arteries in a Rabbit Model of Heart Failure

Chapter 5

Analysis of the Tunica Intima of Resistance Arteries using Laser Scanning Confocal Microscopy

Chapter 6

General Analysis of the Morphological Characteristics of Resistance Arteries revealed by Laser Scanning Confocal Microscopy

Chapter 7

General Discussion

List of tables

Declaration

The experimental work and other research which is contained within this thesis was undertaken by myself with the exception of the histological sectioning required for the study of the collagen content within carotid arteries from rats which underwent coronary artery ligation which was completed by Dr Ian Montgomery.
Some of the results which have been published as detailed below

Publications

Papers:

Arribas SM, Hillier C, Gonzalez C, **McGrory S**, Dominiczak AF, McGrath JC
Cellular aspects of vascular remodelling in hypertension revealed by confocal microscopy.
Hypertension (1997) 30 1455 – 1464

Abstracts:

Arribas, S.M., Hillier, C., **McGrory, S.P.**, Dominiczak, A.F. & McGrath, J.C.
Laser scanning confocal microscopy for the study of vascular structure in mesenteric resistance arteries. Can it solve the problem with remodelling? Hypertension (1996) 28 No 4 709.

Arribas SM, **McGrory SP**, Macmillan JB, McGee A, McGrath JC
Outward hypertophic remodelling in cerebral arteries from a rabbit model of coronary artery ligation. J. Vascular Research (1998) 35 (Suppl 1) O1

Luo, D., Daly, C.J., Mackenzie, J.F., **McGrory, S.P.**, Robert, A. & McGrath, J.C.
3D remodelling of a1-adrenoceptors in live cells using a fluorescent ligand, QAPB and confocal laser scanning microscopy.
Naunyn-Schmiedeberg's Arch. Pharmacol. (1998) 358 Suppl. 2 P6.44.

McGrory SP, Lygate CA, Dominiczak AF, McGrath JC.
Vascular smooth muscle cell remodelling in the coronary artery ligated model of heart failure.
J. Physiology (1999) 521 60P*

Lygate, C.A., **McGrory, S.P.**, Graham, M.J., Brosnan, J.C., McGrath, J.C., Hamilton, C.A. & Dominiczak, A.F.
Irbesartan prevents cardiac and vascular hypertrophy in a model of genetic hypertension.
Hypertension (1999) 34 715

Arribas SM, **McGrory S**, Hamid R, González MC, McGrath JC
Microscopia confocal para el estudio del remodelado vascular en arterias cerebrales y mesentéricas de ratas con hipertensión genética y experimental.
(Confocal microscopy for the study of vascular remodeling in cerebral and mesenteric arteries from rats with genetic and experimental hypertension)
Hipertensión (2000) 17 Numero Extaordinario, Marzo, 144

McGrory SP, McGrath JC.
Media-lumen versus lumen relationship provides a robust framework for the analysis of arterial remodelling.
Hypertension (2002) 40: 568

Abbreviations

ACA:	Anterior Cerebral Artery
ANP:	Atrial Natriuretic Peptide
AT_1:	Angiotensin Type 1 Receptor
BNP:	Brain Natriuretic Peptide
CAL:	Coronary Artery Ligation
CSA:	Cross Sectional Area
EDCF:	Endothelial Derived Contracting Factor
EDRF:	Endothelial Derived Relaxing Factor
H+H:	Hydralazine + Hydrochlorothiazide
I3C:	Indole-3 Carbinol
IEL:	Internal Elastic Lamina
IND:	Inducible Hypertensive Rats
Irb:	Irbesartan
LDCA:	Left Descending Coronary Artery
LSCM:	Laser Scanning Confocal Miscroscopy
NO:	Nitric Oxide
PSS:	Physiological Salt Solution
RAS:	Renin Angiotensin System
s.e.m:	Standard Error of Mean
SHR:	Spontaneously Hypertensive Rats
SHRSP:	Spontaneously Hypertensive Stroke Prone Rats
SMC:	Smooth Muscle Cell
TNF-α:	Tumor Necrosis Factor alpha
WKY:	Wistar Kyoto Rats

Summary

Summary

No single technique has been developed which has the ability to give the experimenter all the results needed to describe in detail the morphological characteristics of an arterial wall. All methods have their advantages and limitations therefore two or more techniques are often used to validate each other.

Quantitative methods for studying remodelling in animal models were used before using human tissue since the ability to use human blood vessels can prove difficult. Patients are often not willing to provide biopsies of healthy tissue which can be compared with diseased tissue. Therefore animal models are valuable in that they allow us to obtain experimental tissue easily under control conditions.

Although thinking of an artery as three distinct individual layers can be useful it is important to remember that the cellular organisation within each of these layers is very complex. Therefore, new techniques are required to advance our understanding of how an artery is constructed at the cellular level and how each individual cell plays its role in the bigger picture. By using Laser Scanning Confocal Microscopy we can show that remodelling in each of the arteries can be defined according to the Mulvany 1996 classification depending on the changes observed within the vascular wall.

In anterior cerebral arteries from a rabbit model of heart failure there was an increase in lumen diameter along with increases in both thickness of the adventitial and medial layers. The

overall increase in wall cross sectional area meant that the changes in the morphology of these arteries could be defined as outward hypertrophic remodelling.

Third order mesenteric arteries from a rat model of heart failure show a decrease in lumen diameter along with a decrease in the density of smooth muscle cells within the ligated animals. There was no difference in the medial cross sectional area therefore arteries undergo eutrophic remodelling.

Remodelling within hypertension was shown in two models.
Firstly, a vasodilator study in genetically hypertensive SHRSP rats. In third order mesenteric arteries from these animals treatment with the angiotensin II type 1 antagonist – Irbesartan, or a combination of the diuretic hydrochlorothiazide and calcium channel blocker hydralazine produced no change in the lumen diameter between control and experimental groups. However a significant decrease in the wall cross sectional area of both experimental groups resulted from a significant decrease in the medial layer thickness with no difference in the number of cells. These arteries undergo hypotrophic remodelling.

The second model of hypertension was an inducible Fischer rat model. Infusion with Indole-3 Carbinol for 14 days results in a hypertensive state. Third order mesenteric arteries from these animals showed no difference in lumen diameter between controls and hypertensive animals. However these arteries displayed an increase in adventitial thickness along with a reduction in medial thickness resulting in no overall difference in the wall thickness as the decrease medial thickness cancelled the increased adventitial thickness. These results would suggest

that mesenteric arteries from an inducible model of hypertension undergo eutrophic remodelling.

What these results show is that by using Laser Scanning Confocal Microscopy more precise estimations of the type of remodelling within an artery wall can be made. The results show that by using the classification developed by Mulvany *et al.*, (1996) most types of remodelling can be explained but it also shows that there are gaps in the accepted classification. Remodelling within the vasodilator hypertension study can not be classified any further than hypertrophic remodelling. This is due to the fact that there was not an observed difference in the lumen diameter so remodelling can not be further described as inward or outward.

CHAPTER 1

Introduction

Introduction

The study of vascular morphology in particular the morphology of the resistance vessel wall has wide implications for the further understanding of many pathological conditions attributable to cardiovascular disease. Indeed, it is necessary to understand the architecture of the blood vessel wall to allow comparison between normal and diseased states. Morphological changes have been reported in hypertension (Mulvany *et al.*, 1993), chronic heart failure (Heeneman *et al.*, 1995), cerebral vascular injuries (Baumbach *et al.*, 1985) and others such as pre-eclampsia (Craven *et al.*, 1998, Goldman-Whol *et al.*, 2000). All of these diseases involve an alteration in the morphology of the blood vessel wall which reflects the underlying pathology and can aid its understanding.

1.1 Arterial Morphology

Resistance arteries may be defined as pre-arteriolar vessels with a luminal diameter of less than 500 μm (Bloom *et al.*, 1968; Johnson *et al.*, 1962). In common with larger arteries, resistance arteries comprise an outer tunica adventitia, a central tunica media and an inner tunica intima.

The tunica adventitia is composed of connective tissue containing elastin and collagen. The most common cell type found in the adventitial layer is the adventitial fibroblast; this makes up more than 90% of the cell population. Other cell types found include macrophages, leukocytes, mast cells and adipocytes (Faber *et al.*, 2001). This layer also contains the nerves which are associated with sympathetic innervation (Lee *et al.*, 1983; Rhodin *et al.*, 1980).

These nerves stimulate the release of a number of neurotransmitters, predominantly noradrenaline.

The tunica media comprises vascular smooth muscle cells bound by an internal and external elastic lamina. In small resistance-sized arteries the external elastic lamina can be fragmented or absent (Lee *et al.*, 1983; Carlson *et al.*, 1982). The smooth muscle cells are arranged circumferentially around the vessel diameter with an angular pitch (Gattone *et al.*, 1986; Miller *et al.*, 1987; Walmsley *et al.*, 1982,1983.) from the horizontal axis. Reports vary as to the extent of this pitch. Some believe it to be as small as 2° while others have reported a pitch of 10° (Mulvany *et al.*, 1976; Walmsley *et al.*, 1983.). The number of layers of smooth muscle within the blood vessel wall is directly proportional to the diameter of the vessel (Lee *et al.*, 1983). In vessels with a diameter of around 300 μm there are approximately 6 layers of smooth muscle in the media whereas there may be only a monolayer of vascular smooth muscle cells in the media layer of arteries with a diameter of between 30 to 50 μm (Gattone *et al.*, 1986; Miller *et al.*, 1987; Walmsley *et al.*, 1982). The tunica media comprises approximately 70 - 80 % of the vessel wall (Lee *et al.*, 1983; Miller *et al.*, 1987; Mulvany *et al.*, 1978; Walmsley *et al.*, 1983) regardless of the lumen diameter.

The inner-most layer of a blood vessel is the tunica intima. This layer comprises a loosely packed monolayer of endothelial cells orientated in the direction of the long axis of the artery and in the direction of blood flow. This layer is bound by a sheath of elastin known as the internal elastic lamina.

The ability of an artery to modulate its tone is linked to the endothelial layer. This is due to the ability of its cells to produce a number of vasoactive compounds which can affect vascular tone either through relaxation or contraction. These compounds are commonly known as endothelium derived relaxing factors (EDRF) or endothelium derived contracting factors (EDCF). Of all of the EDRFs arguably the most important is nitric oxide. This substance is released when some form of stimulation acts on the surface of the endothelial cells. The release of EDRF or nitric oxide may be as a result of mechanical factors such as sheer stress across the endothelial surface related to changing viscosity or flow or to chemical stimulus by agonists or other agents (Langille *et al.,* 1993). Within the internal elastic lamina there are small holes known as fenestrations, which allow nutrients and other substances to pass through the blood vessel wall in both directions i.e. from blood to tissues and from tissues to the blood.

1.1.1 A Description of Vascular Remodelling

Mulvany *et al.,* (1996) described a change in the media:lumen ratio without a change in media cross sectional area as "remodelling" i.e. a rearrangement of material around a changed lumen. The term remodelling is now commonly used to describe any alteration in architecture of a blood vessel wall. To better describe the process of remodelling Mulvany *et al.,* (1996) devised a nomenclature, which specifies the type of remodelling taking place; this is shown in figure 1. They suggested that inward or outward remodelling of the lumen may occur which can be further characterised as hypotrophic (a decrease in the cross sectional area), eutrophic (no change in the cross sectional area) or hypertrophic (increase in cross sectional area). Zervoudaki *et al.,* 2003 reviews the current and past literature agreeing with Mulvany's classification and giving an excellent description of remodelling of resistance arteries in

essential hypertensive patients. Since the proposal of this nomenclature there have been many debates as to how descriptive it is. Other researchers view this as incomplete or not descriptive enough. For example in SHR and SHRSP, remodelling occurs at a young age. Therefore the above method does not take into consideration growth changes in an artery (Korner & Angus, 1997). In human hypertension remodelling occurs in mature adults. Therefore it is different from hypertensive rat models in that elevation in blood pressure occurs over a number of years thus making it difficult to make comparisons between both models. In the scenario where there is no change in the lumen diameter, there is no provision for this in the nomenclature suggested by Mulvaney *et al* (Lee *et al.*, 1997). They point out the difficulties in using different techniques to study vascular structure. When using wire myography stretching of the vessel on wires is non-physiological and alters the normal shape of the artery. When using pressure myography the increase in pressure causes a longitudinal stretch on the vessel altering the lumen diameter. They suggest that *in-vivo* pressure fixation and confocal microscopy is the best technique to study arterial structure.

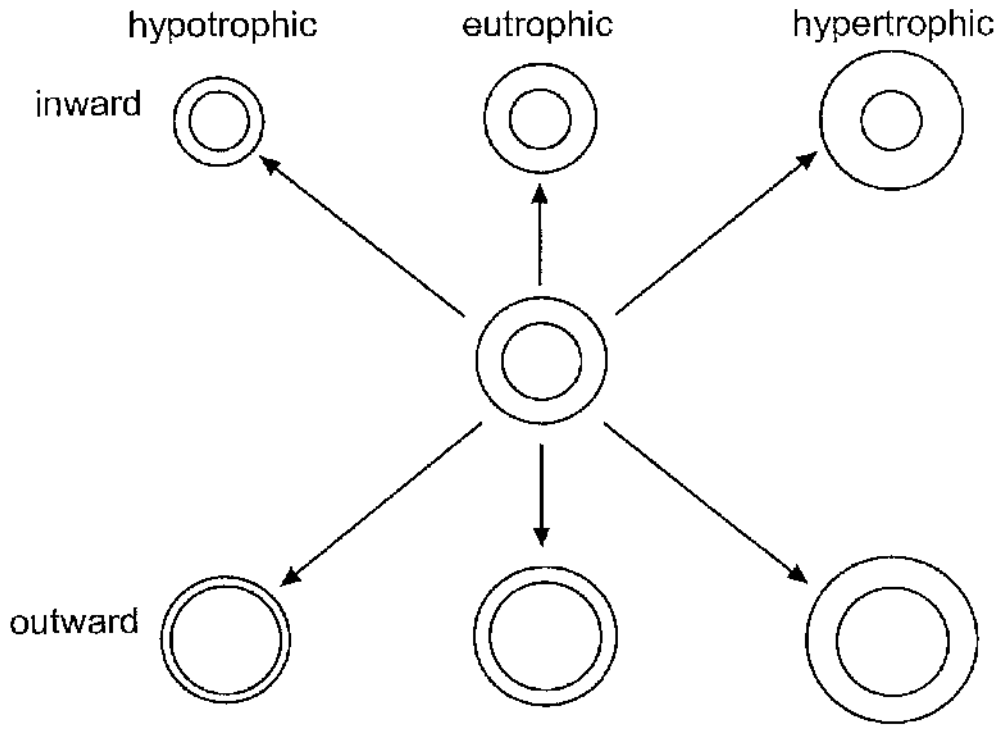

Figure 1.1 : Mulvany *et al.* Diagram of Vascular Remodelling

1.2 Techniques Used to Study Arterial Structure

1.2.1 Classical Techniques used to Study Arterial Structure

Over the years there have been many techniques used to further the understanding of the structure of blood vessels. Beginning in the mid part of the 19th and the earlier years of the 20th centuries histological methods were developed. These techniques concentrated on the basic histological structure of blood vessels using only simple staining techniques (Johnson *et al.*, 1867). These methods did not give very much information about the fine detail of the architecture of the artery.

1.2.2 Wire and Pressure Myography

Both of these methods have advantages and disadvantages over each other but a common advantage is the possibility for further histological studies of the fixed artery (Thybo *et al.*, 1995; Bevan *et al.*, 1972).

The wire myograph was developed by Bevan and Osher (1972) to study functional responses in resistance arteries. They wanted to record changes in wall tension of small blood vessels in-vitro. It was not until the late 1970's that Mulvany along with Halpern first used wire myography to study the structure of arteries from hypertensive rats (Halpern *et al.*, 1978).

This technique involves mounting resistance arteries of approximately 2 mm in length on to two 40μm wires. One wire is attached to a micrometer and the other to a force transducer. This allows the tension and the internal circumference of the artery to be measured and controlled. Measurements such as wall to lumen ratio and the cross sectional area of the vessel wall can be measured by placing the myograph on to the stage of a microscope fitted with a 10 X magnification water objective lens. Other important parameters that can be measured include the internal diameter and length of the vessel, the mean wire thickness and the mean distance between the inner edges of the wires. By using these measurements the internal circumference of an artery mounted on a wire myograph can be calculated.

By using the value for the internal circumference and a measurement of force (F) exerted on the transducer other vessel measurements can be made: Wall Tension, Active Wall Tension, and Active Wall stress.

On the wire myograph an artery can then be set to an effective transmural pressure similar to that *in-vivo*. This allows experiments to be carried out with the vessel maintained at its correct diameter and is known as 'normalisation'. This procedure of stretching the vessel in steps of around 10μm until the wall tension is approximately 1nN/mm is continued until the wall tension reaches 13.3 Kpa (equivalent to 100mmHg). Once a vessel has been normalised a value can be obtained for the internal circumference corresponding to the point on the exponential curve for which the effective transmural pressure is equal to 100mmHg (L_{100}). This allows an estimate to be made of the lumen diameter of the vessel *in-situ*, relaxed and under a transmural pressure of 100mmHg:

$l_{100} = L_{100}/\pi$

Most experiments are carried out at internal circumferences less than that of L_{100}, usually $_{0.9}L_{100}$, i.e. 90% of the internal circumference at L_{100}.

Vessels normalised on a wire myograph can yield biophysical values described above but they do not give details on the structural aspects of blood vessels. To do this histological or other visualisation techniques must be used. The wire myograph aids this by holding the artery at L_{100} or other set values while fixation occurs. One of the biggest disadvantages of using wire myography as a means of fixing blood vessels is that the wires pull the vessel therefore flattening it. This does not give a true representation of the circumferential aspects of the lumen or wall. A better and more physiological method is pressure myography.

Pressure myography was developed as a tool for studying the function of small artery preparations from normotensive and hypertensive rats (Halpern, W *et al.*, 1978). This

technique involves securing a resistance vessel to glass cannulae, which are filled with physiological salt solution (PSS). A system of PSS filled tubing is attached to the cannulae via a pressure transducer with one end of the tubing attached to either a servo-pump or a fluid reservoir raised to a preset height so as to control the pressure to which the vessel is exposed. The myograph is placed on the stage of a microscope and, with a video camera attached to a microscope, images can be taken of the blood vessel. The signal is fed into a video dimension analyser or similar computer program; this allows continuous measurements of the lumen diameter and wall thickness to be made. It also allows measurements along the length of the vessel to be made as the position of the lines on the monitor can be adjusted manually or by using measurement software. These measurements can be added together and a mean arterial wall thickness and lumen diameter can be calculated. Other measurements that can be made using this myograph system include external arterial diameter and arterial length. These can be used to calculate wall and media to lumen ratios etc. This method of using video measurements is very precise as the measuring lines on the monitor can be calibrated using a calibration grid placed on the microscope stage. The disadvantages to video based measurements are that they are very subjective and open to experimenter bias as the experimenter has to decide which points to measure the arterial wall. In addition variations in light intensity from the microscope can result in different measurements being taken as the vessel wall will appear to be thicker at lower intensities. Despite these disadvantages, pressure myography has a high rate of reproducibility; a 5% error was noted between observers looking at the same vessel. In one study by Lew *et al.*, (1992) a computerised diameter measuring system was used to make a comparison with video measurements. The results showed an excellent correlation between the computerised diameter measurements and manual

measurements - the regression coefficient was 0.992 showing that there are near similarities and validity between both methods.

Once again, pressure myography can be combined with histological techniques allowing a more detailed analysis of the structure of the blood vessel walls to be made. Arguably pressure myography offers more physiologically correct conditions for blood vessels. With this in mind mechanical characteristics can be calculated which are comparable to those values seen if the blood vessel was still *in-vivo*.

1.2.3 Dissector Stereological Technique

The dissector technique (Sterio *et al.*, 1983, Mulvany *et al.*, 1985; Bamdrup *et al.*, 1985; Korsgaard *et al.*, 1988) is a stereological method used by several researchers to estimate parameters such as volume fraction of smooth muscle cells in the media and also average cell dimensions including cell volume, length and cross sectional area and average nuclear length. This method of studying vascular morphology can be linked with wire myography to include the number of cells per segment length and the active force per cell. However, it is not very user friendly and can be time consuming. For this reason simple and more exact methods have been sought.

1.2.4 Laser Scanning Confocal Microscopy (LSCM)

A state of the art method currently being used to study vascular morphology is the technique combining pressure myography or in-vitro fixation with laser scanning confocal microscopy. Together these methods allow the experimenter to visualise the component cells within the

vessel wall. Several methods have been described using confocal microscopy to study the vascular wall at the cellular level. They mostly rely on staining the nucleus of cells with a fluorescent dye thus allowing the identification of cells types and thickness of constituent wall layers from these cell types (Baumbach *et al.*, 1989; Dickhout *et al.*, 1997). Each layer within the vessel wall can be clearly seen and can be distinguished from the others by cell shape and orientation.

Images obtained on a confocal microscope allow measurements of cross-sectional area, wall thickness, wall to lumen ratio, internal diameter and sometimes external diameter to be made. Wall thickness measurements can be made in an X-Y plane or a Z-axis. X-Y measurements can be used for the calculation of lumen diameter and Z-axis measurements show adventitial, medial and endothelial cells thus allowing wall measurements to be made using the different cell types as markers within the wall.

It has also been shown that staining the nuclei from vascular cells is a valid method for imaging and therefore further analysing the vessel wall (Arribas *et al.*, 1997). This method was validated by comparing the pattern of the staining with Hoechst 33342- a nuclear stain, and the widely used Haematoxylin and Eosin method of histological staining (Korsgaard *et al.*, 1993). By looking at both the LSCM images and the histological images similarities could be seen in the pattern of nuclei of both methods when taken at similar magnifications, although greater resolution can be achieved with confocal images.

The method of using confocal microscopy to study vascular morphology is advantageous as it gives clear and high resolution images of the vessel wall allowing 3 dimensional models to be constructed giving a virtual feel of the arterial morphology. There are some disadvantages to using confocal microscopy; these include the need for good quality specimens for imaging and the cost of running such a machine.

1.3 Animal Models

Animal models are required to study the basic mechanisms of cardiovascular disease which are observed in humans. Animal models are useful as age and sex matched experimental groups can be used under controlled experimental conditions. Rats are the most common species used in cardiovascular research because they are relatively low cost, have a short growth period to sexual maturity and therefore have rapid disease progression. They are also suited to invasive techniques with few resulting problems making them ideal for comparative studies. Other species commonly used include mice, rabbit and dog. The use of genetically engineered mice in cardiovascular studies has become very popular with several groups using knockout mice to study adrenoceptor pharmacology and its links with vascular remodelling while others study angiotensin receptor knockouts and their effect on blood pressure (Tanaka *et al., 1999, Akishita et al.,* 1999).

Cardiovascular disease can either be surgically induced in a species or bred into a species. In this study animal models which have been used include SHRSP rats, heart failure induced rats and rabbits and hypertension induced rats- a brief description of each model follows.

1.3.1 Spontaneously Hypertensive Stroke Prone Rats

Spontaneously Hypertensive Stroke Prone rats (SHRSP) were used in this study as a model of cerebrovascular disorders. These rats were developed by Okamoto *et al.* as a model for essential hypertension (Okamoto *et al.*, 1974). These rats have increased systemic blood pressure with ageing along with associated organ failure (Takakura *et al.*, 1994) and the incidences of cerebral vascular disorders are increased within these rats especially spontaneous stroke. Within the smaller cerebral arteries of these rats fibrinoid necrosis occurs which progressively leads to occlusion and stroke. Larger cerebral arteries lose their ability to regulate pressure via a decrease in compliance; this may also participate in the development of stroke by contributing to alterations in downstream cerebral microcirculation.

The susceptibility of this strain of rat to stroke or cerebral occlusion is believed to be genetically inherited. It is understood that infarction resulting from occlusion is inherited from one generation to the next as an autosomal recessive trait and that decreases in lumen diameter of anastasomes between the middle cerebral artery and the anterior cerebral artery are in fact responsible for the pathophysiology associated with cerebral occlusion. (Gratton *et al.*, 1998).

1.3.2 Antihypertensive Vasodilator Drug Study

Irbesartan, an angiotensin II type 1 receptor (AT_1) antagonist, was investigated to see whether it could prevent the pathology associated with stroke-prone spontaneously hypertensive rats (SHRSP). Irbesartan treatment from 6 weeks of age was compared to untreated control SHRSP, as well as rats given hydralazine (vasodilator via calcium binding on smooth muscle cells) and hydrochlorothiazide (a diuretic), (H+H). The hypothesis was that blockade of AT_1

receptors provides additional benefits over and above the ability of irbesartan to just lower blood pressure. This study focuses only on the effect that treatment with antihypertensives may have on the vascular morphology of SHRSP rats.

1.3.3 Controlled Inducible Hypertensive Rats

This model of hypertension has been generated in Professor John J Mullin's laboratory at the University of Edinburgh Medical School. These are inbred Fischer rats in which inducible hypertension is achieved via the expression of the mouse *Ren-2* gene. This gene is a renin transgene under the transcriptional control of the cytochrome P450, *Cyp1a1* promoter. Incorporation of this transgene results in a situation whereby expression leads to the animals becoming hypertensive. Induction of the transgene expression is regulated by the administration of Indole-3 Carbinol (I3C) and removal of this natural xenobiotic reverses this phenomenon (Kantachuvesiri *et al.*, 2001).

1.3.4 Coronary Artery Ligated Rabbits

Vascular morphology remodelling can be observed in experimental heart failure. It is believed that as a result of heart failure the peripheral vasculature will remodel to compensate for decreases in stroke volume, which leads to a decrease in cardiac output. Our model of heart failure involves ligation of the major branch of the left coronary artery resulting in a reduction in blood flow to the left ventricle. This reduction in flow results in ischaemic areas forming leading to reduction in cardiac function.

This model has been used extensively to investigate haemodynamic performance in comparison with other models. (Pye *et al.*, 1996). Echocardiography can be used as a non-invasive method to determine if this model of heart failure is representative of the condition seen in humans.

1.3.5 Coronary Artery Ligated Rats

This model was developed as a less expensive alternative to a rabbit model of heart failure. Male Wistar-Kyoto (WKY) rats were obtained from Professor Anna Dominiczak's colony at Glasgow's Western Infirmary. Similar to our rabbit model these rats had left ventricular dysfunction induced by ligation of their left anterior descending coronary artery. Left ventricular dysfunction was assessed by echocardiography, ligated animals showing a significant decrease in ejection fraction compared to sham operated controls (Lygate C,A. 2000; University of Glasgow PhD thesis). This method of inducing heart failure has been investigated by other researchers (Buss *et al.*,., 1999; Heeneman *et al.*,., 1995) although the architecture of the arteries has never been investigated using laser scanning confocal microscopy.

CHAPTER 2

Materials and Methods

Methods

2.1 Solutions and Drugs

The Krebs-Hensleit solution used as the physiological salt solution in which all blood vessels were dissected and stored in before use was of the following composition (mM): Sodium Chloride (112), Potassium Chloride (5.9), Magnesium Chloride (1.2), Calcium Chloride (2), Sodium Hydrogen Carbonate (25), Sodium Hydrogen Phosphate (1.2), Glucose (11.5) and Na_2EDTA (0.023).

All vessels were fixed using neutral buffered formalin of the following composition (mM): 10% formaldehyde, Sodium Phosphate monobasic ($NaH_2PO_4H_20$) (135), Sodium Hydroxide (NaOH) (105)- pH 7.4.

The following compounds were used:

Propidium Iodide (Sigma)

These investigations conform with the Guide for the Care and Use of Laboratory Animals published by the US National Institute of Health (NIH publication No. 85-23, revised 1996). All experiments were performed using the highest quality reagents and under levels of safety required by the Control of Substances Hazardous to Health regulations.

2.2 Animals used and anatomical location of Arteries

Spontaneously hypertensive stroke prone (SHRSP) and Wistar Kyoto (WKY) rats were obtained from Professor Anna Dominiczak's colony in the Western Infirmary, Glasgow. Fischer rats were obtained from Professor John Mullin's colony in the Medical School, University of Edinburgh. All rats were used at a similar age (~12 – 14 weeks). New Zealand White rabbits (~ 20 weeks) were obtained from Glasgow Royal Infirmary's biological services unit. All animals were killed by lethal overdose of Euthetal. Third order mesenteric ateries in the rat and anterior cerebral arteries from rabbits are located as shown in figure 2.1 and removed from the animals. Connective tissue from around the artery was dissected under a stereo dissecting microscope. The intention of this thesis is not to compare vascular remodelling in the same arteries from various animal experimental models but to show that laser scanning confocal microscopy can be used as a tool to study vascular remodelling.

Rat Mesenteric (MES) **Rabbit Anterior Cerebral (ACA)**

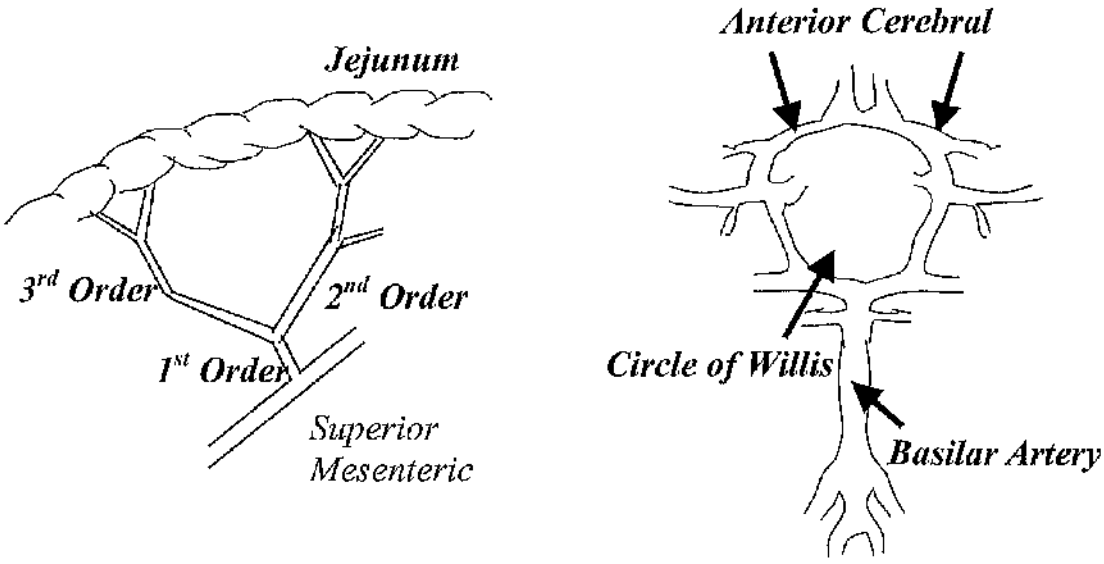

Figure 2.1: Indication of anatomical position of both the 3rd order mesenteric artery in the rat and the anterior cerebral arteries in the rabbit.

2.3 Laser Scanning Confocal Microscopy

After dissection the arteries were mounted on a pressure myograph (Living Systems Instruments); pressurized and fixed with neutral buffered formalin. Pressure settings for each artery are calculated from initial wire myograph (Danish MyoTechnology A/S) experiments except in the case of the study using SHRSP rats and irbesartan and Hydralazine + Hydrochlorothiazide. In these experiments ½ systolic blood pressure was used as the fixation pressure (Halpern W *et al.*, 1991). This was possible because initial blood pressures were known for these animals whereas in the other experimental groups initial blood pressures were not measured. The fixation pressures used for each study are given in table 2.1

				Mean Pressure (mmHg)		
Study	**Species**	**Method**	**Artery**	***Control***	***Exp. Group 1***	***Exp. Group 2***
1. Heart Failure	Rabbit	CAL	Anterior Cerebral	55	60	-
2. Heart Failure	Rat	CAL	Mesenteric	50	50	-
3. Hypertension	Rat	IND	Mesenteric	50	50	-
4. Hypertension	Rat	REV	Mesenteric	83	62	60

Table 2.1: Fixation pressures for arteries in all experimental groups studied.
CAL: Coronary Artery Ligation; Ind: Inducible Hypertension;
Rev: Reversible Hypertension treatment with Irb (Exp group1) and H+H (Exp group2)

Nuclei were stained by incubation with 10 μmol/L propidium iodide for 45 minutes, then washed 3 times for 10 minutes each in physiological salt solution.

2.3.1 Setup of Arteries on Glass Slides

Arteries were mounted on glass slides within a small square of vacuum grease to ensure that the cover-slip did not press against the surface of the blood vessel therefore ensuring a circular shape was maintained.

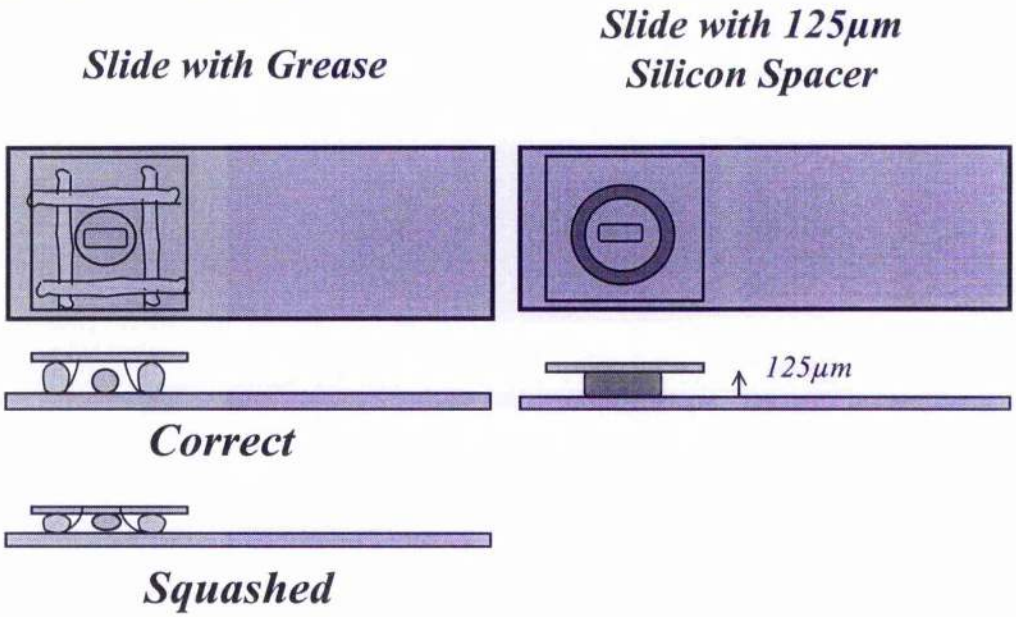

Figure 2.2: Artery setup on a glass slides using both vaccuum grease and silicone spacer showing the correct and squashed shape of the blood vessel.

Blood vessel images were obtained using a method described by Arribas *et al.*, (1997) with an Odyssey Real Time Laser Scanning Confocal Microscope (Noran Instruments).

Imaging parameters were an excitation wavelength of 488nm from an argon ion laser and an emission filter of 515nm with a slit size of 15μm. The lumen was visualized with a X10 air objective at the point mid-way through the blood vessel wall. A X40 water immersion objective was used for wall thickness measurements, 1μm thick optical sections were taken through the vessel wall. Metamorph software (Universal Imaging Corporation) was used

to make measurements from three lumen measurements and two wall thickness stacks per vessel.

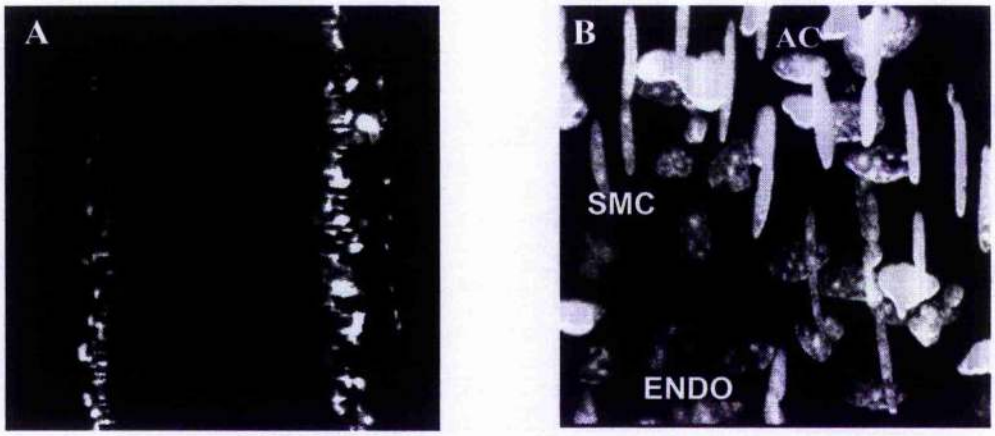

Figure 2.3

Image A: mid point through the vessel wall where lumen diameter measurements are made. Image B: 3 dimensional reconstruction of artery wall; Adventitial cells (AC), Smooth muscle cells (SMC) and endothelial cells (ENDO).

2.4 Method of Cell Counting

From within the wall thickness the number of cells within each layer was counted manually through the z-series. The method used for this ensured that nuclei were counted only once. Nuclei which bisected the left and bottom limits of the image were counted but those which bisected the upper and right limits were not. As each image was taken from different areas in the artery we can be sure that the same cell is not counted more than once.

By orientating the artery horizontally along the field of view different cell types can be identified by shape and orientation. Adventitial cells are irregular and dispersed in the outer regions of the stack. Smooth muscle cells are long and narrow and are located in the mid region of the stack, orientated circumferencially around the vessel wall and endothelial

cells are short and narrow and orientated perpendicular to the Smooth muscle cells (SMC) in the inner most layer of the stack. The following data is measured directly from the images obtained on the LSCM: lumen diameter, wall thickness (adventitial, medial and intimal thickness) and cell numbers in each layer. Other parameters such as cross-sectional area (CSA) and wall volume are calculated as outlined below using the above data. The assumption is that the vessels are of uniform thickness along their length and circumference.

2.5 Calculations from Confocal Images

The image area remained constant throughout all experiments (102.4 x 102.4μm)- at a magnification of 40 times- thus allowing a further calculation of the density of each cell type to be made as outlined below:

Area of image = 102.4μm x 102.4μm = 10485μm2 = 0.010485 mm2

The number of endothelial cells (nEC) is counted from a set of 4 –10 images and calculated as the number of endothelial cells per mm^2.

nEC/mm^2 = Total nEC / (Area of image x Number of images)

The external diameter was not measured directly in any of the experimental groups but can be easily calculated as,

External diameter = lumen diameter + (2 x wall thickness)

Using an established method of calculating cross sectional area (CSA) (Miller *et al.*, (1987), Lee *et al.*, (1983), Arribas *et al.*, (1997), Kvist *et al.*, (2003)) we estimate that by using the previously calculated data CSA= πr^2, where r = radius of the artery [wall thickness + the distance from the centre of the artery to the inner surface of the intima].

Vessel wall CSA = [π(External diameter/2)^2] – [π(lumen diameter/2)^2]

Adventitial CSA was calculated using the above equation by including medial and intimal thickness with lumen radius when calculating internal dimensions. Media and intima CSA's were calculated in a similar way.

A measurement of volume could then be obtained by multiplying CSA by length of vessel, assuming the vessel to have a cylindrical shape. A standard segment length of 1mm was chosen, such that CSA in mm^2 was equal to volume of a 1 mm segment in mm^3.

The volume of a stack was calculated as,

Volume of stack mm^3 = Area of image x Wall thickness

Since we know the volume of the stack and the number of SMC counted within it, then it is possible to calculate the total number of SMC in a 1mm segment of artery by calculating the number of stacks required to represent that artery.

Number of stacks / 1 mm length of vessel = Wall volume / Volume of stack
Total nSMC = (Number of stacks / 1 mm length of vessel) x (nSMC in stack)

Cell density can be calculated by correcting total cell number for volume of the appropriate layer.

SMC density (n/mm^3) = nSMC / Media volume

The equivalent parameters for adventitial cell number and density were calculated in a similar manner.

Media : Lumen Ratio (%) = (Media thickness / Lumen diameter) x 100

The equivalent parameter for wall : lumen ratio can be calculated by substituting the value for media thickness with wall thickness.

2.6 Measurement of Wall Thickness

Stacks of 1μm thick serial optical slices were taken in z–axis from the first adventitial to the last endothelial nuclei. Each layer was identified as being when the first nuclei of the specific cell type was visible and ending when the first nucleus of the next layer was visible.

2.7 Analysis of Confocal Images

Analysis of the images obtained from the LSCM using specialized software allowed detailed information to be obtained regarding the size, shape and orientation of the nucleus in the various levels within the vessel wall. This information is important for the classification of the type of remodelling occurring in the vessel wall i.e. hyper or hypoplasia.

2.8 Total Number of Cells

The total number of adventitial and smooth muscle cells can be calculated for each 1mm^3 volume of blood vessel. This is achieved by multiplying the number of adventitial or smooth muscle cells per image by the number of stacks per 1 mm^3 vessel.

Using the equations:

Total number of Adventitial Cells =

Number of stacks / 1 mm^3 X number of adventitial cells

(or Smooth Muscle Cells)

number of stacks / 1 mm length of vessel =

Wall Volume / Volume of Image

Wall Volume (mm$^{3)}$ =

(Outer Adventitial CSA – Inner Adventitial CSA) / 1000000

Volume of Image (mm$^{3)}$ =

(Area of the image X Vessel Thickness) / 1000000000

2.9 Analysis of Carotid Artery Images

Carotid arteries from Sham (n=9) and Ligated (n=8) New Zealand white rabbits were dissected, mounted and pressurised on a Living Systems pressure myograph at 120mmHg. They were then fixed using neutral buffer formalin overnight. Once fixed the arteries were prepared for paraffin wax embedding by dehydration through increasing percentages of ethanol to absolute ethanol. The arteries then were put through a series of increasing

concentrations of acetone to absolute acetone. From acetone the arteries were embedded in paraffin wax and stored until sectioned. Sections were cut at 10μm thickness using a Richert Jung microtome. After sectioning cut sections were mounted on glass slides and stained with picro-sirius red, a collagen specific stain, (Junqueira L. *et al.*, 1979). Under bright field microscopy collagen is stained red against a yellow background (counterstaining by picric acid). The intensity of the red staining can be measured by optical densitometry to provide an estimate of the extracellular collagen component in the tissue. An estimate of the extracellular component was made for the adventitial and medial layers in both control and ligated rabbits in the heart failure rabbit study. This was calculated as the percentage area within the image that the red stained material occupied. A grey scale value between 0 and 255 was obtained as an indicator of the optical density of the collagen. For each artery several segments of the preparation were examined. Image analysis was used to calculate the total area of the adventitial and medial layers. Within the computer protocol the software took into consideration any holes in the section caused by tearing during processing and sectioning. Thus, a true estimate can be made of the collagen component in the arterial wall.

2.10 Analysis of results

The average value of each measurement and calculated parameter is presented in tabular form in appendix AP1-AP4. All data was analysed using Microsoft Excel and GraphPad Prism 3.01 (Institute for Scientific Information, San Diego, California, USA). All equations and nomenclature used in the text are taken from Microsoft Excel and GraphPad Prism 3.01. Statistical comparison of control and experimental data was performed using an unpaired t test. A p value of less than 0.05 was considered to be significant.

CHAPTER 3

Tunica Adventitia

Analysis of the Tunica Adventitia of Resistance Arteries using Laser Scanning Confocal Microscopy and the Quantification of Collagen within the Adventitial Layer of Carotid Arteries in a Rabbit Model of Heart Failure

For the purpose of clarity the following key will be used throughout this and all results sections.

	Control	Exp. Group 1	Exp. Group 2
Rabbit ACA	Sham (n=9)	Ligated (n=7)	-
Rat HF	Sham (n=7)	Ligated (n=9)	-
Vasodilator Study	Control (n=8)	H+H (n=6)	Irb (n=7)
Rat Induced Hypertension	Control (n=16)	Hypertensive (n=19)	-

Table 3.1 Definition of terms used in table and Figure headings and keys.
Control: animals under same experimental conditions except ligation was not done.
Ligated: descending left coronary artery ligated animal,
H+H: Hydralazine/ Hydrochlorothiazide treated rat,
Irb: Irbesartan treated rats,
Hypertensive: hypertension induction.

3.1 Adventitial Characteristics

Adventitial cells are irregular in shape and dispersed without any obvious regular pattern throughout the outer most layers of the arterial wall. Staining with Propidium Iodide allows us to visualise the location and number of cells within the adventitial wall (Appendix 6)

3.2 Adventitial Thickness

Measured values of adventitial thickness were made directly from confocal images using the previously described method. No difference was seen in the thickness of any of the adventitial layers in the blood vessels measured. Figures 3.1, 3.2

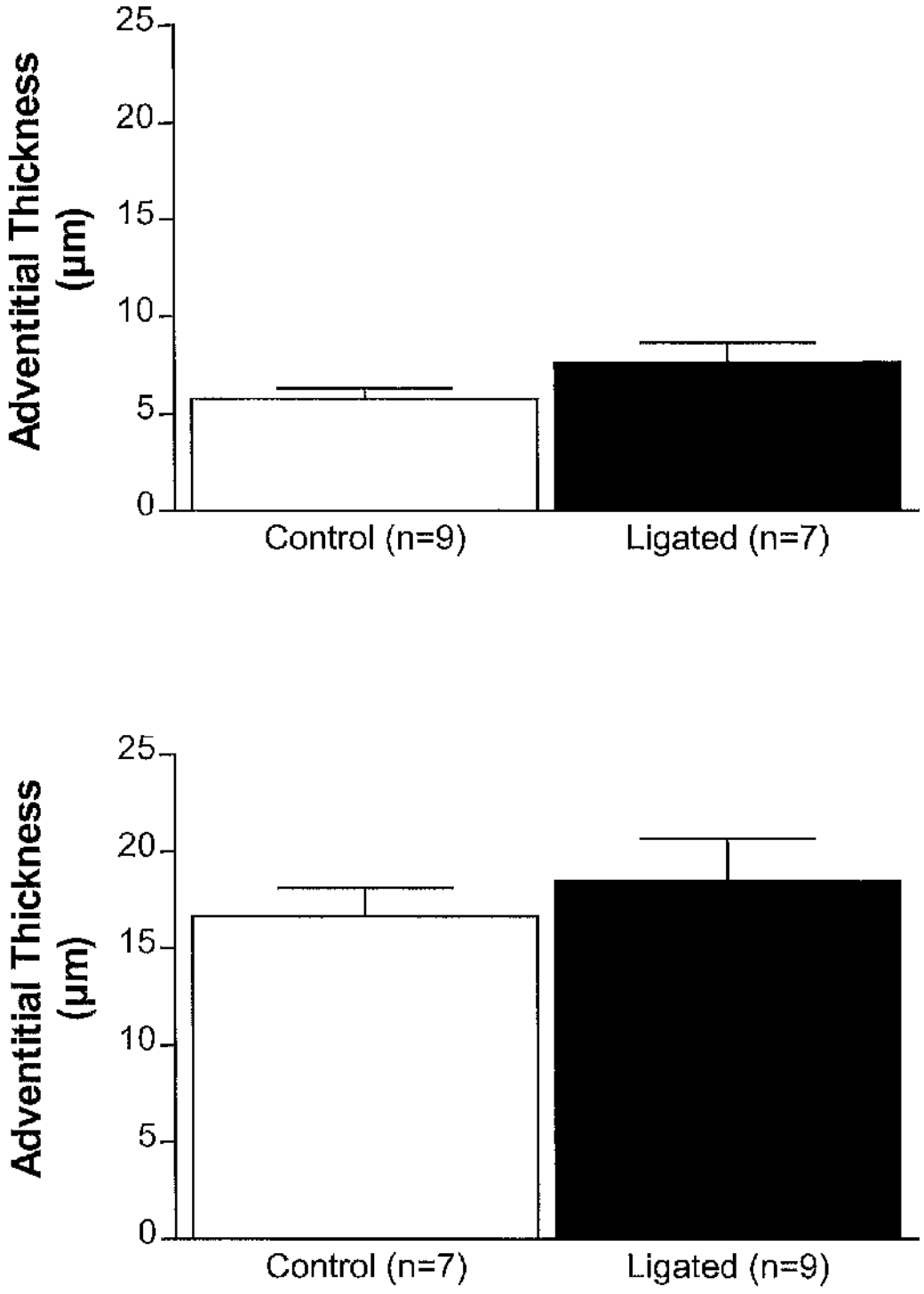

Figure 3.1 :- Thickness of the adventitial layer in arteries from heart failure models. Anterior cerebral arteries from the rabbit model of heart failure (top) and third order mesenteric arteries form the rat model of heart failure (bottom) showed no significant difference in adventitial thickness. Data is presented as mean ± s.e.m for the number of arteries indicated in brackets.

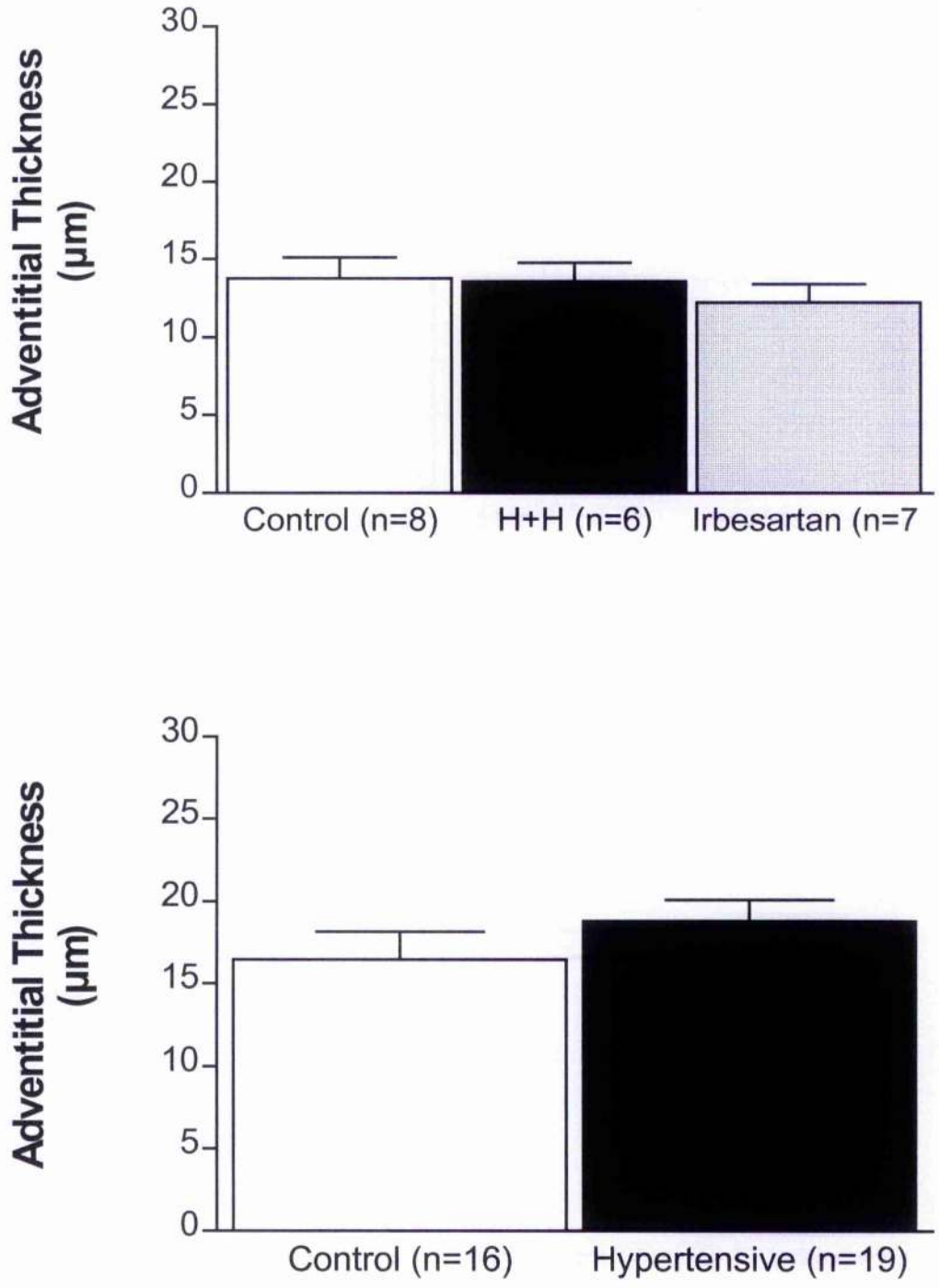

Figure 3.2 :- Thickness of the adventitial layer in arteries from hypertensive models. Third order mesenteric arteries from the hypertension treatment with H+H or irbesarten (top) from the rat model of inducible hypertension (bottom) showed no significant difference in adventitial thickness. Data is presented as mean ± s.e.m for the number of arteries indicated in brackets.

3.3 Count of Adventitial Cell Number per Stack

There was no difference observed between the experimental groups except in the H+H group and the inducible hypertension study. With H+H treatment the number of adventitial cells was significantly reduced. The control rats have 19.5±1.52 cells per region, whilst the hydralazine/hydrochlorothiazide group had 15.38±0.88 ($p<0.05$). In the inducible hypertensive study the hypertensive rats had a significantly increased number of adventitial cells. The control rats had 18.38±2.49 whereas the hypertensive animals had 32.82±2.33 ($p<0.005$).

	Control	Exp. Group 1	Exp. Group 2
Rabbit ACA	13.94±1.31	16.06±2.48	-
Rat HF	20.96±3.24	18.36±1.89	-
Vasodilator Study	19.5±1.52	15.38±0.88*	17.64±1.67
Rat Induced Hypertension	18.38±2.49	32.82±2.33**	-

Table 3.2 Adventitial Cell Number (cell number ± SEM).
* $p < 0.05$ control v Hydralazine/Hydrochlorothiazide treatment.
** $p < 0.001$ Control v hypertensive

3.4 Estimation of Adventitial Cell Density

Using values from measurements made of adventitial thickness and cell number we can calculate the density of the adventitial cells as the number of adventitial cells per mm^3. The only group observed which showed a difference in the density of adventitial cells was the hypertensive rats in the inducible hypertension study. The control rats had an adventitial cell density of 127±10 thousand cells per mm^3, whereas there was a significant increase in the adventitial cell density in the hypertensive rats 155±11thousand cells per mm^3 ($P<0.05$).

	Control	Exp. Group 1	Exp. Group 2
Rabbit ACA	232±2	242±76	-
Rat HF	131±33	106±27	-
Vasodilator Study	127±11	100±10	140±25
Rat Induced Hypertension	103±12	160±11*	-

Table 3.3 Adventitial Cell Density (thousand cells / mm3 ± SEM).
* $p < 0.05$ control v hypertensive

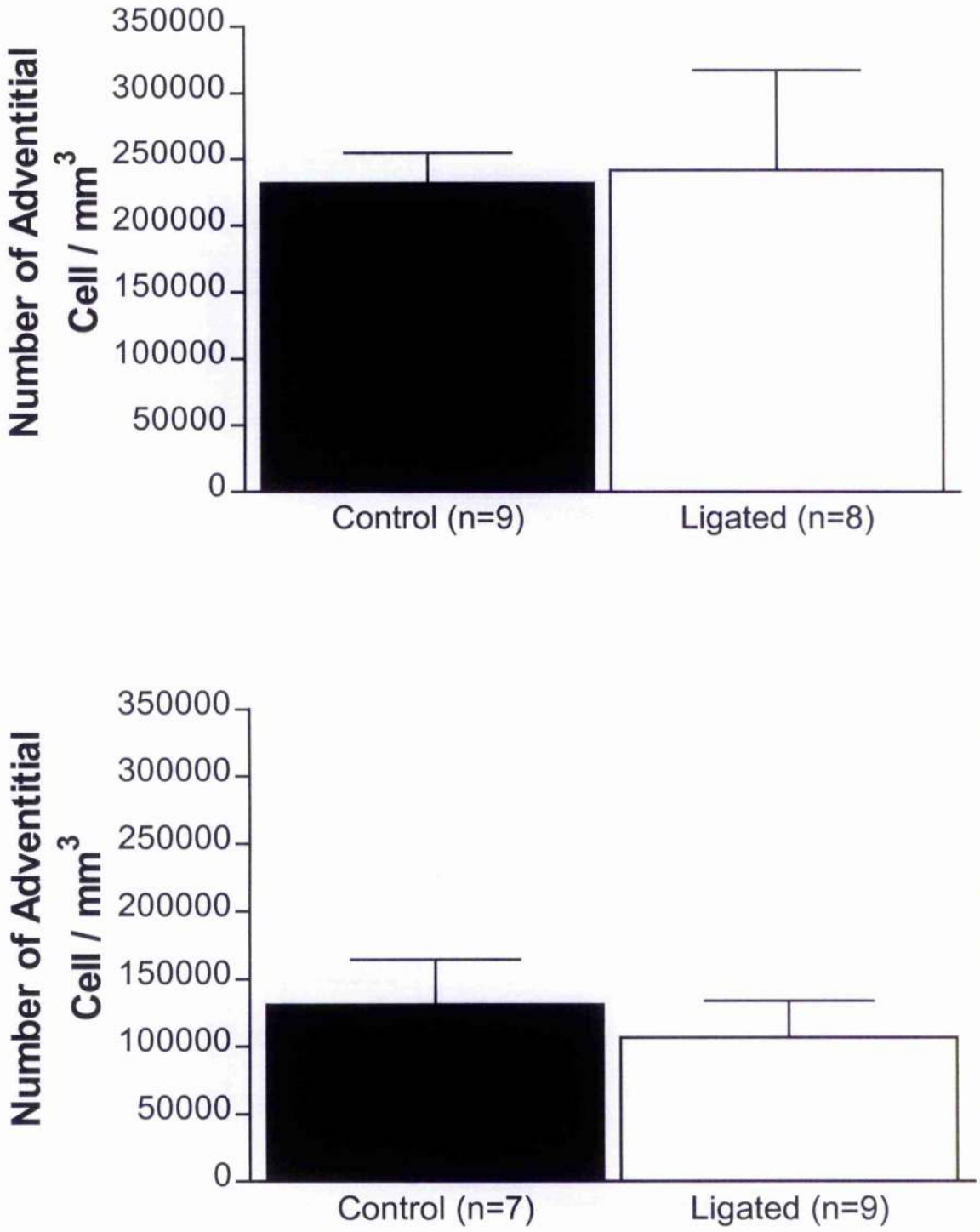

Figure 3.3: Density of Adventitial cells from Heart Failure Models. Anterior Cerebral Arteries from the rabbit model of heart failure (top) and third order mesenteric arteries from the rat model of heart failure (bottom) showed no significant difference in adventitial cell number density.

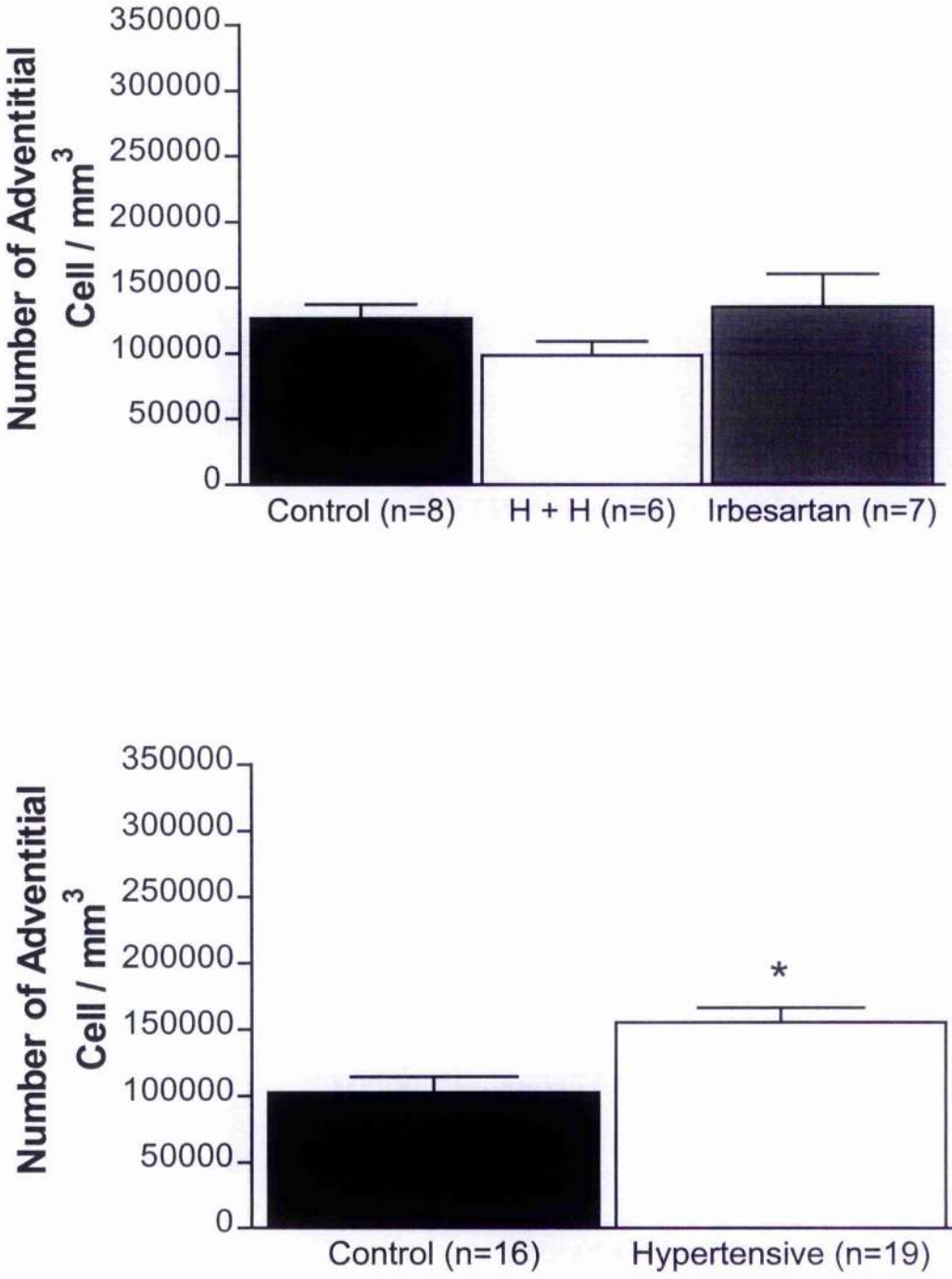

Figure 3.4: Density of Adventitial cells from Hypertensive Models. Third order mesenteric arteries from the hypertension treatment with H+H or irbesartan (top) showed no significant difference in adventitial cell density whereas third order mesenteric arteries from the inducable hypertension rats showed a significant increase in adventitial cell density. ($p<0.005$ control v hypertensive).

3.5 Total Number of Adventitial Cells

Within all the groups there was no difference in the total number of adventitial cells within a 1mm length of artery.

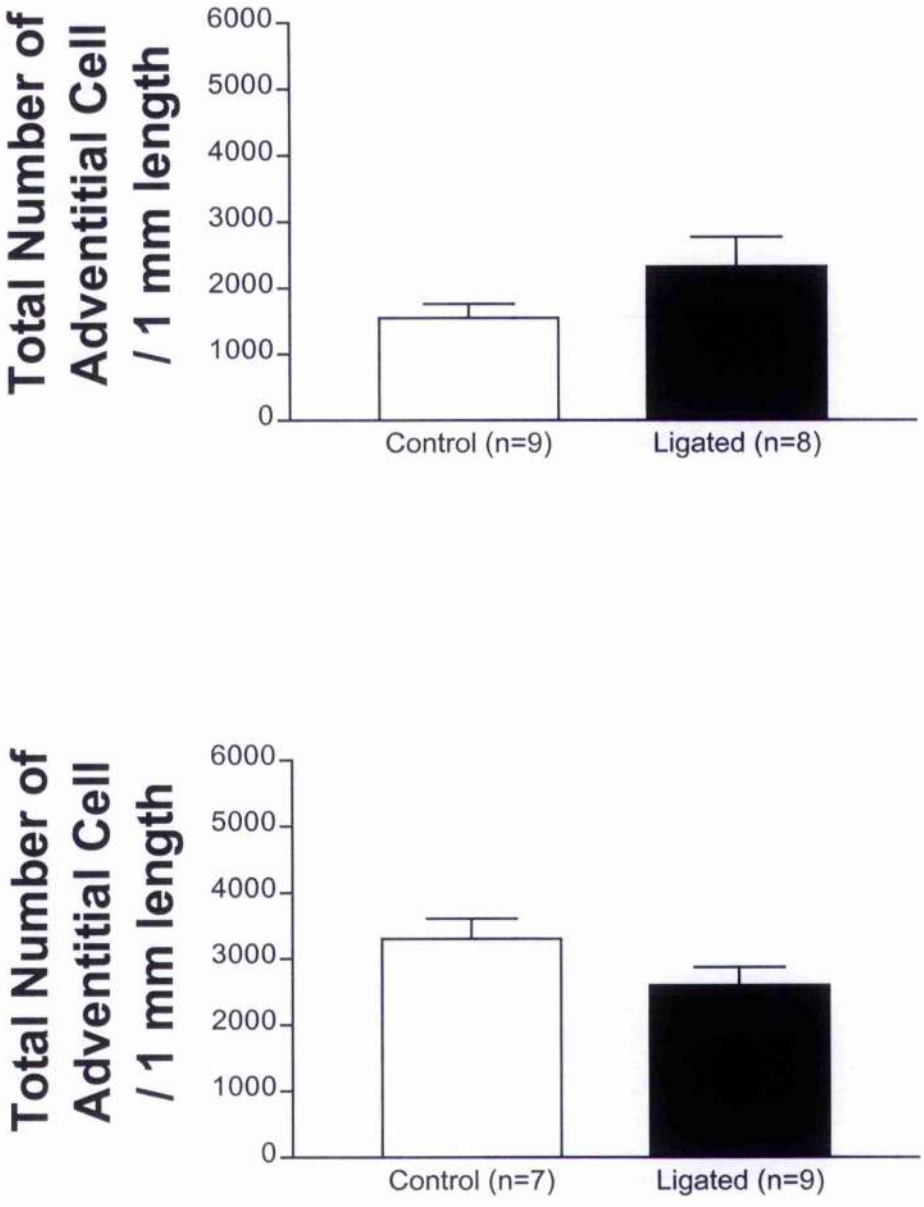

Figure 3.5 Total number of Adventitial cells from Heart Failure Models. Anterior Cerebral Arteries from the rabbit model of heart failure (top) and third order mesenteric arteries from the rat model of heart failure (bottom) showed no significant difference in total adventitial cell number / 1mm length of artery.

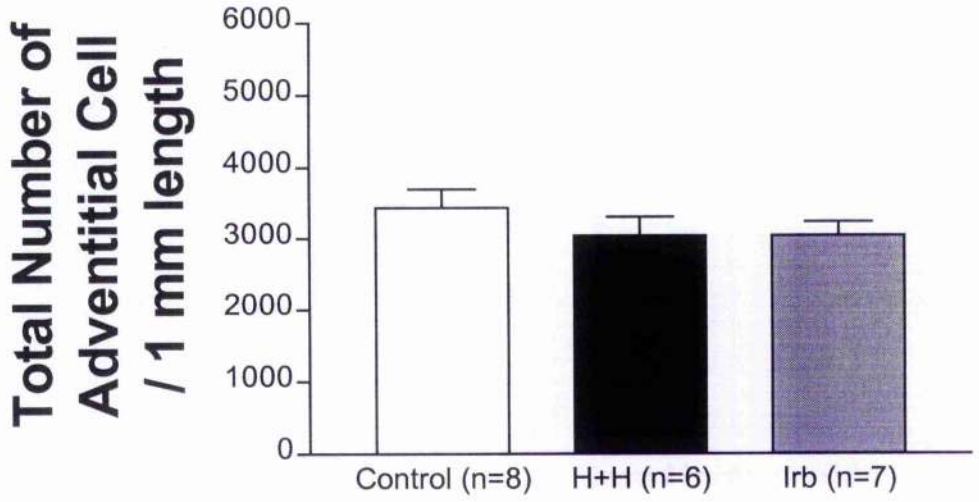

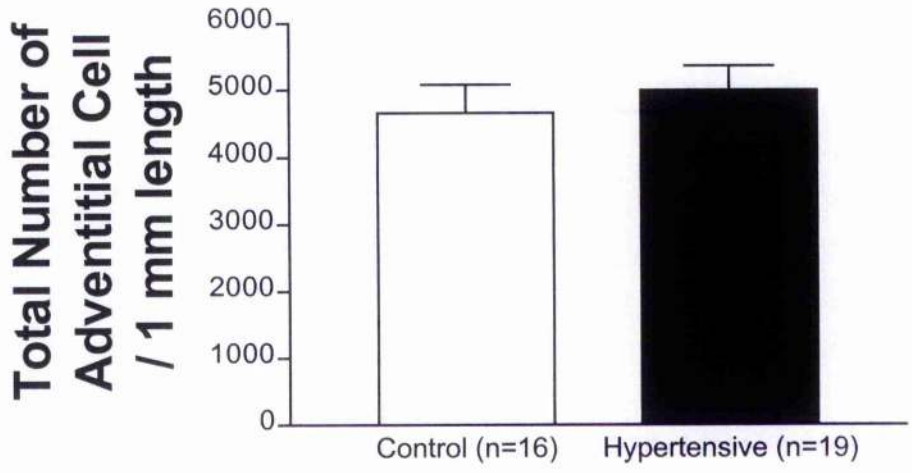

Figure 3.6 Total Number of Adventitial cells from Hypertensive Models. Third order mesenteric arteries from hypertension treatment with H+H or irbesartan (top) and from the inducable hypertension rats (bottom) showed no significant difference in total adventitial cell number.

3.6 Collagen Content within the Tunic Adventitia

The collagen component within the carotid arteries of the ligated rabbits was significantly reduced.

	Total Adventitial Area (μm^2) x 10^3	Collagen content in Adventitial Layer (%)
Control (n=8)	4.95 +0.15	82.01 ± 0.51
Ligated (n=9)	4.47 ± 0.17 *	82.33 ± 0.58

Table 3.4 Collagen content within the tunica adventitia of carotid arteries from control and ligated rabbit. Student's T-Test, * $p<0.005$

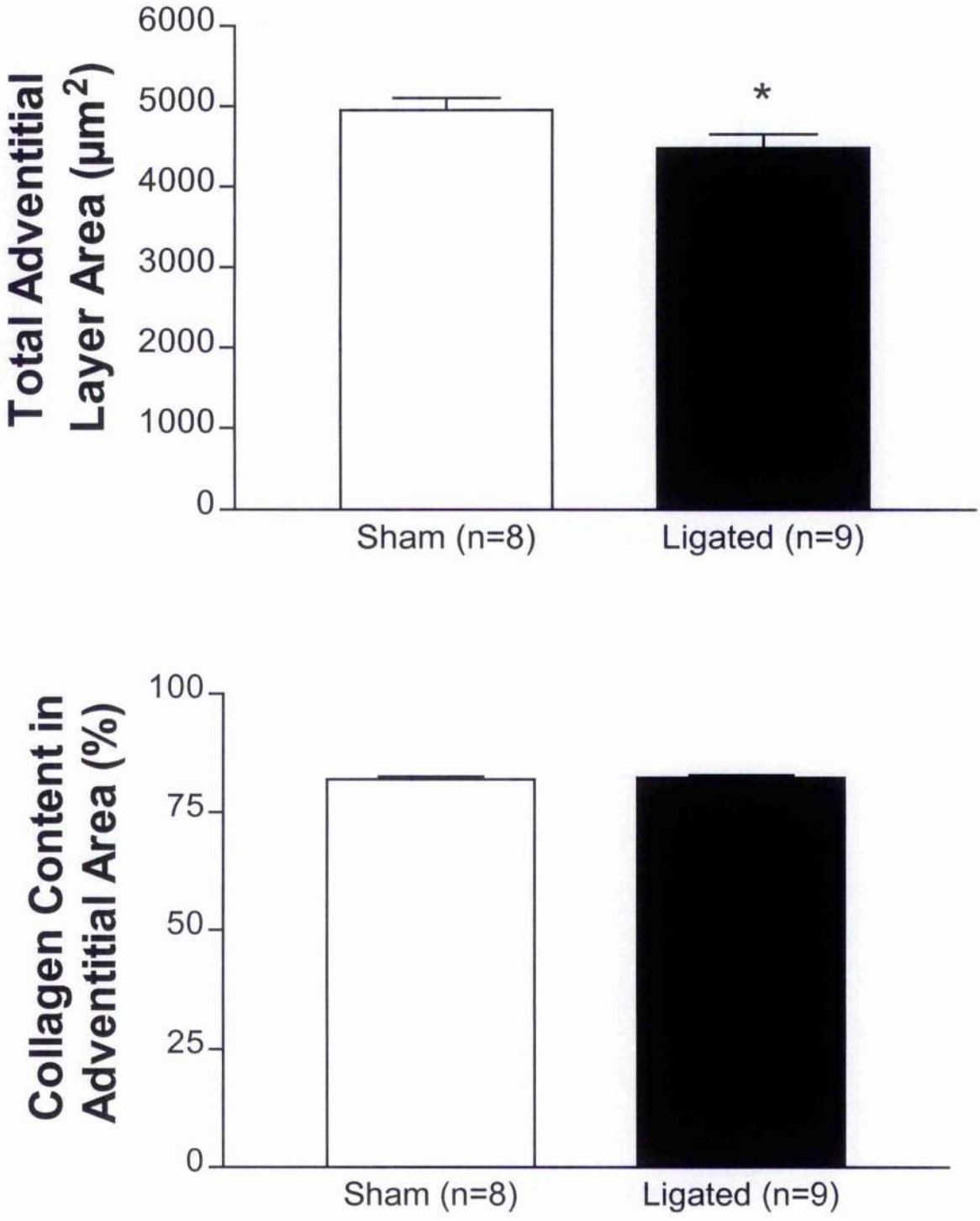

Figure 3.7 Parameters calculated from histological images obtained from rabbit carotid arteries. Total adventitial area (top) within the section was calculated and from this the percentage collagen content obtained from picosirius red staining was measured (bottom).

3.7 Collagen Staining in the Rabbit Carotid Artery

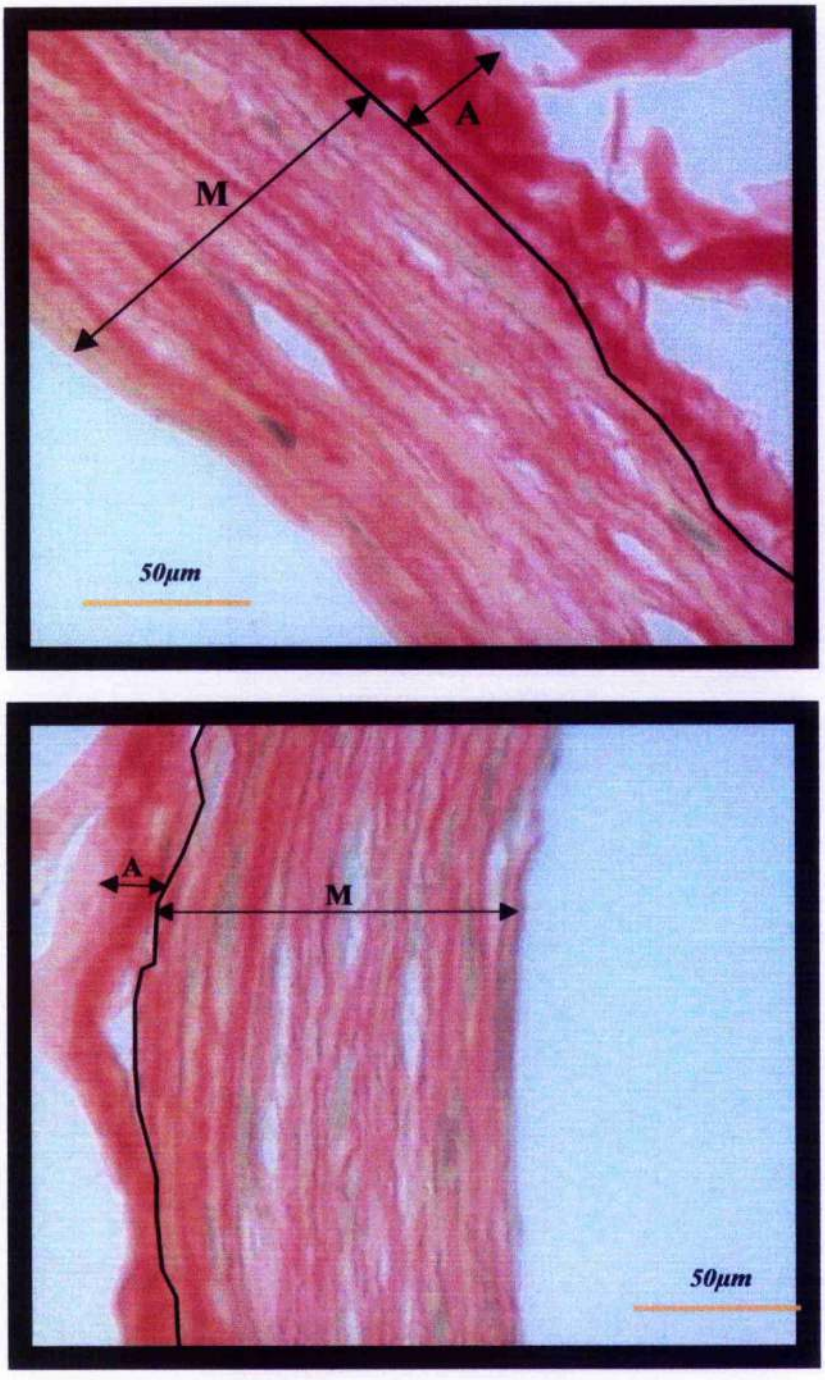

Figure 3.8 Histological images obtained from Sham (top) and Ligated (bottom) rabbit carotid arteries stained with picosirius red for collagen. The adventitial-medial border is marked thus allowing the software to distinguish between both layers for the purpose of calculations. The adventitial layer (A) is the smaller outermost area of the section whereas the medial layer (M) comprises the majority of the image.

CHAPTER 4

Tunica Media

Analysis of the Tunica Media of Resistance Arteries using Laser Scanning Confocal Microscopy and the Quantification of Collagen within the Medial Layer of Carotid Arteries in a Rabbit Model of Heart Failure

4.1 Medial Characteristics

Smooth Muscle Cells (SMC) are regular in shape and dispersed throughout the middle layer of the arterial wall. Staining with propidium iodide (PI) allows us to visualise the location and number of cells within the medial layer (Appendix 6).

4.2 Medial Thickness

Values of medial thickness were measured directly from confocal images using the previously decribed method. An increase in the medial thickness was observed in both the anterior cerebral arteries in the rabbit model of heart failure (Sham 12.72 ± 1.13 μm; Ligated 20.19 ± 2.62 μm, $p<0.05$) and also in mesenteric arteries from the inducible hypertension rat model (Sham 19.47 ± 1.42μm; Ligated 24.95 ± 1.86μm, $P<0.05$). A decrease in the medial thickness was shown in SHRSP rats treated with Irbesartan or H+H (SHRSP control 26.81 ± 2.05; H+H 20.63 ± 1.26*; Irb 20.00± 1.18†, *$p<0.05$, †$p<0.05$). No difference was seen in the thickness of any of the medial layers in blood vessels in the other experimental groups measured. (Figure 4.5)

4.3 Measurement of Smooth Muscle Cell Number per Stack

There was no difference in the number of smooth muscle cells observed per stack in the experimental groups. (Figure 4.7)

	Control	Exp. Group 1	Exp. Group 2
Rabbit ACA	52.06±3.41	56.56±3.38	-
Rat HF	45.43±3.39	37.11±3.41	-
Vasodilator Study	49.13±2.83	49.50±1.73	44.50±2.24
Rat Induced Hypertension	46.56±2.72	48.26±2.99	-

Table 4.1 :- Smooth Muscle Cell Number (cell number ± SEM).

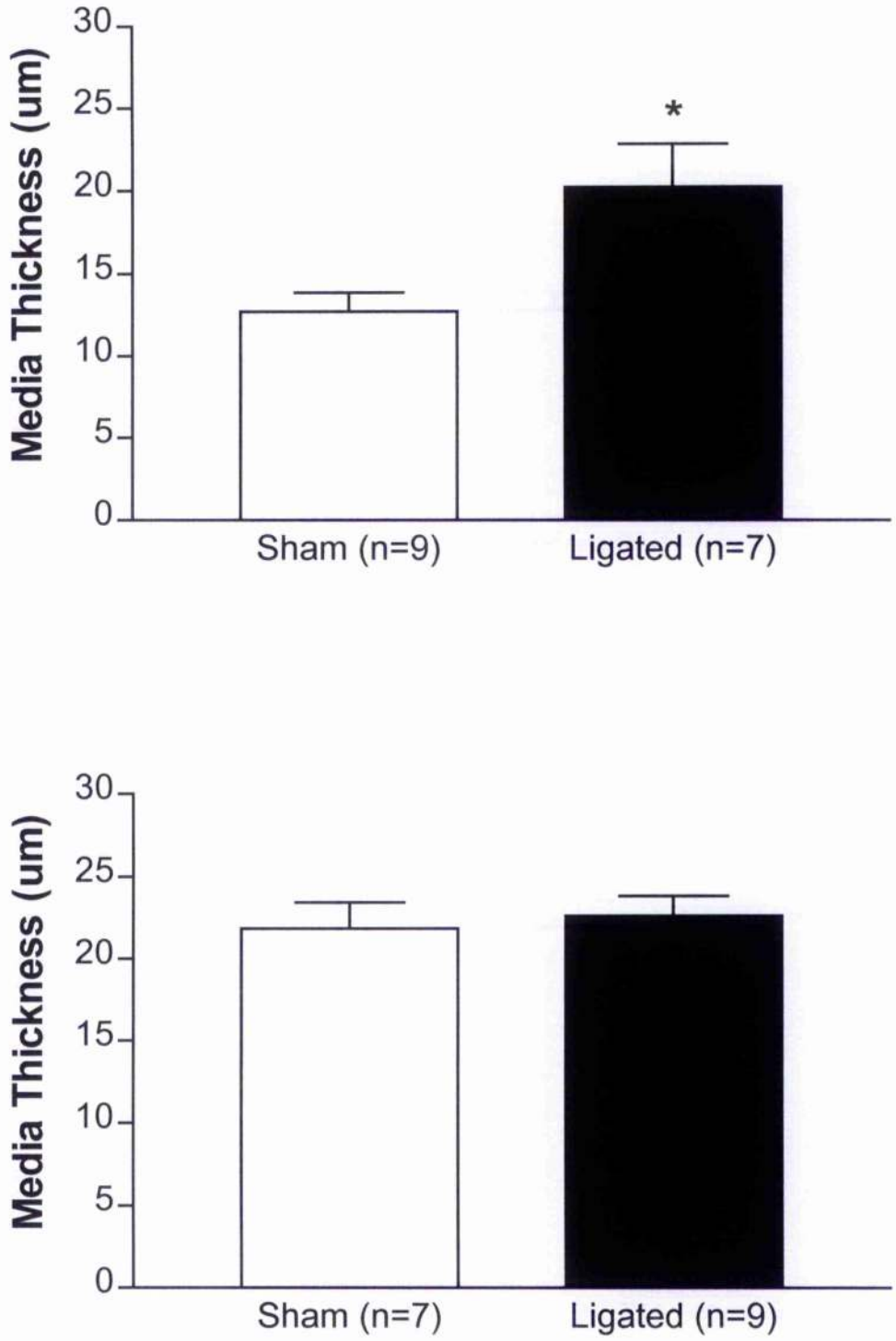

Figure 4.1 :- Thickness of the medial layer in arteries from heart failure models. Anterior cerebral arteries from the rabbit model of heart failure (top) and third order mesenteric arteries form the rat model of heart failure (bottom). Data is presented as mean ± s.e.m for the number of arteries indicated in brackets.

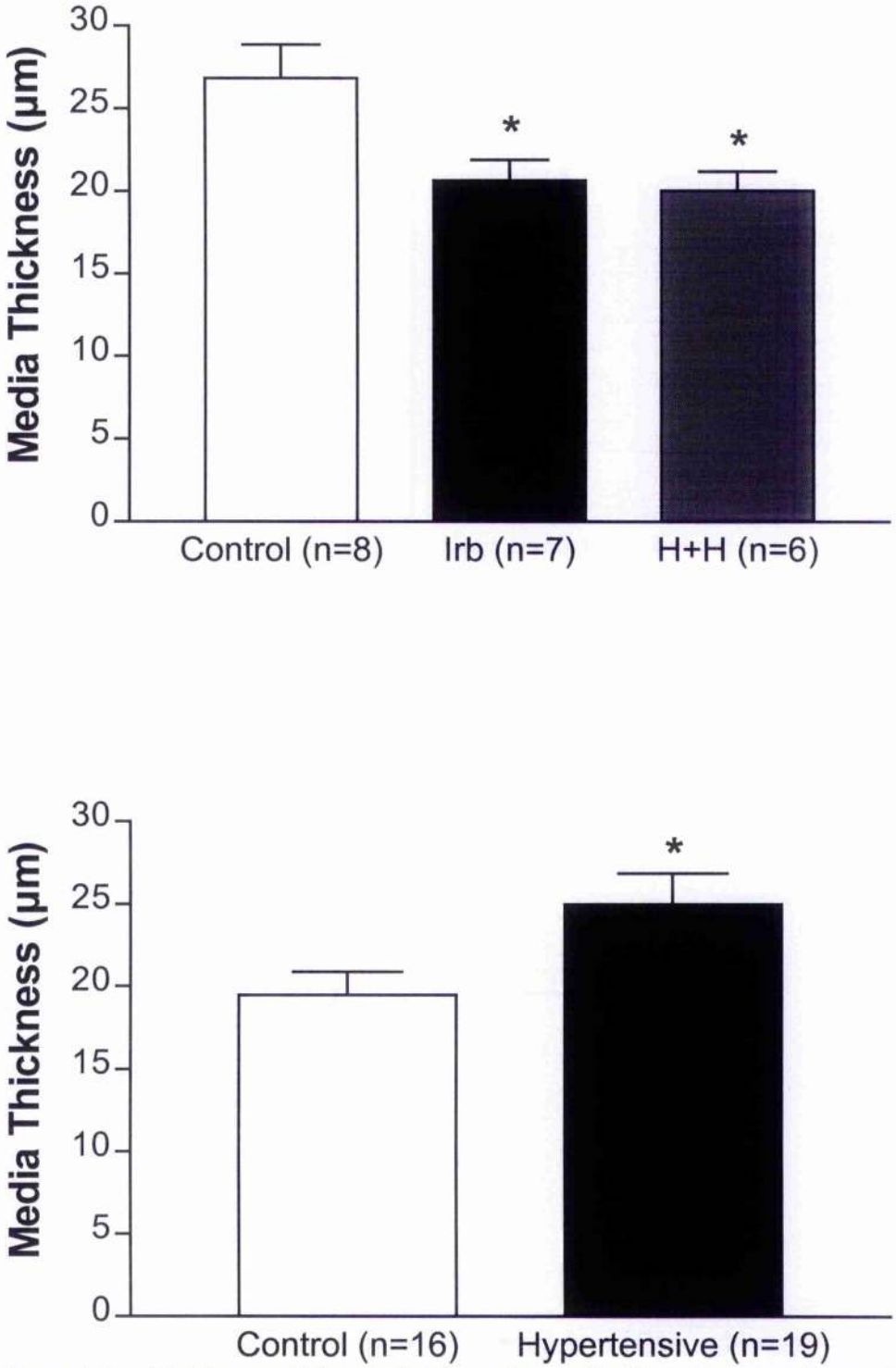

Figure 4.2 :- Thickness of the medial layer in arteries from hypertensive models. Third order mesenteric arteries from the hypertensive treatment with H+H or Irb (top) and the rat model of inducible hypertension (bottom). Data is presented as mean ± s.e.m for the number of arteries indicated in brackets.

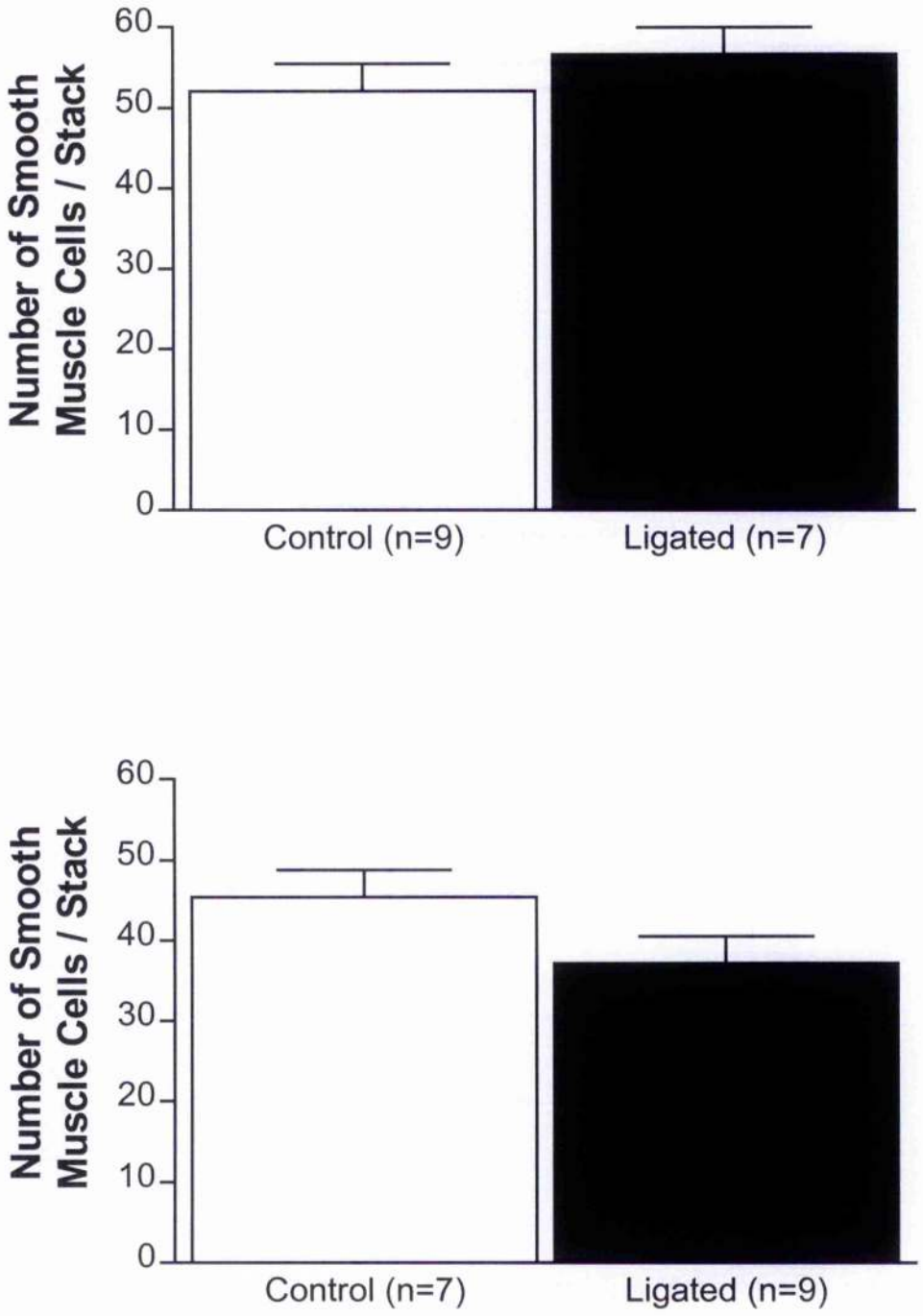

Figure 4.3 :- Number of Smooth Muscle Cells per stack in the medial layer in arteries from heart failure models. Anterior cerebral arteries from the rabbit model of heart failure (top) and third order mesenteric arteries form the rat model of heart failure (bottom). Data is presented as mean ± s.e.m for the number of arteries indicated in brackets.

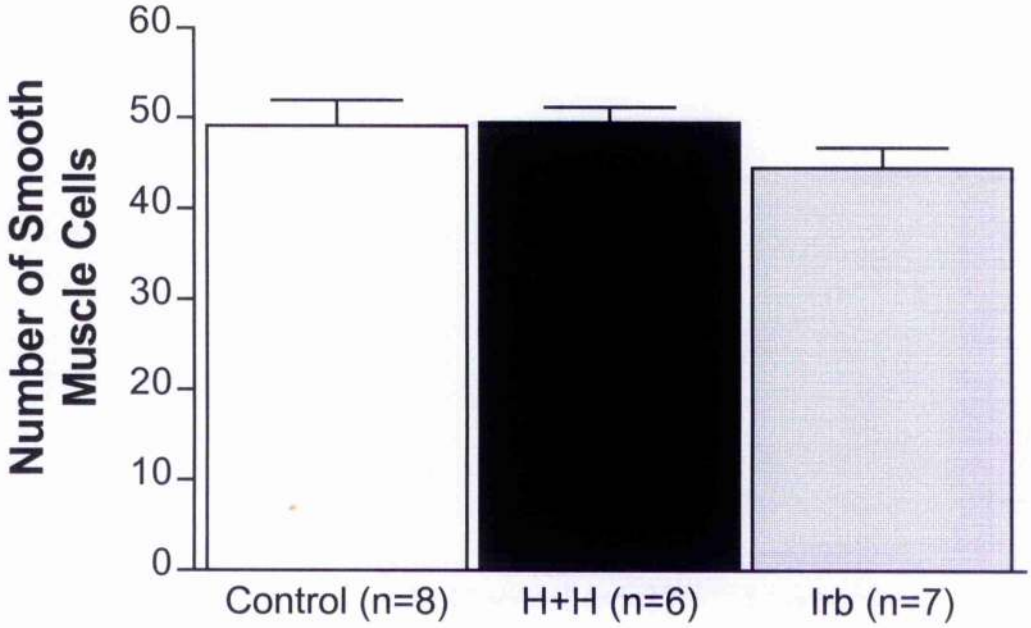

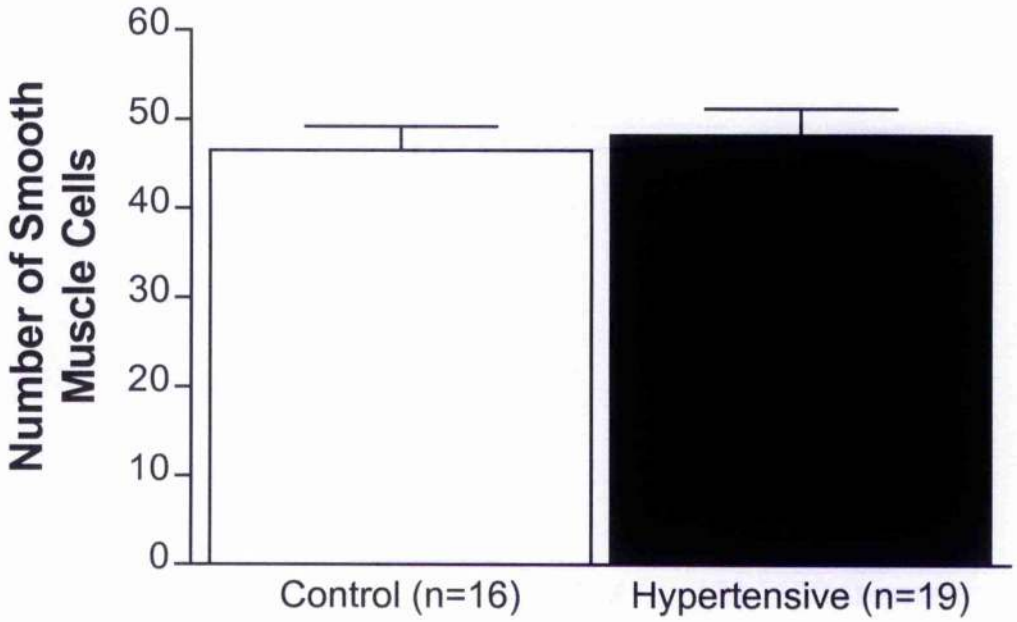

Figure 4.4 :- Number of smooth muscle cells per stack of the medial layer in arteries from hypertensive models. Third order mesenteric arteries from the hypertensive treatment with H+H or Irb(top) and the rat model of inducible hypertension (bottom). Data is presented as mean ± s.e.m for the number of arteries indicated in brackets.

4.4 Estimation of Smooth Muscle Cell Density

Using measurements of medial thickness and cell number we were able to calculate the density of SMC's as the number of SMC's per mm^3. The anterior cerebral arteries in the rabbit model of heart failure and mesenteric arteries from both the rat model of heart failure and inducible hypertension showed a decrease in the density of SMC's per mm^3. The only group observed which showed an increase was in the H–H treated hypertensive rats.

	Control	Exp. Group 1	Exp. Group 2
Rabbit ACA	415.3±48.3	285.4±25.1*	-
Rat HF	215.4±13.1	168.9±9.1**	-
Vasodilator Study	179.9±14.3	238.7±13.8†	218.6±18.7
Rat Induced Hypertension	246.6±18.6	199.3±10.7#	-

Table 4.2 :- Smooth Muscle Cell Density (Thousand cells / 1 mm length ± SEM).
* $p < 0.05$ Control v Ligated; ** $p<0.005$ Control v Ligated, † $p<0.05$ Control V H+H, # $p<0.05$ Control v Hypertensive

4.5 Estimation of the Total Number of Smooth Muscle Cells

Within all the groups there was no difference in the total number of smooth muscle cells within a 1mm length of the arterial wall.

	Control	Exp. Group 1	Exp. Group 2
Rabbit ACA	5868.83±800.88	8257.15±842.17	-
Rat HF	3185.74±308.57	2448.76±269.75	-
Vasodilator Study	3435.70±259.56	3041.31±265.14	3040.80±201.03
Rat Induced Hypertension	4659.59±423.90	4994.16±369.78	-

Table 4.3 :- Total Number of Smooth Muscle Cells in 1 mm^3 volume of arterial wall (total number of cells / 1mm length of wall ± SEM).

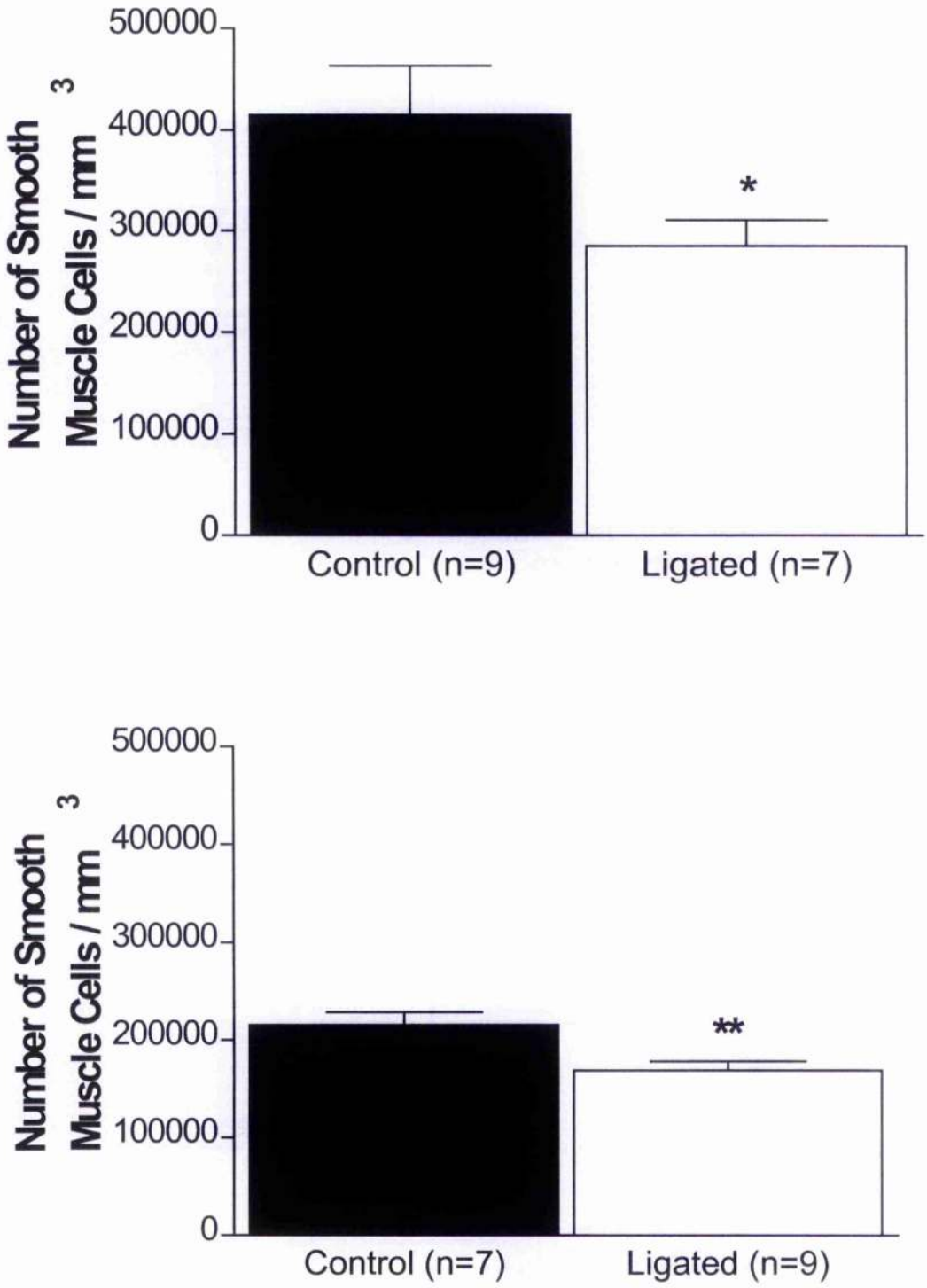

Figure 4.5 :- Density of Smooth Muscle Cells in the medial layer in arteries from heart failure models. Anterior cerebral arteries from the rabbit model of heart failure (top) and third order mesenteric arteries form the rat model of heart failure (bottom). Data is presented as mean ± s.e.m for the number of arteries indicated in brackets.

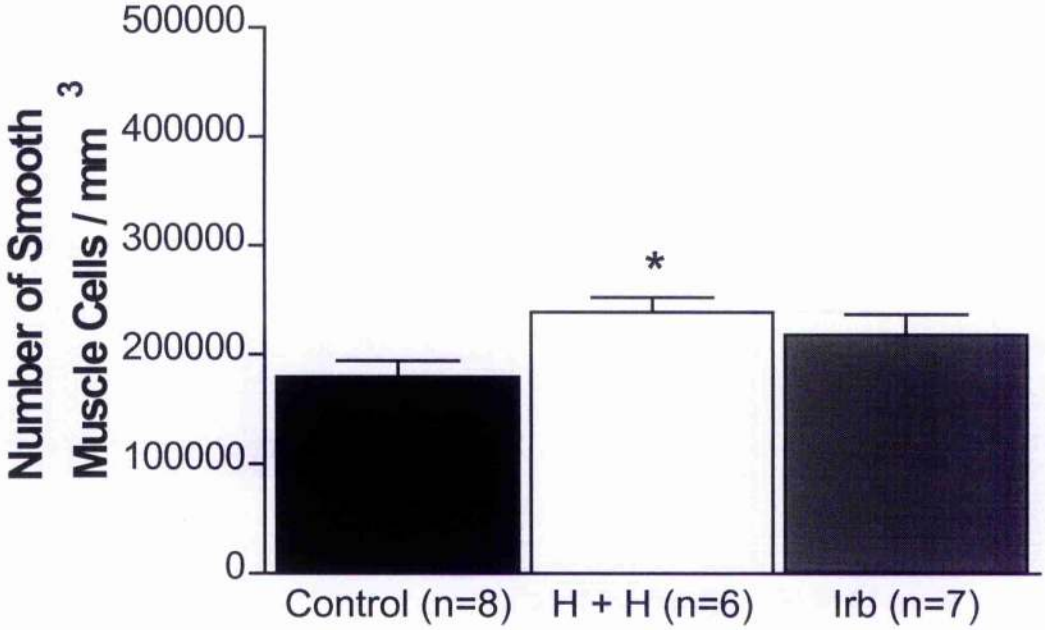

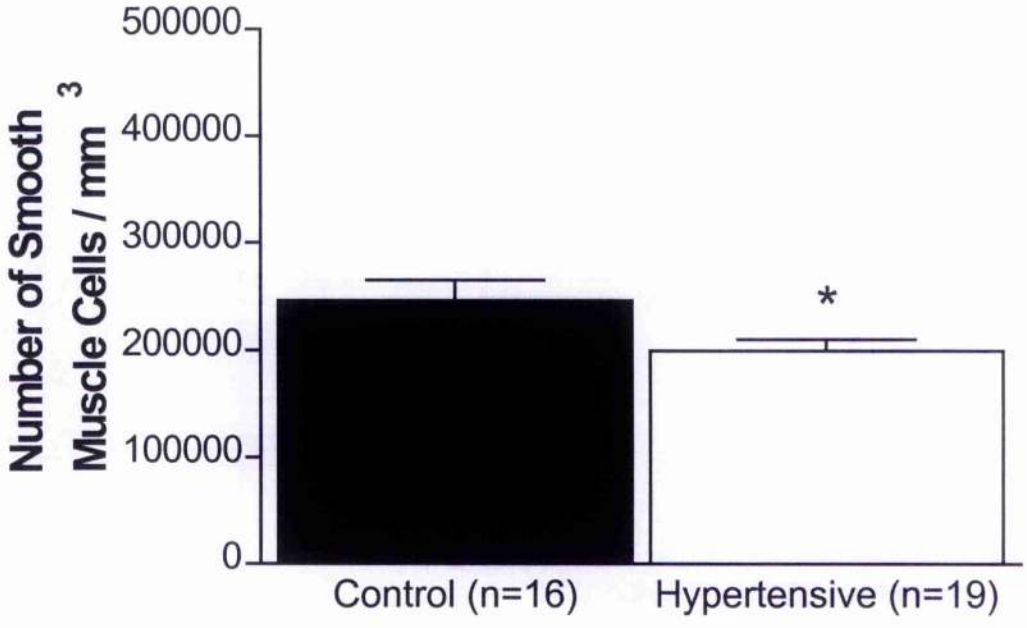

Figure 4.6 :- Density of smooth muscle cells of the medial layer in arteries from hypertensive models. Third order mesenteric arteries from the hypertensive treatment with H+H or Irb(top) and the rat model of inducible hypertension (bottom). Data is presented as mean ± s.e.m for the number of arteries indicated in brackets.

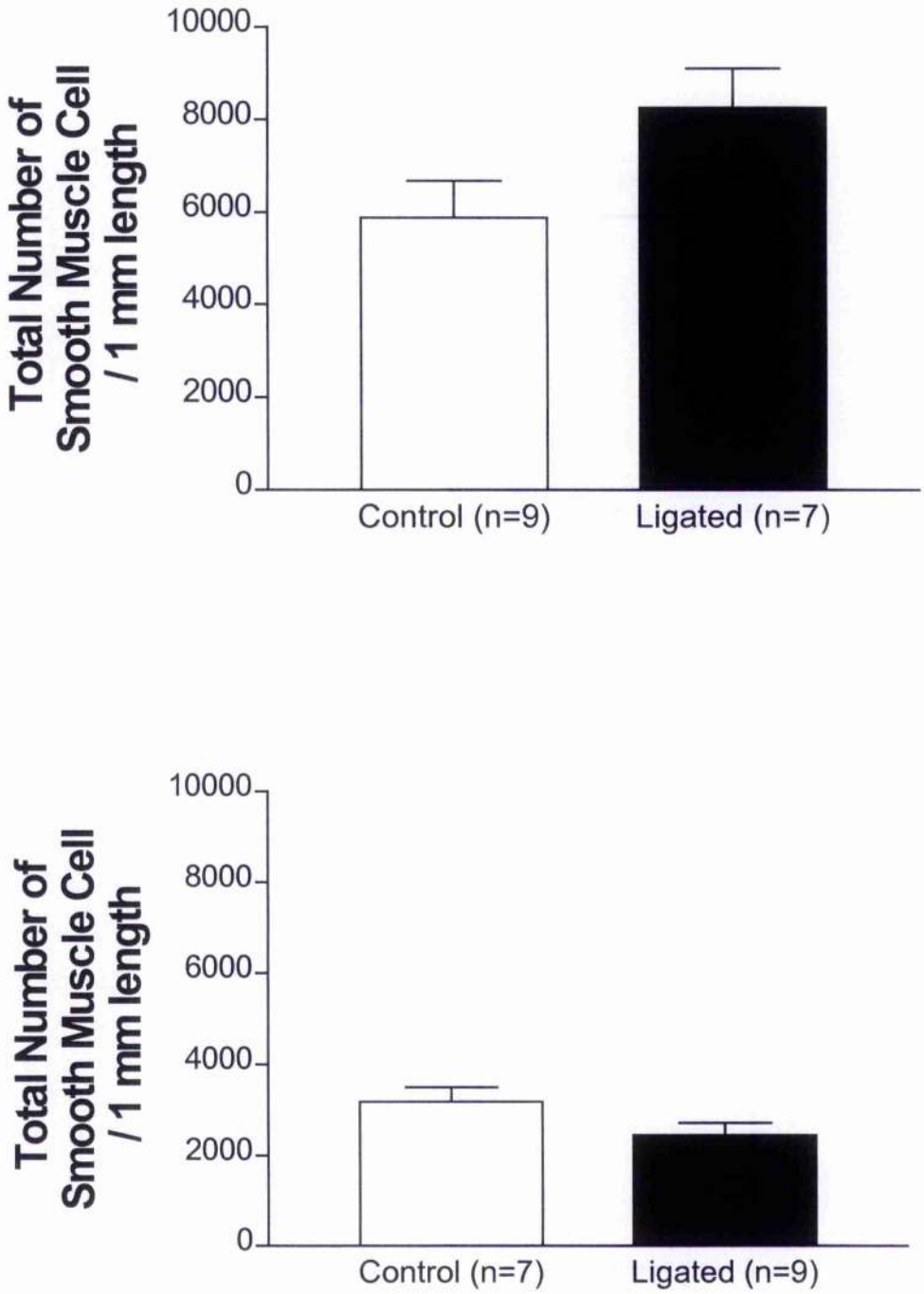

Figure 4.7 :- Total number of Smooth Muscle Cells per 1 mm length of medial layer in arteries from heart failure models. Anterior cerebral arteries from the rabbit model of heart failure (top) and third order mesenteric arteries form the rat model of heart failure (bottom). Data is presented as mean ± s.e.m for the number of arteries indicated in brackets.

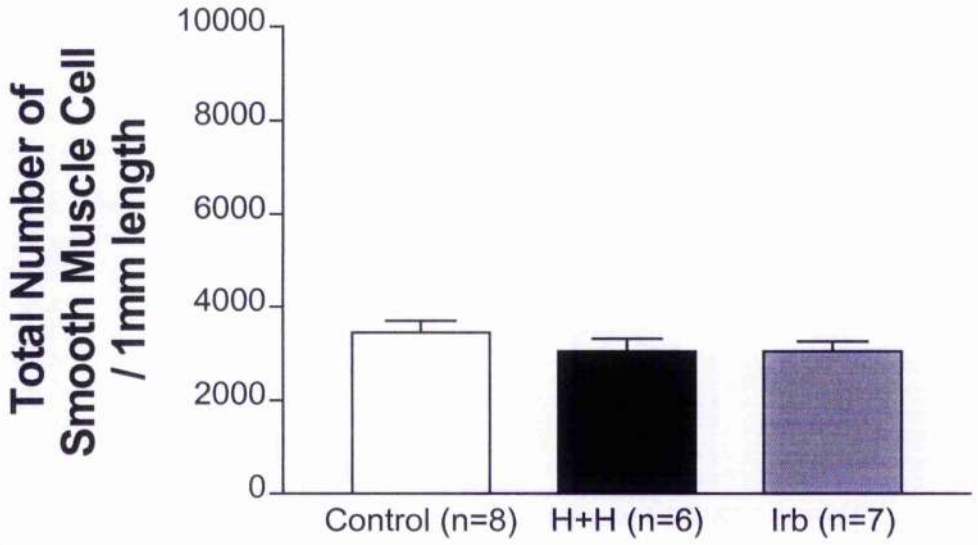

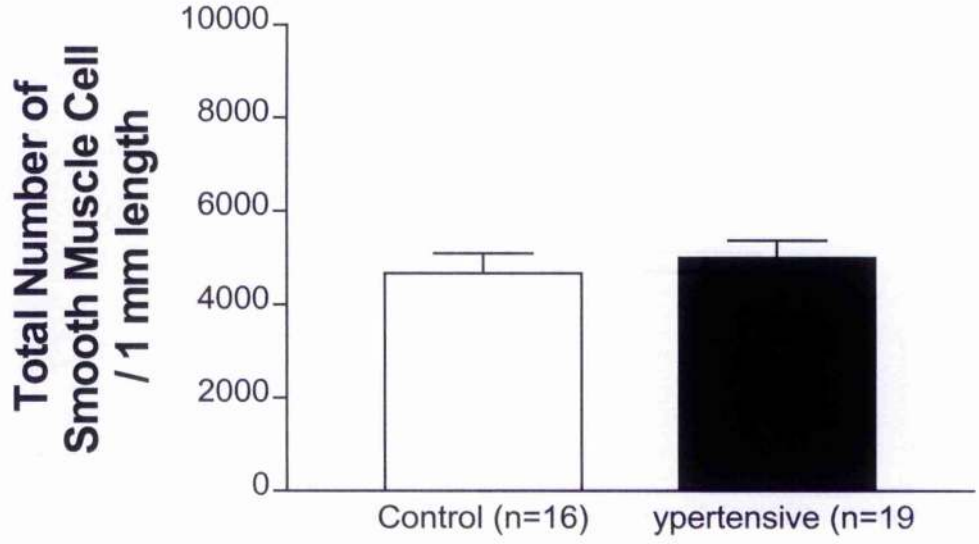

Figure 4.8 :- Total number of smooth muscle cells in 1mm length of medial layer in arteries from hypertensive models. Third order mesenteric arteries from the hypertensive treatment with H+H or Irb(top) and the rat model of inducible hypertension (bottom). Data is presented as mean ± s.e.m for the number of arteries indicated in brackets.

4.6 Measurement of the Collagen Content within the Tunic Media of Coronary artery Ligated Rabbits

The collagen component within the carotid arteries of the ligated rabbits was not changed although there was a significant reduction in the area of the medial layer.

	Total Media Area (μm^2)	Collagen content medial layer (%)
Control (n=8)	7527.92 ±183.72	76.9 ±0.87
Ligated (n=9)	6494.01 ± 169.29 ***	78.06 ± 0.94

Table 4.4 :- Collagen content within the tunica media of carotid arteries from control and ligated rabbit in a model of heart failure. Student's T-Test, *** $p<0.001$

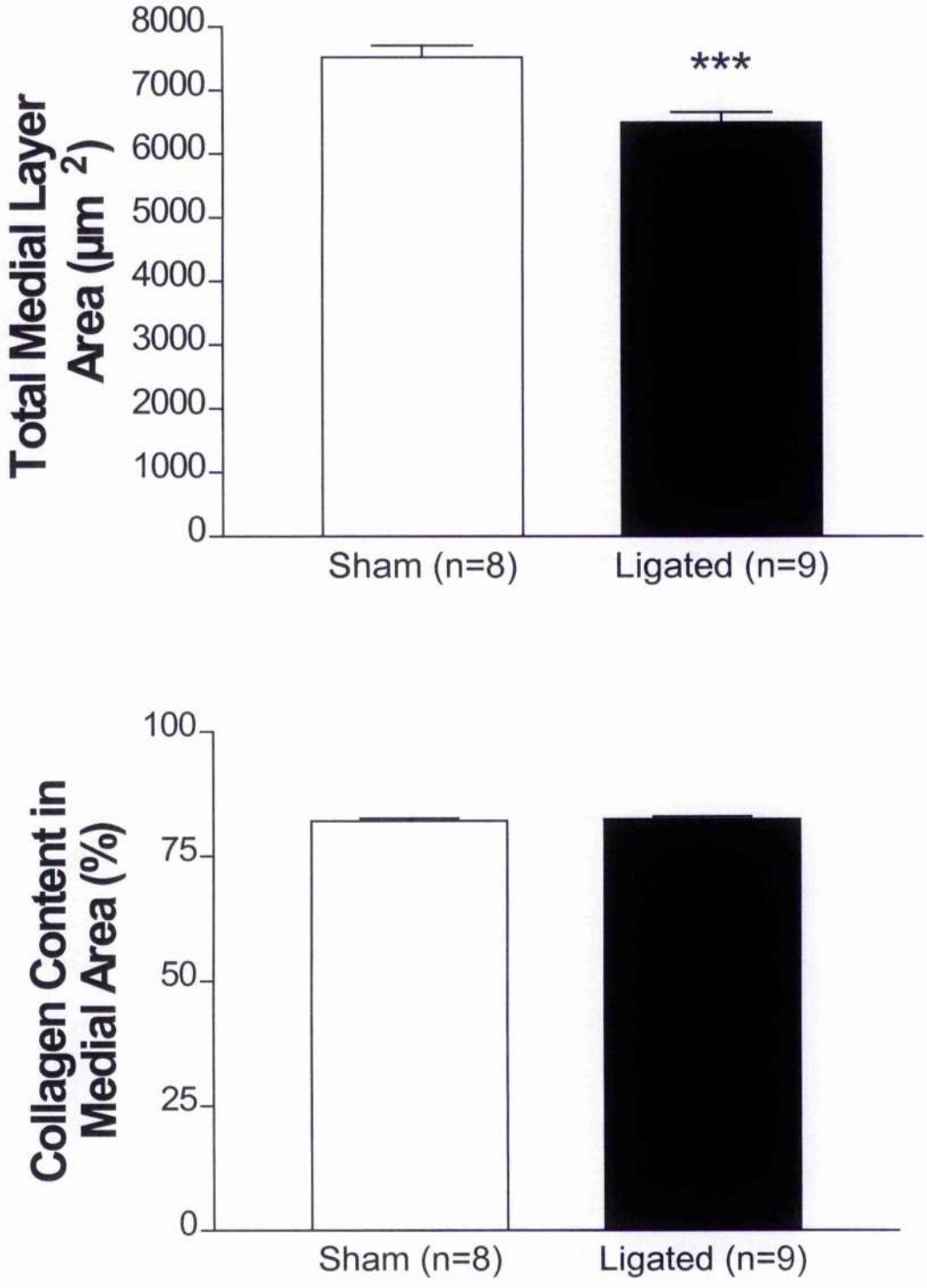

Figure 4.9 :- Parameters calculated from histological images obtained from rabbit carotid arteries. Total medial area (top) within the section was calculated and from this the percentage collagen content obtained from picosirius red staining was measured (bottom).

4.7 Collagen Staining in the Rabbit Carotid Artery

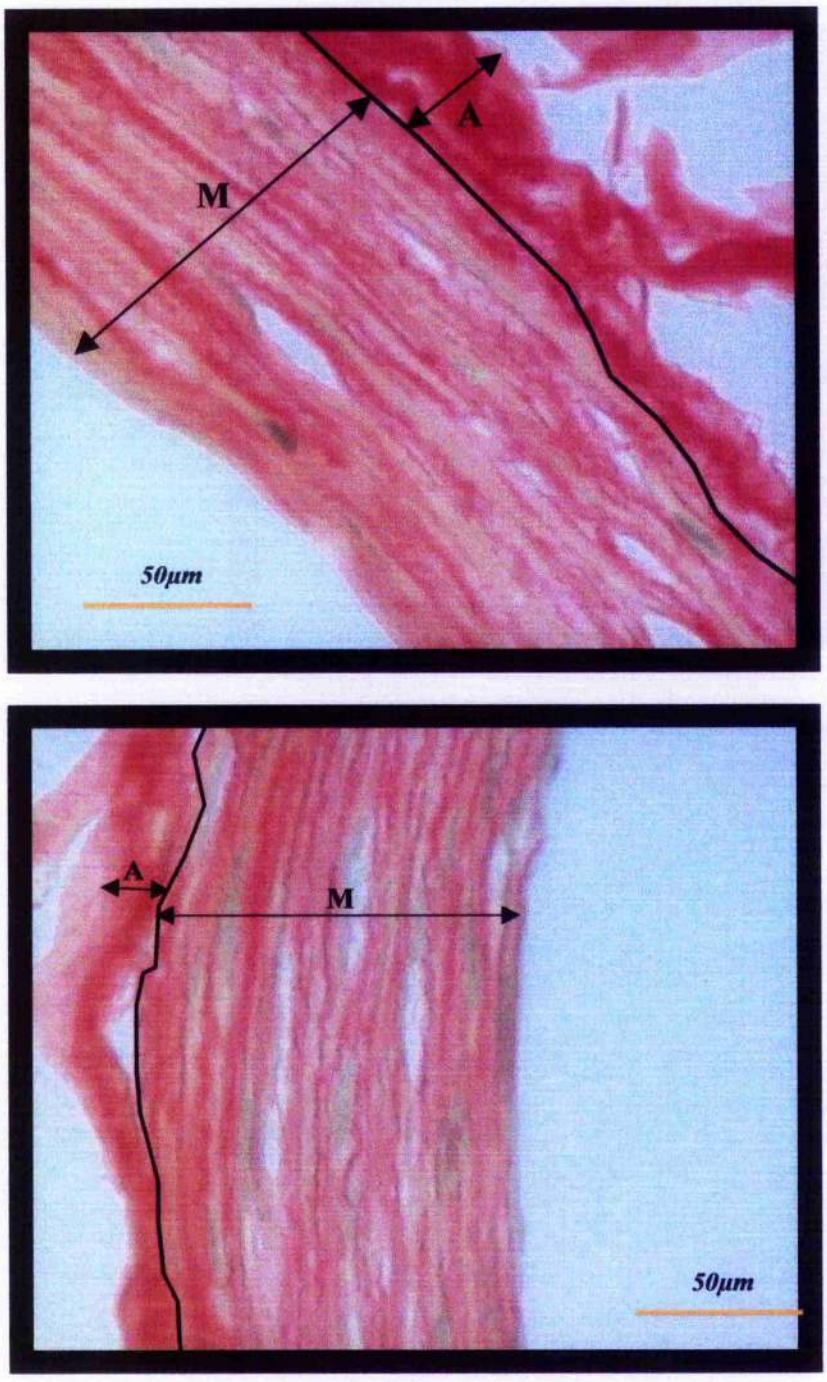

Figure 4.9 Histological images obtained from Sham (top) and Ligated (bottom) rabbit carotid arteries stained with picosirius red for collagen. The adventitial-medial border is marked thus allowing the software to distinguish between both layers for the purpose of calculations. The adventitial layer (A) is the smaller outermost area of the section whereas the medial layer (M) comprises the majority of the image.

4.8 Smooth Muscle Cell Nuclei Characteristics

From measurements made of the nuclei in the Anterior Cerebral Arteries of control and heart failure rabbits it can be seen that although the length and breadth of the nuclei were not significantly different the area that these structures covered changed significantly. The nuclei from control ACA smooth muscle cells were 5.4±0.17 μm wide with a length of 24.34±0.35 μm long whereas in the ligated rabbits the smooth muscle cell nuclei were 5.84±0.18 μm wide and 25.42±0.51 μm long. The area of the same nuclei was 385.71±11.54 μm^2 in the controls versus 451.45±15.74 μm^2 in the ligated and the perimeter of the smooth muscle cell nuclei also significantly increased in the ligated from 51.78±0.73 in the controls to 54.52±1.02 μm in the ligated.

		Width (μm)	Length (μm)	Area (μm2)	Perimeter (μm)
Control	**Mean**	5.4	24.34	385.71	51.78
	SD	1.33	2.74	89.37	5.68
	SEM	0.17	0.35	11.54	0.73
Ligated	**Mean**	5.84	25.42	451.75	54.52
	SD	1.62	4.56	140.7	9.1
	SEM	0.18	0.51	15.74	1.02
	P value	0.093	0.153	0.002 **	0.042 *

Table 4.5 :- Parameters measured from smooth muscle cell nuclei from the anterior cerebral artery of control and ligated rabbits.

CHAPTER 5

Tunica Intima

Analysis of the Tunica Intima of Resistance Arteries using Laser Scanning Confocal Microscopy

5.1 Intimal Characteristics

Endothelial cells are regular in shape and dispersed throughout the inner layer of the arterial wall. Staining with Propidium Iodide allows us to visualise the location and number of cells within the intimal layer.

5.2 Measurement of Intimal Thickness

Intimal thicknesses were measured directly from confocal images using the previously decribed method. Changes were observed in the intimal thickness of SHRSP rats treated with H+H (SHRSP control 13.44 ± 0.96; H+H 10.06 ± 1.12). No other chages in intimal thickness were observed in any of the other models studied. Figure 5.5

	Control	Exp. Group 1	Exp. Group 2
Rabbit ACA	6.83±0.85	8.81±1.67	-
Rat HF	8.93±1.48	14.67±2.35	-
Vasodilator Study	13.44±0.96	10.06±1.12*	10.71±1.42
Rat Induced Hypertension	10.84±0.82	9.16±0.87	-

Table 5.1 :- Intimal Thickness (thickness ± SEM; * $p < 0.01$).

5.3 Estimation of the Endothelial Cell Number

The number of endothelial cells was expressed as the number of endothelial cells per mm^2 luminal surface area. No differences were seen in the number of endothelial cells per mm^2 in any of the experimental groups. (Figure 5.5)

	Control	Exp. Group 1	Exp. Group 2
Rabbit ACA	1950.91±105.48	1692.58±152.22	-
Rat HF	1273.54±122.26	1082.93±167.22	-
Vasodilator Study	1583.47±208.84	1492.91±117.9	1718.44±216.14
Rat Induced Hypertension	1234.11±72.51	1199.27±47.45	-

Table 5.2 :- Endothelial Cell Number (number ± SEM; * $p < 0.01$).

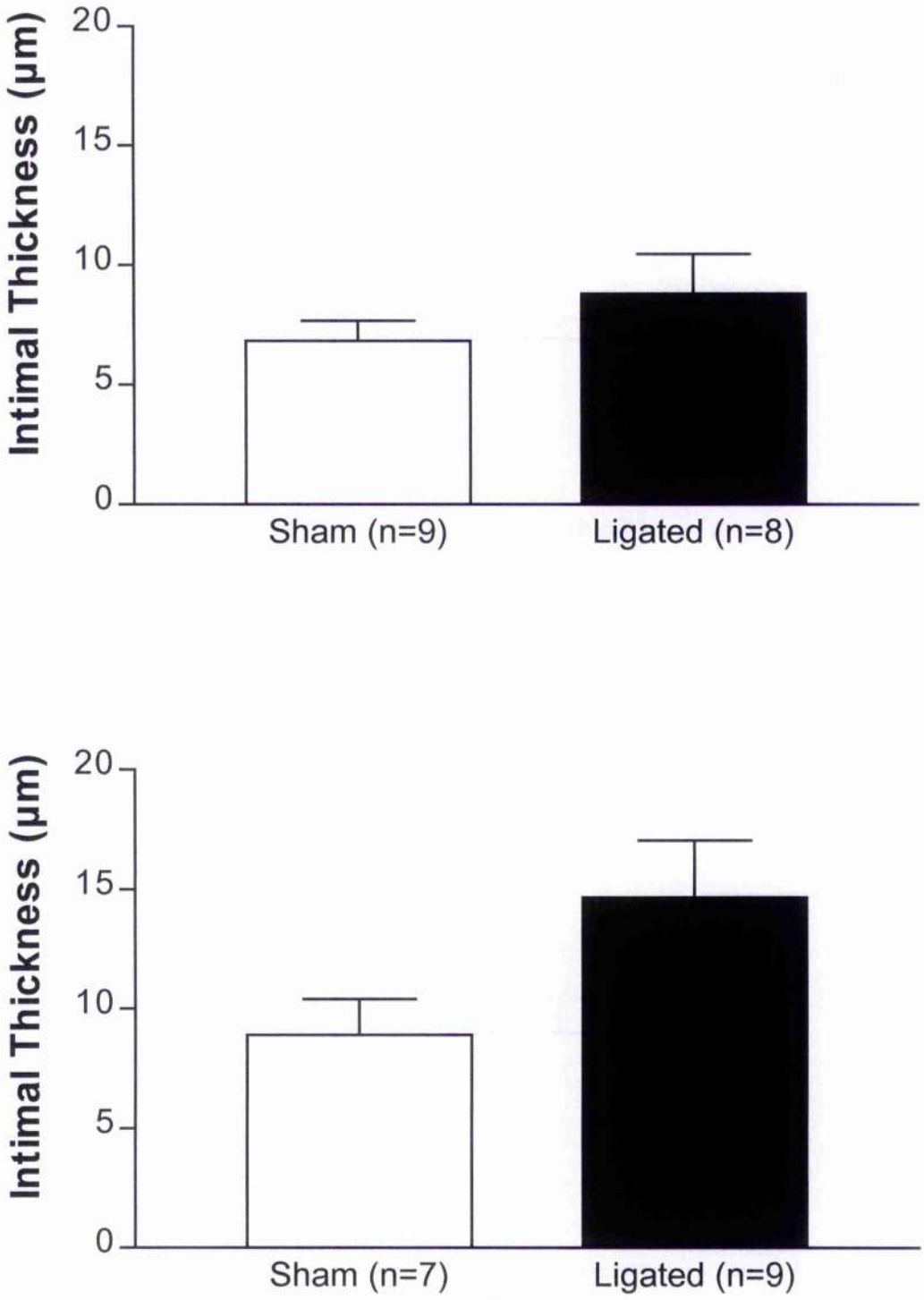

Figure 5.1 : - Thickness of the intimal layer in arteries from heart failure models. Anterior cerebral arteries from the rabbit model of heart failure (top) and third order mesenteric arteries from the rat model of heart failure (bottom). Data is presented as mean ± s.e.m for the number of arteries indicated in brackets.

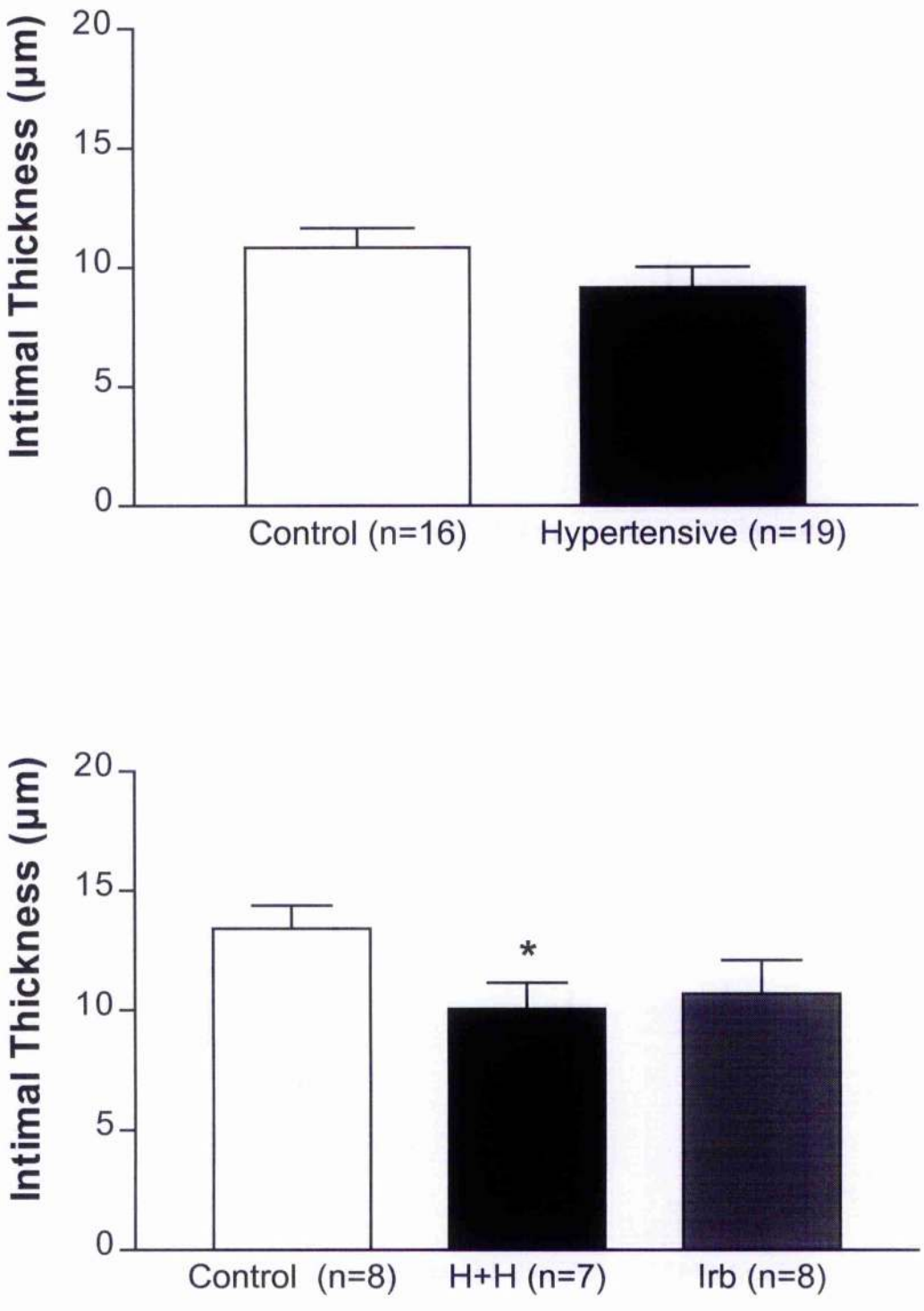

Figure 5.2 : - Thickness of the intimal layer in arteries from hypertensive models. Third order mesenteric arteries from hypertensive treatment with H+H or Irb (top) and the rat model of inducible hypertension (bottom). Data is presented as mean ± s.e.m for the number of arteries indicated in brackets. Students' T-Test * $p<0.05$

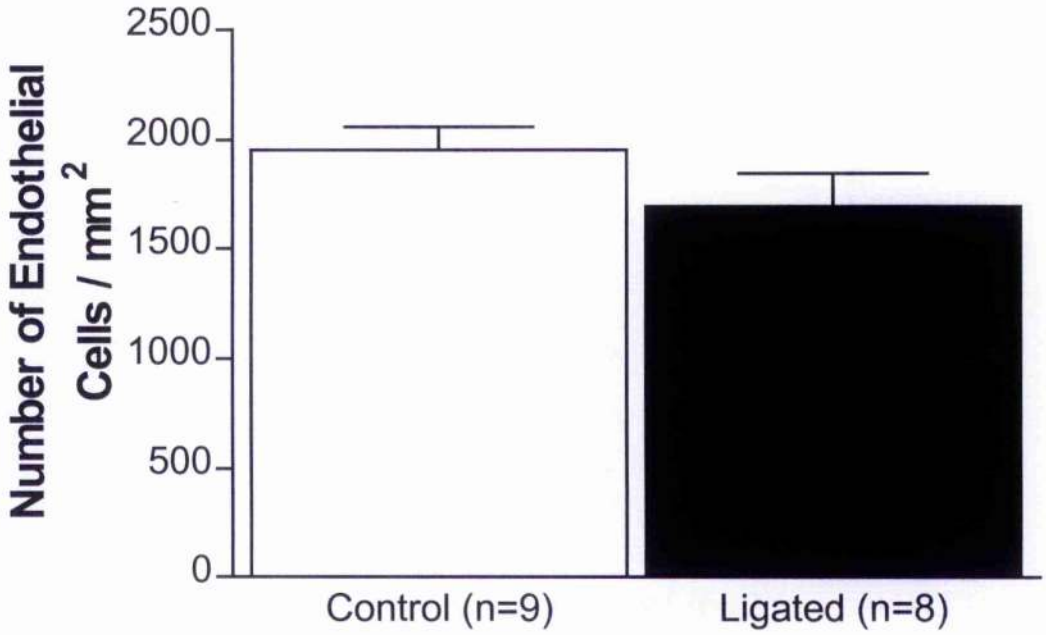

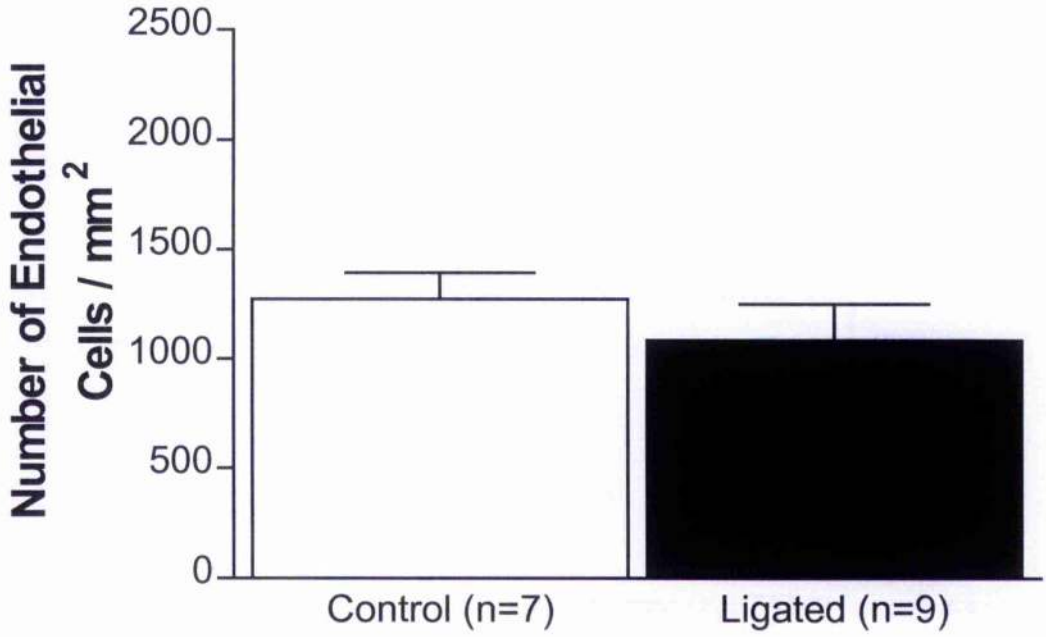

Figure 5.3 : - Number of endothelial cells/mm^2 in the intimal layer of arteries from heart failure models. Anterior cerebral arteries from the rabbit model of heart failure (top) and third order mesenteric arteries form the rat model of heart failure (bottom). Data is presented as mean ± s.e.m for the number of arteries indicated in brackets.

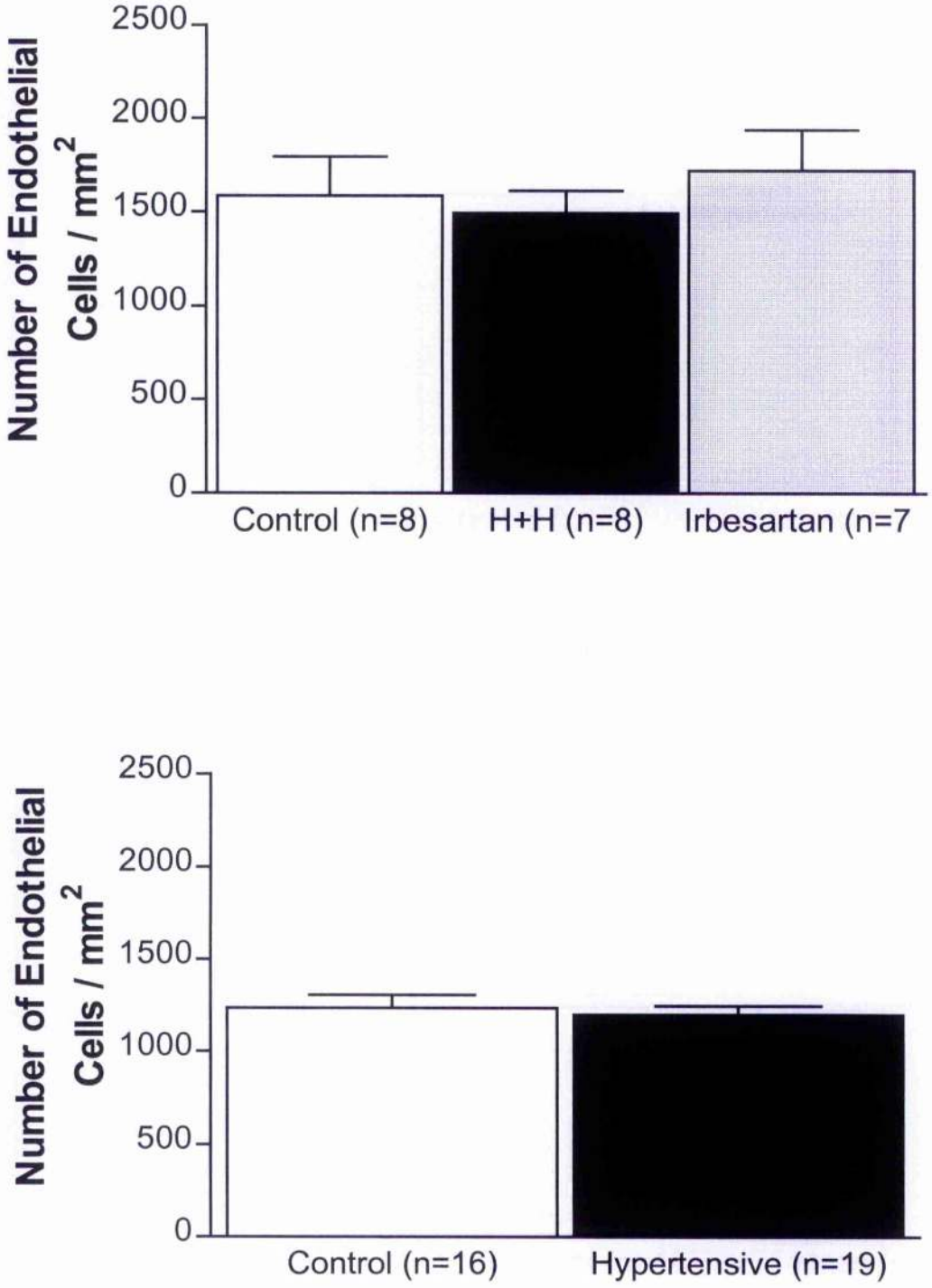

Figure 5.4 : - Number of endothelial cells/mm^2 in the intimal layer in arteries from hypertensive models. Third order mesenteric arteries from hypertensive treatment with H+H or Irb(top) and the rat model of inducible hypertension (bottom). Data is presented as mean ± s.e.m for the number of arteries indicated in brackets.

CHAPTER 6

General Analysis of the Morphological Characteristics of Resistance Arteries revealed by Laser Scanning Confocal Microscopy

General

6.1 Further Measurable Characteristics

Further analysis of the data collected from the tunicas adventitia, media and intima along with other measurements allows calculations to be made of various parameters other than those measured directly from the confocal images which may further describe blood vessel architecture.

6.2 Measurement of Lumen Diameter

Lumen diameter measurements were made directly from confocal images at 10 times magnification using the described method. The lumen diameter in the rabbit model of heart failure was the only model which showed a change. (Figure 6.1)

	Control	Exp. Group 1	Exp. Group 2
Rabbit ACA	343.15±33.08	445.99±25.44*	-
Rat HF	200.39±22.72	176.88±9.88	-
Vasodilator Study	181.24±13.32	160.00±15.14	184.85±10.76
Rat Induced Hypertension	280.31±13.55	292.64±13.07	-

Table 6.1 :- Lumen Diameter measurements (μm ± SEM, * $p<0.01$).

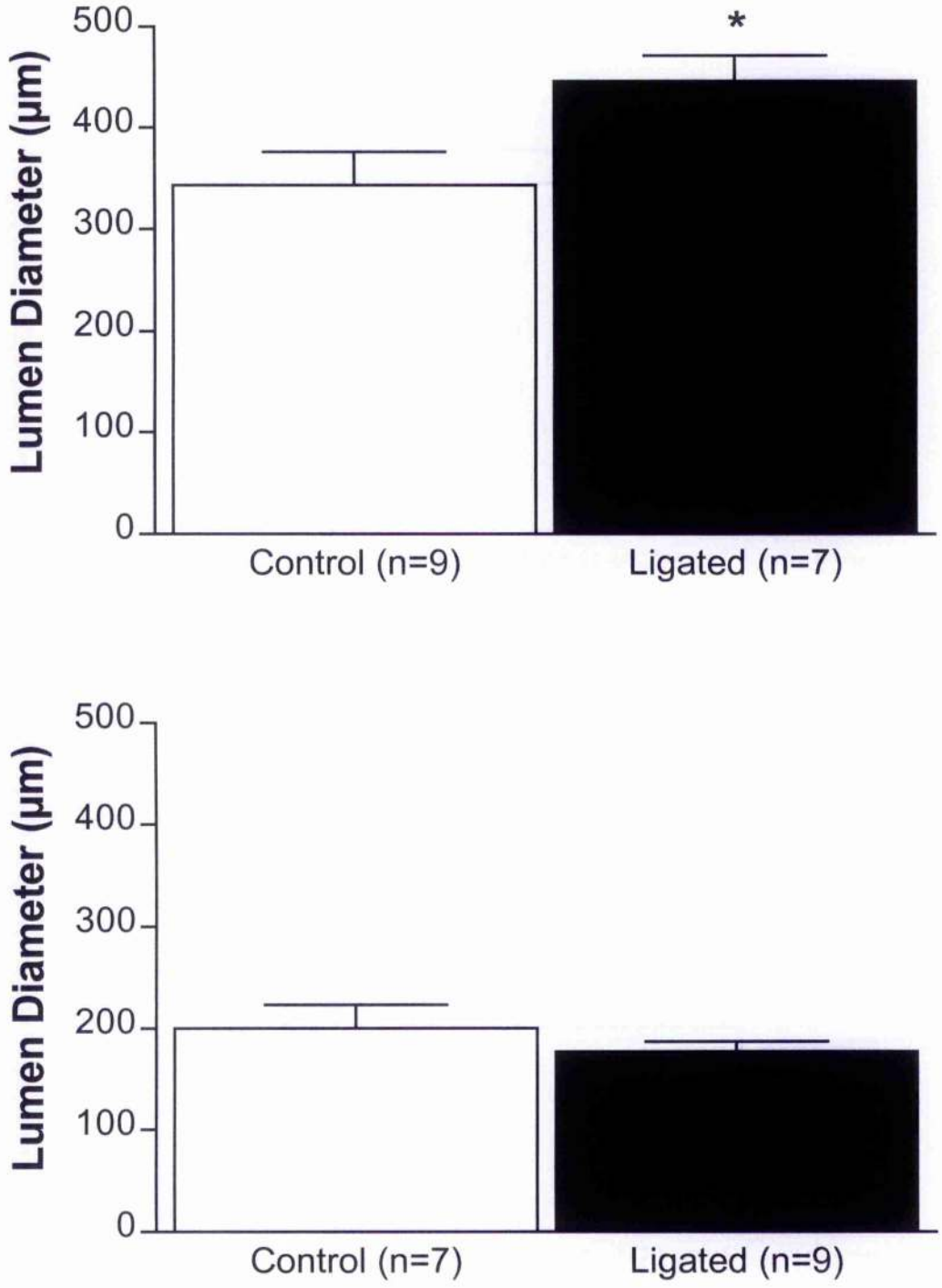

Figure 6.1 :- Lumen Diameter of arteries from heart failure models. Anterior cerebral arteries from the rabbit model of heart failure (top) and third order mesenteric arteries from the rat model of heart failure (bottom). Data is presented as mean ± s.e.m for the number of arteries indicated in brackets. Student's T-test * $p<0.05$

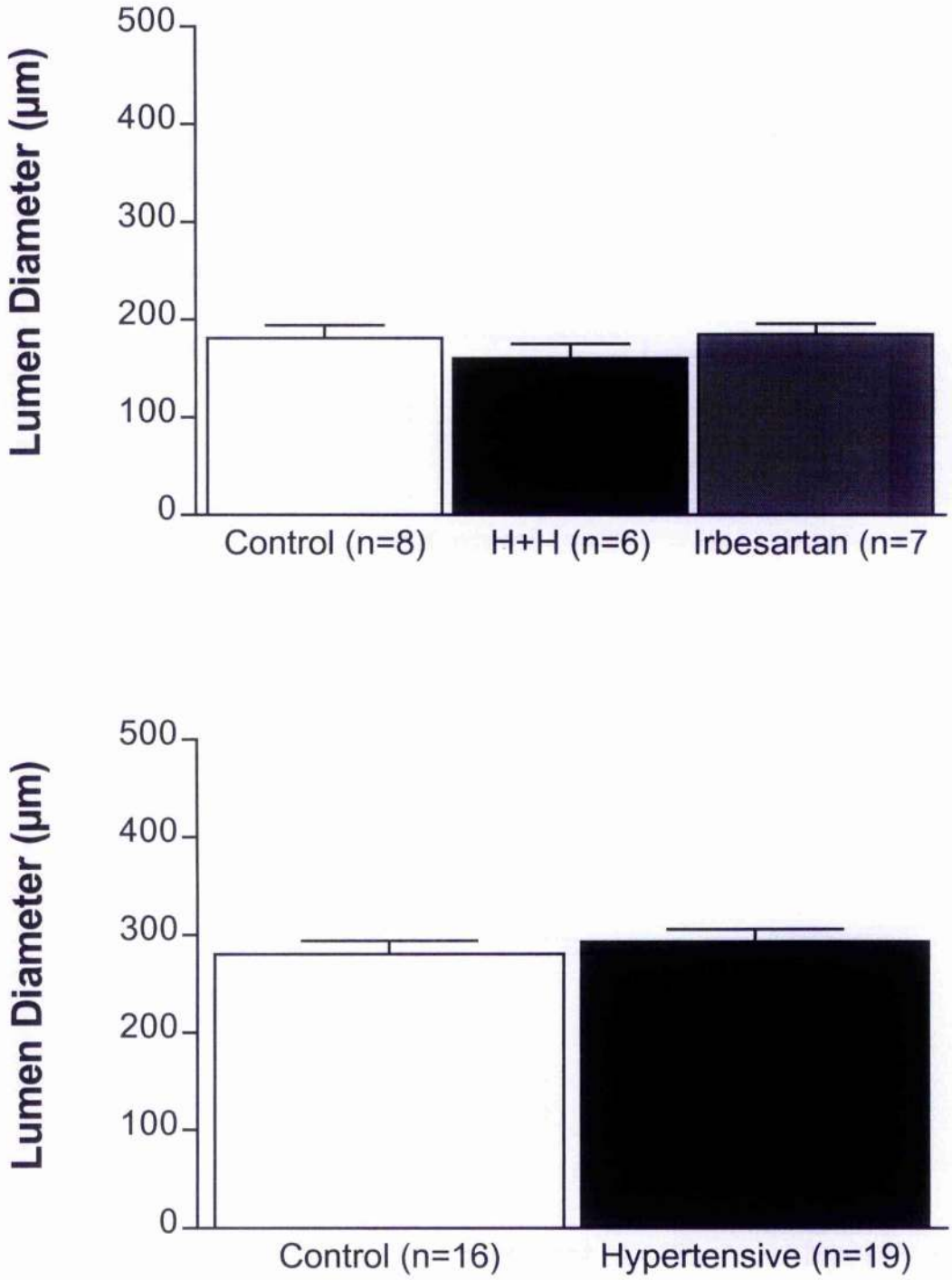

Figure 6.2 :- Lumen diameter of arteries from hypertensive models. Third order mesenteric arteries from hypertensive treatment with H+H or Irb (top) and the rat model of inducible hypertension (bottom). Data is presented as mean ± s.e.m for the number of arteries indicated in brackets.

6.3 Calculation of Wall : Lumen Ratio

Within the data measured there was no difference in the wall : lumen ratio in the experimental groups. (Figure 6.3)

	Control	Exp. Group 1	Exp. Group 2
Rabbit ACA	7.98±0.87	8.33±0.97	-
Rat HF	25.15±15	32.33±2.96	-
Vasodilator Study	30.98±3.64	29.40±2.95	23.81±2.41
Rat Induced Hypertension	17.17±1.35	18.97±1.44	-

Table 6.2 :- Wall : Lumen Ratio (% ± SEM).

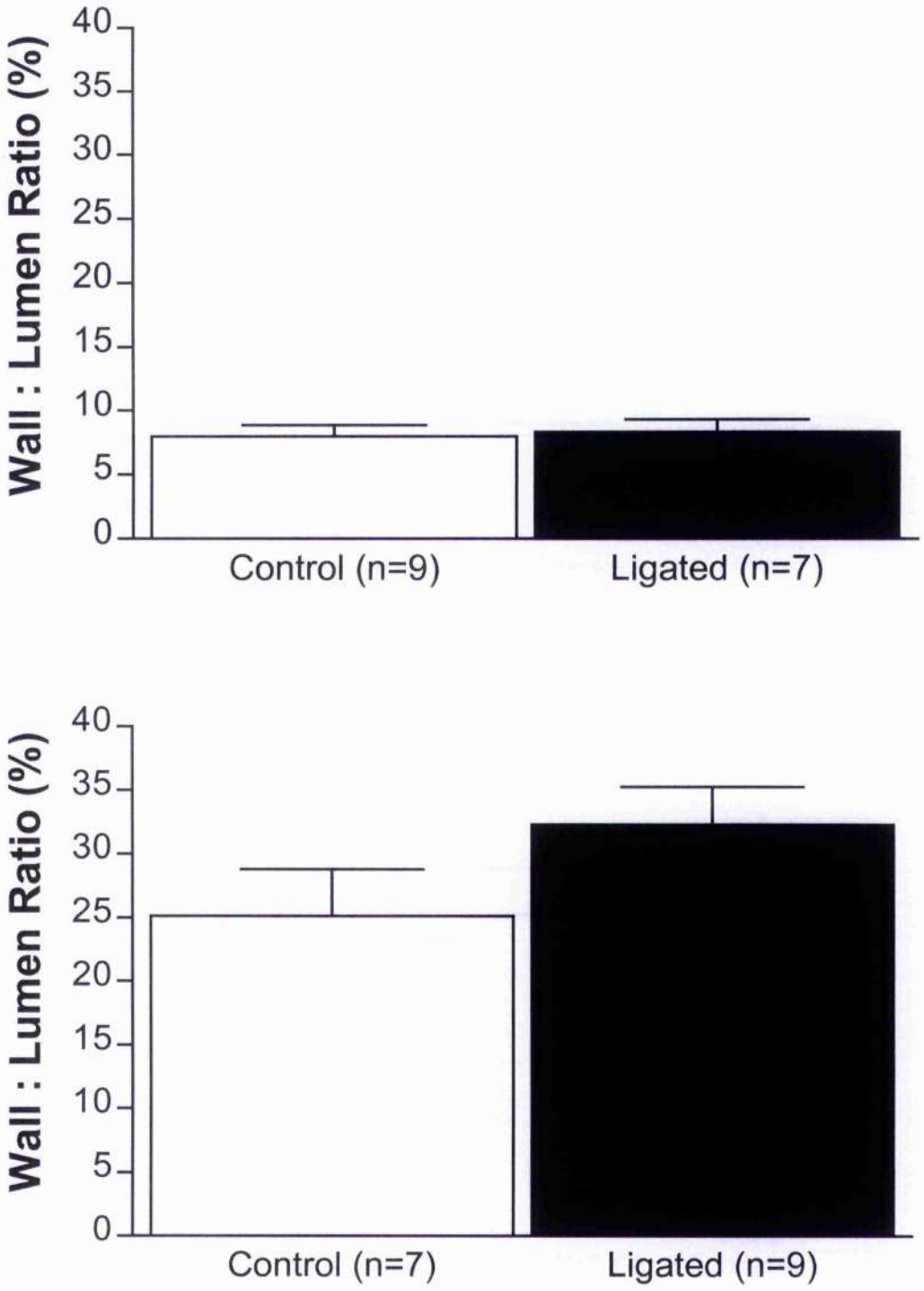

Figure 6.3 :- Wall : Lumen ratio of arteries from heart failure models. Anterior cerebral arteries from the rabbit model of heart failure (top) and third order mesenteric arteries from the rat model of heart failure (bottom). Data is presented as mean ± s.e.m for the number of arteries indicated in brackets.

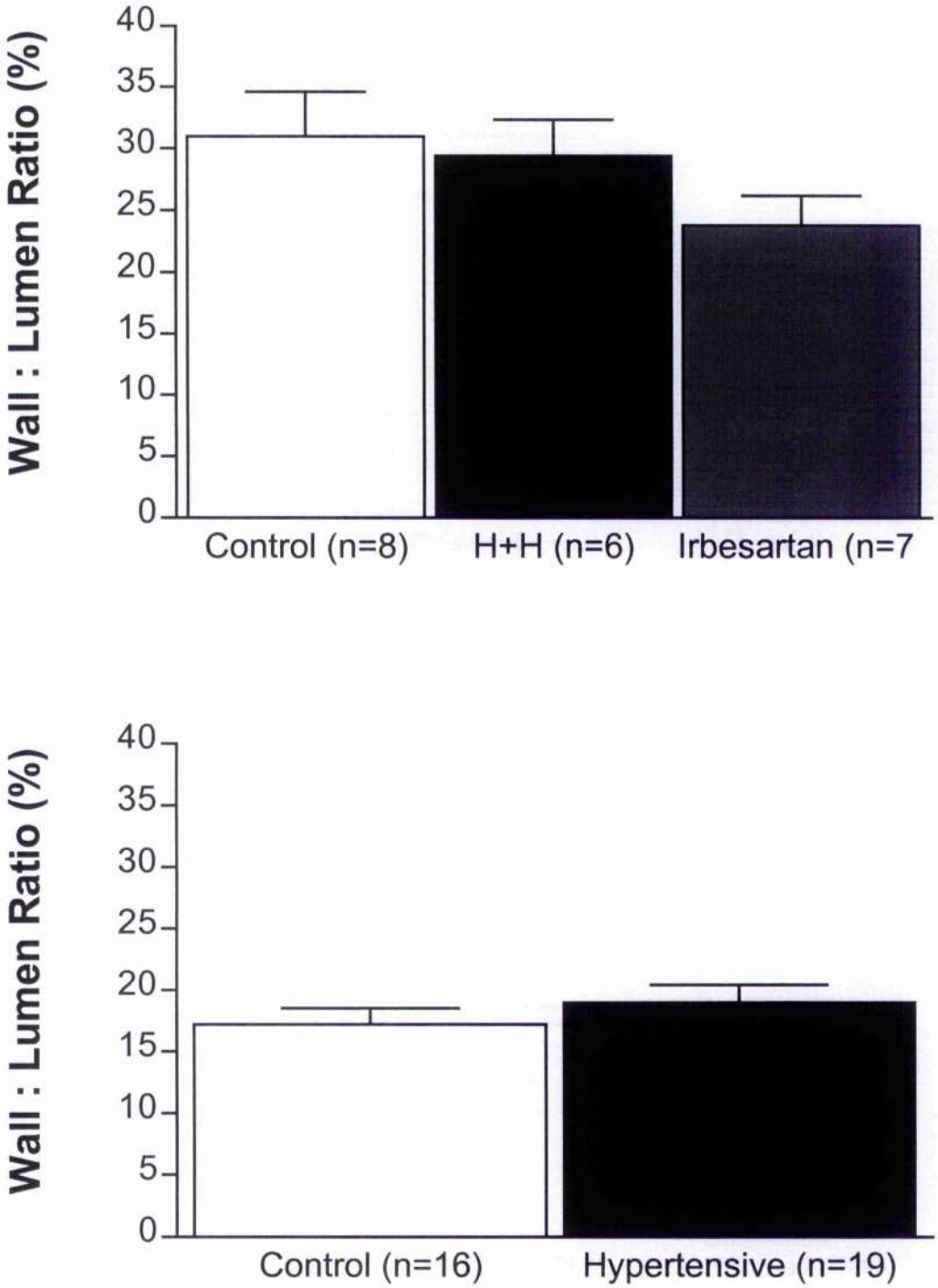

Figure 6.4 :- Wall : Lumen ratio of arteries from hypertensive models. Third order mesenteric arteries from hypertensive treatment with H+H or Irb (top) and the rat model of inducible hypertension (bottom). Data is presented as mean ± s.e.m for the number of arteries indicated in brackets.

6.4 Calculation of Wall Cross Sectional Area

Using measurements made of wall thickness and lumen diameter it was possible to calculate the wall cross sectional area. Anterior cerebral arteries from the rabbit model of heart failure showed an increase in the cross sectional area of the artery wall (Sham 29032.51 ± 2772.96, Ligated 55545.13 ± 8093.75**, $p < 0.005$) whereas mesenteric arteries from the rat model of H+H and Irb treated hypertension showed a decrease in the wall cross sectional area. (SHRSP 39146.13 ±2635.11, H+H 28728.58 ±3023.29*, Irb 30444.14 ± 2297.21*, $p < 0.01$). Other arteries showed no difference in the cross sectional area within their walls, (Figure 6.5)

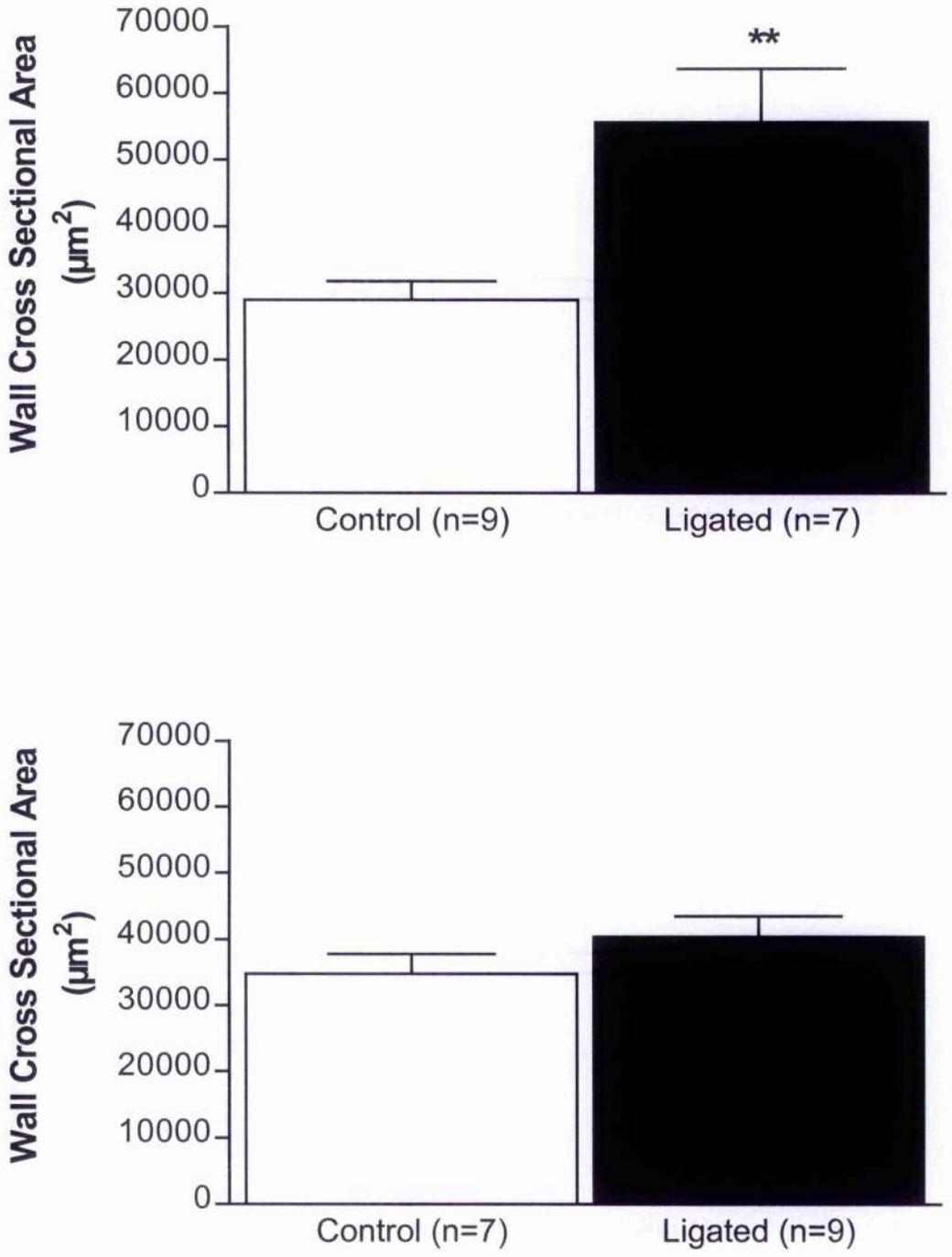

Figure 6.5 :- Wall cross sectional area of arteries from heart failure models. Anterior cerebral arteries from the rabbit model of heart failure (top) and third order mesenteric arteries from the rat model of heart failure (bottom). Data is presented as mean ± s.e.m for the number of arteries indicated in brackets.

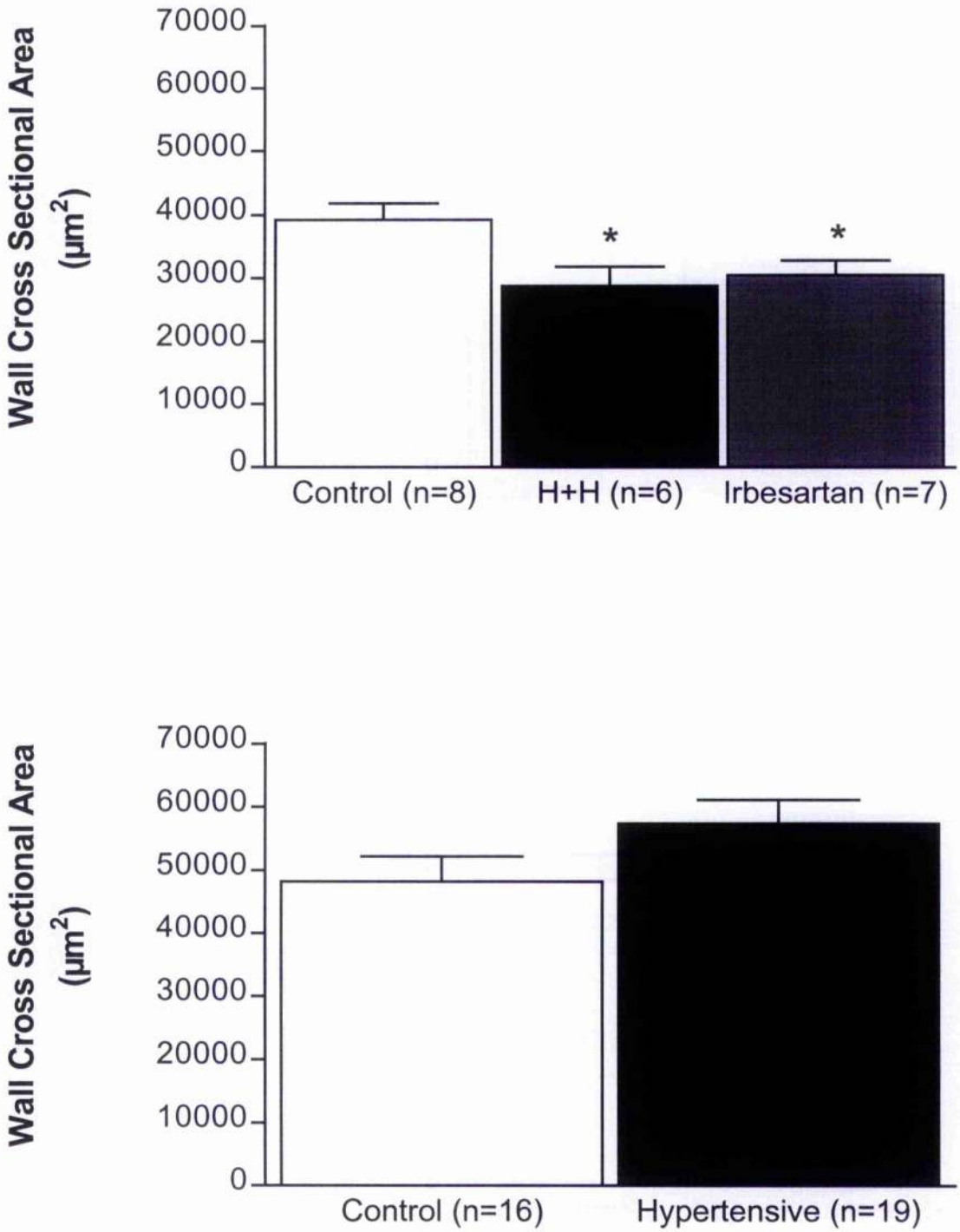

Figure 6.6 :- Wall cross sectional area of arteries from hypertensive models. Third order mesenteric arteries from hypertensive treatment with H+H or Irb (top) and the rat model of inducible hypertension (bottom). Data is presented as mean ± s.e.m for the number of arteries indicated in brackets.

6.5 Calculation of Media : Lumen Ratio

Within all the groups except in the inducible hypertension rat model there was no difference in the media : lumen ratio.

	Control	Exp. Group 1	Exp. Group 2
Rabbit ACA	3.96±0.44	4.57±0.56	-
Rat HF	11.85±1.55	13.14±1.11	-
Vasodilator Study	15.98±2.76	13.57±1.29	11.15±1.12
Rat Induced Hypertension	7.00±0.45	8.81±0.70*	-

Table 6.3 :- Media : Lumen Ratio (% ± SEM, * $p < 0.05$).

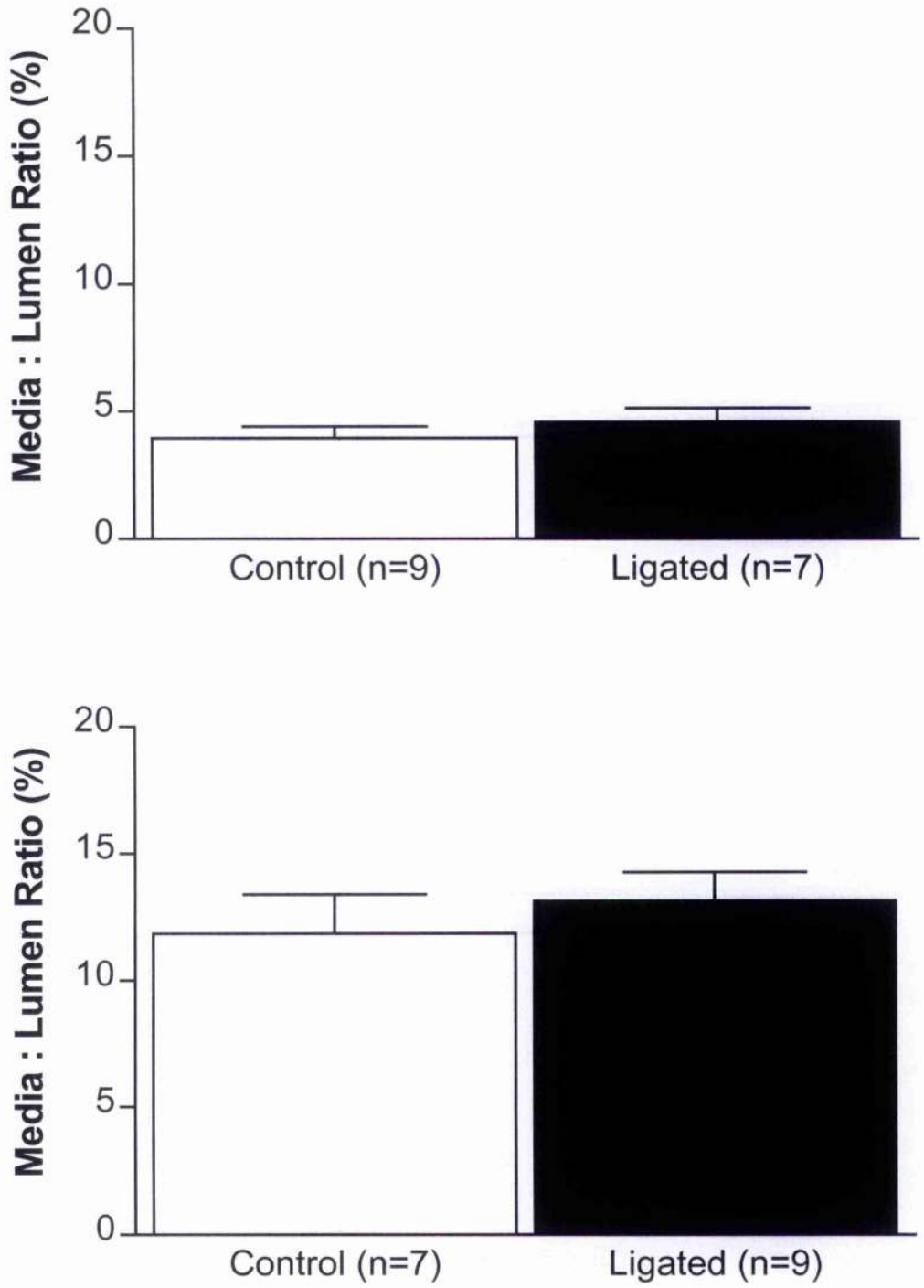

Figure 6.7 :- Media : Lumen ratio of arteries from heart failure models. Anterior cerebral arteries from the rabbit model of heart failure (top) and third order mesenteric arteries from the rat model of heart failure (bottom). Data is presented as mean ± s.e.m for the number of arteries indicated in brackets.

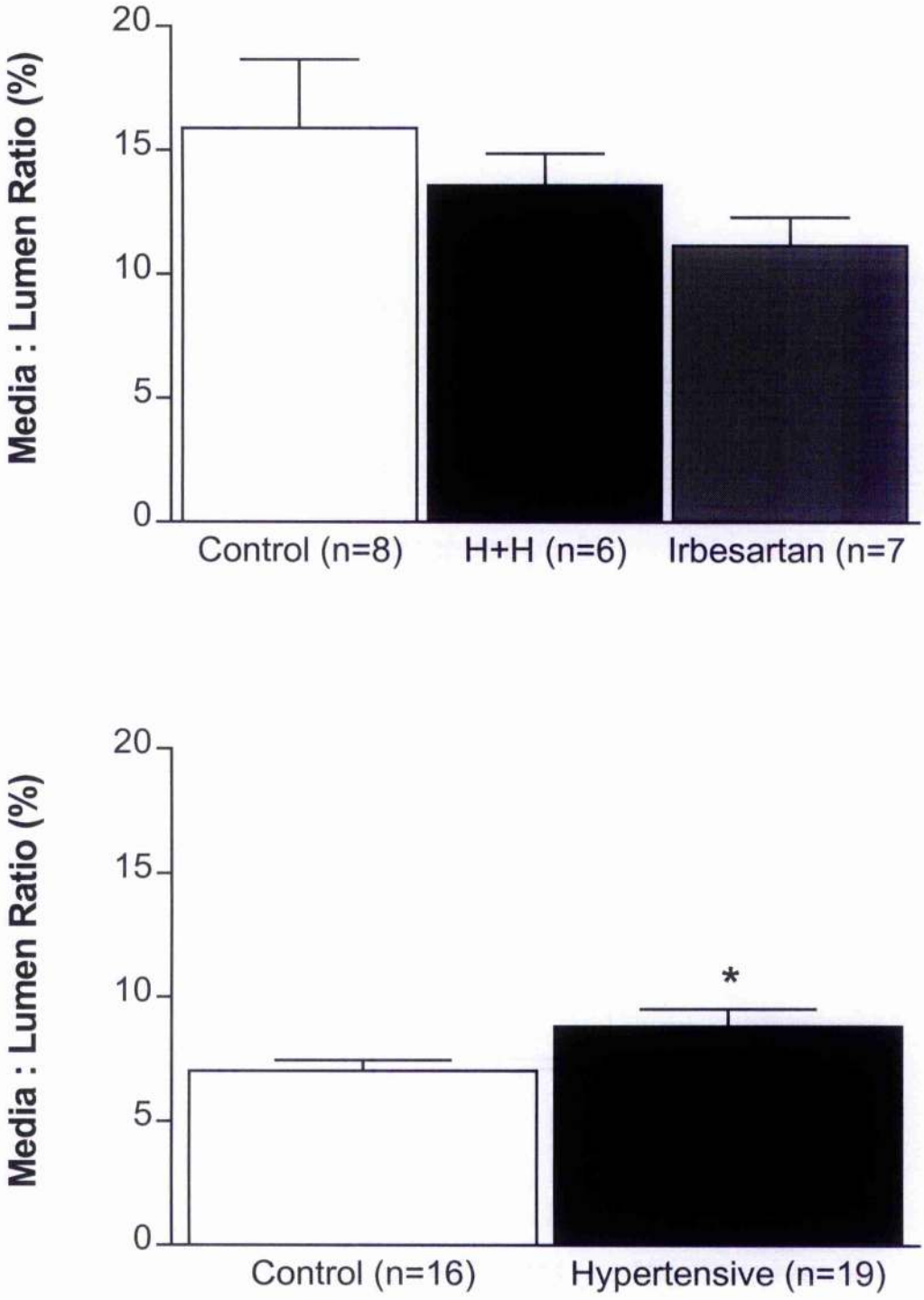

Figure 6.8 :- Media : Lumen ratio of arteries from hypertensive models. Third order mesenteric arteries from hypertensive treatment with H+H or Irb (top) and the rat model of inducible hypertension (bottom). Data is presented as mean ± s.e.m for the number of arteries indicated in brackets

6.6 Calculation of Media Cross Sectional Area

Similarly to wall cross sectional area by using the values obtained for the medial thickness it is possible to calculate the media cross sectional area. Increases in the media cross sectional area were observed in the rabbit model of heart failure and decreases in the rat model of hypertension treated with H+H or Irb but the other models used did not show any differences.

	Control	Exp. Group 1	Exp. Group 2
Rabbit ACA	14985.34±2256.52	31380.56±5496.05*	-
Rat HF	16357.10±1659.15	16323.45±1320.79	-
Vasodilator Study	19518.67±1251.28	13185.79±1576.43**	14161.71±902.71**
Rat Induced Hypertension	20234.88±2140.88	26629.11±26629.11	-

Table 6.4 :- Media Cross Sectional Area (μm ± SEM, * $p< 0.05$, ** $p< 0.01$).

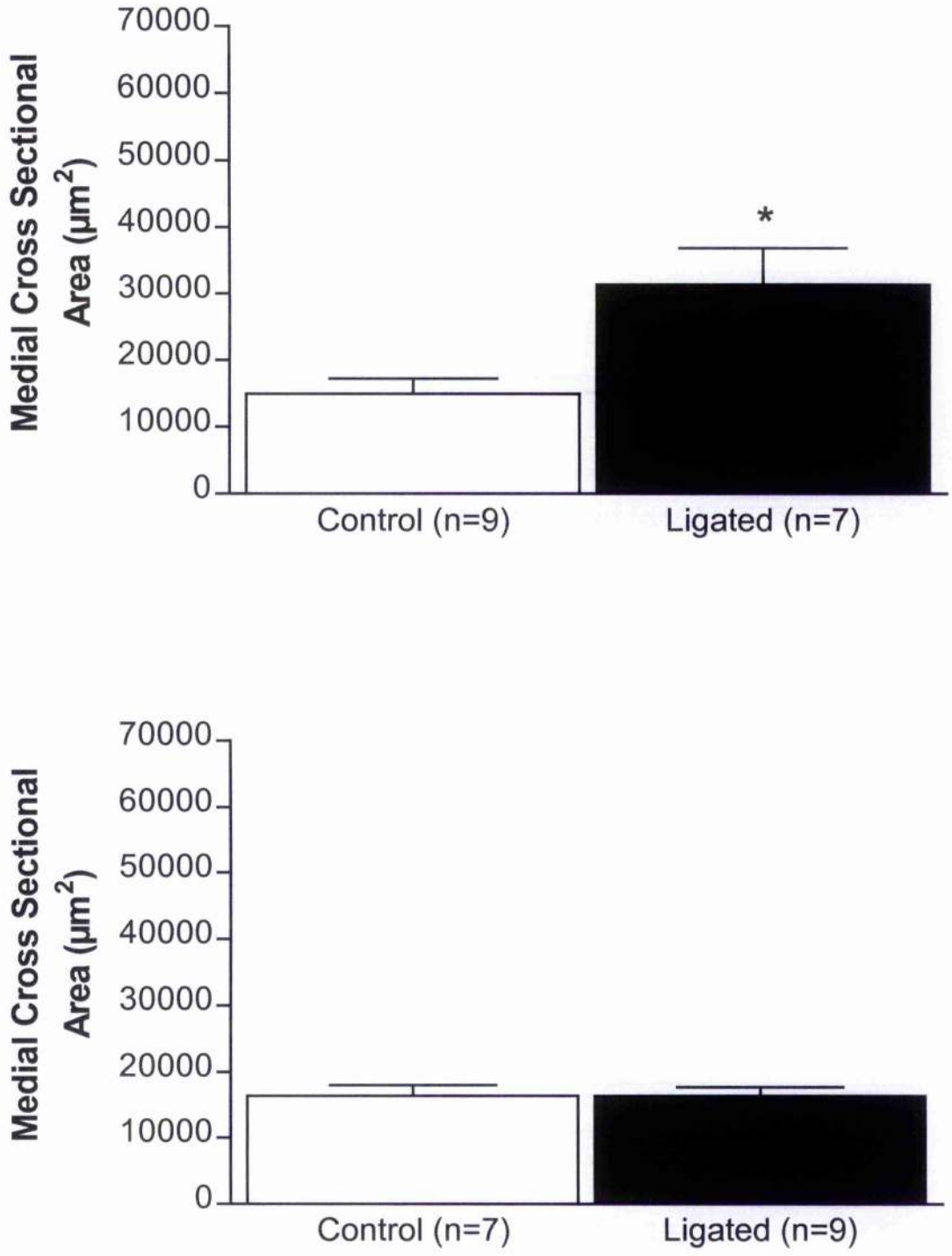

Figure 6.9 :- Media cross sectional area of arteries from heart failure models. Anterior cerebral arteries from the rabbit model of heart failure (top) and third order mesenteric arteries from the rat model of heart failure (bottom). Data is presented as mean ± s.e.m for the number of arteries indicated in brackets.

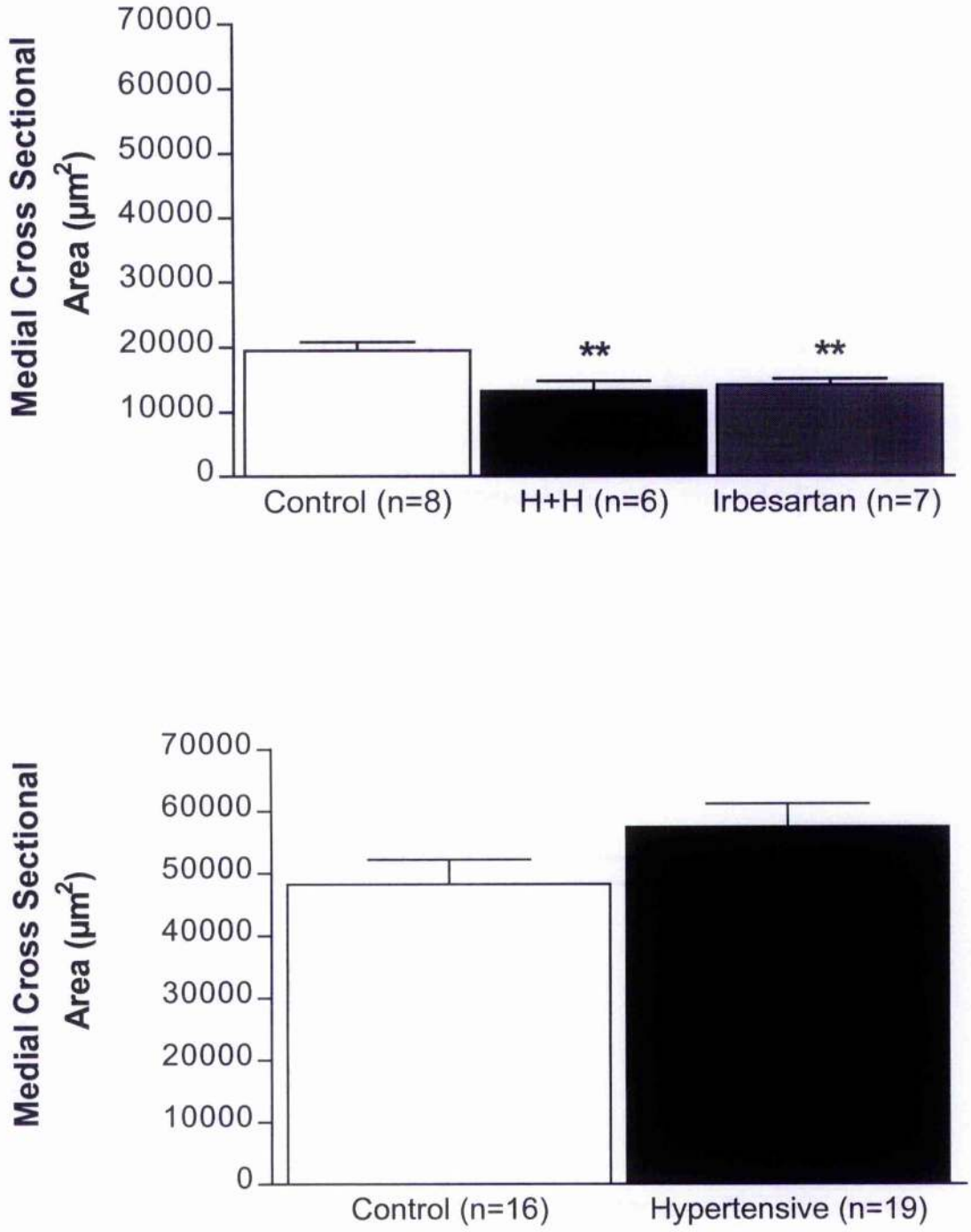

Figure 6.10 :- Media cross sectional area of arteries from hypertensive models. Third order mesenteric arteries from hypertensive treatment with H+H or Irb (top) and the rat model of inducible hypertension (bottom). Data is presented as mean ± s.e.m for the number of arteries indicated in brackets.

6.7 Calculation of the Total Number of Cells within 1mm length of artery

A measure of the total number of cells contained within 1 mm^3 was calculated. This was made by the addition of the number of cells found in the tunica adventitia, tunica media and tunica intima. It allows an estimate to be made of the total number of cells within a defined volume of the artery wall. From the values obtained the only group which showed a change was the induced hypertensives in the rat model of inducible hypertension (Control 7520.11 ± 563.08, Hypertensive 9518.48 ± 652.54, * $p<0.05$). The other models showed no change; ACA (control 9556.75 ± 1241.74, Ligated 13001.33 ± 1150.24); heart failure rats (controls 5543.82 ± 631.22, ligated 4274.98 ± 439.13); Irb study (SHRSP control 5737.08 ± 485.85, WKH 4728.83 ± 391.93, Irb 5223.93 ± 322.77).

	Control	Exp. Group 1	Exp. Group 2
Rabbit ACA	9556.75±1241.74	13001.33±1150.24	
Rat HF	5543.82±631.22	4274.98±439.13	
Rat Vasodilator	5737.08±485.85	4728.83±391.93	4274.98±439.13
Rat Inducible	7520.11±563.08	9518.48±652.54*	

Table 6.5 :- Calculation of the total number of cells within 1mm length of artery (Number of cells ± SEM, * $p< 0.05$).

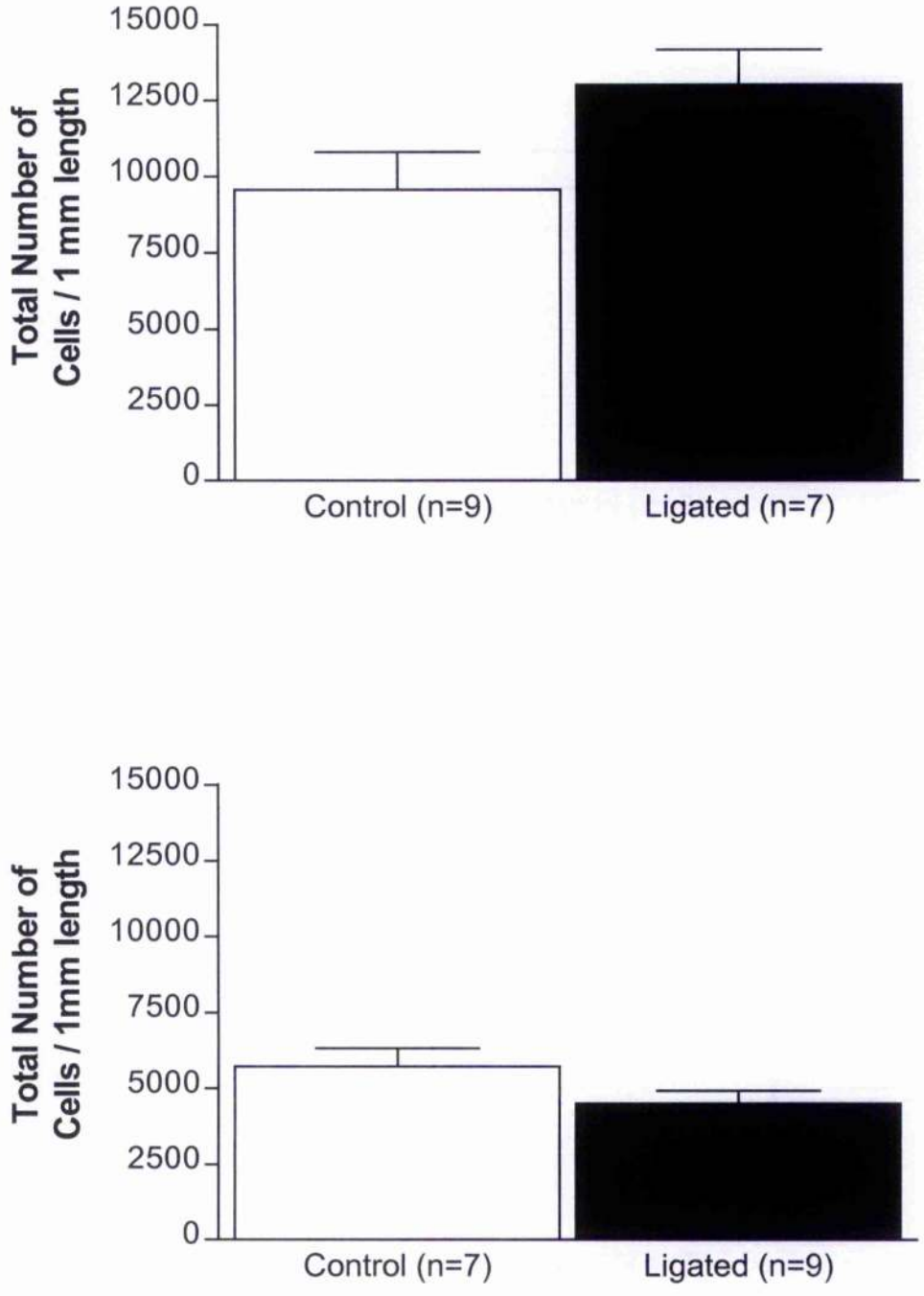

Figure 6.11 :- Total number of cells per 1 mm length of artery in arteries from heart failure models. Anterior cerebral arteries from the rabbit model of heart failure (top) and third order mesenteric arteries from the rat model of heart failure (bottom). Data is presented as mean ± s.e.m for the number of arteries indicated in brackets.

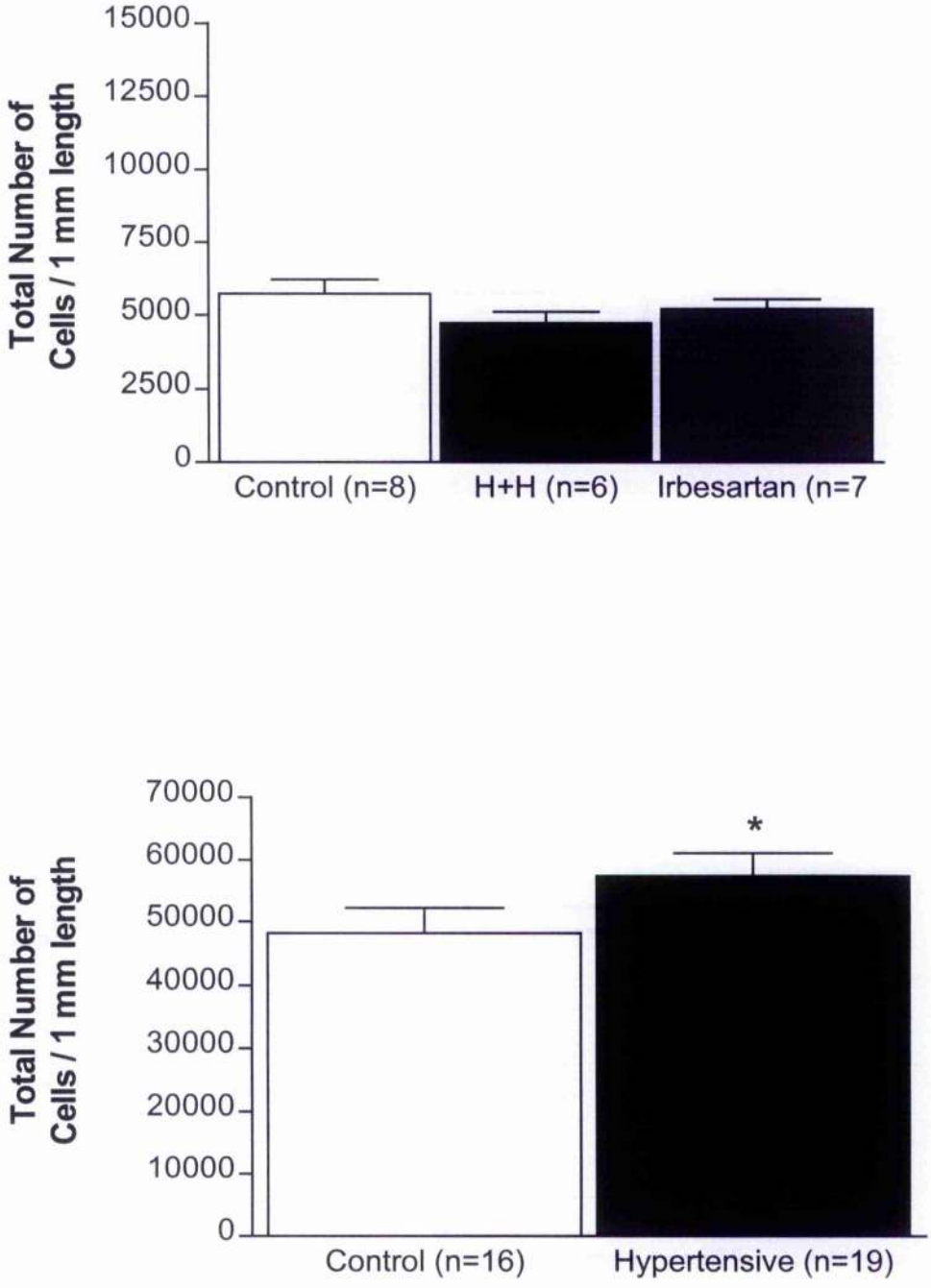

Figure 6.12 :- Total number of cells per 1 mm length in arteries from hypertensive models. Third order mesenteric arteries from hypertensive treatment with H+H or Irb (top) and the rat model of inducible hypertension (bottom). Data is presented as mean ± s.e.m for the number of arteries indicated in brackets

CHAPTER 7

General Discussion

Discussion

Within this study I have made a direct quantitative analysis of the cellular basis of the vascular structure and remodelling in cardiovascular diseases using a method developed within Professor Ian McGrath's laboratory in the University of Glasgow based on LSCM in intact blood vessels.

These studies have shown that LSCM provides an accurate method for the determination of the morphology of whole resistance arteries compared to other previously used methods. (Arribas *et al.*, 1997).

There are several advantages of using this LSCM method over previous methods for morphological measurements. Firstly, it allows us to obtain high resolution images, thus allowing straightforward measurements at the cellular level with image analysis software including counting of different cell types as well as determination of several cell parameters such as nuclear shape, orientation and area. Secondly, it can be performed on intact arteries without the need for histological sectioning. Third, it gives objective and bias free data of basic dimensions.

In addition, LSCM shows differences that had not been found previously at the various levels within the arterial wall. This provides evidence that LSCM can show potentially important information which has not been shown before regarding the remodelling process in various cardiovascular diseases. This is relevant in the understanding of the pathogenesis of the disease and also towards developing new therapautic approaches in tackling the disease.

7.1 Remodelling in each animal model

7.1.1 Rabbit Anterior Cerebral Artery and Rat Mesenteric Artery models of Heart Failure

It is known that left ventricular dysfunction and heart failure can lead to progressive structural changes in the distal vasculature of both animals and humans. The aim of this study was to determine the structural modifications in the cerebral vasculature induced by a reduction in cardiac function for 8 weeks but not the mechanisms responsible for this remodelling. This model of CAL has been characterised in previous studies (Pye *et al.*, 1996) and is felt to best resemble myocardial failure in man. Eight weeks after ligation several alterations can be observed: firstly, an increase in left ventricular weight can be seen. This indicates cardiac remodelling or compensatory hypertrophy. Secondly, an increase in right ventricular weight was observed, suggesting a right ventricular afterload and finally an increase in lung and liver weights could be found, typical of organ congestion (Denver *et al.*, 1996, Ng *et al.*, 1998, Denver *et al.*, 1998).

An important feature of the compensatory mechanism in heart failure is an increase in total peripheral resistance. This helps preserve central haemodynamics at the cost of microcirculatory function. There is evidence that increased peripheral resistance is related to small artery structural changes (Mulvany and Aalkjaer 1990). However, studies of vascular remodelling in heart failure yield conflicting results. Several reports show no structural changes in resistance arteries from rats with 3 to 26 weeks CAL (Stassen *et al.*, 1997., Mulder *et al.*, 1997 and Buss *et al.*, 1999) although after one year of ligation some other studies have demonstrated changes in mesenteric arteries towards an increase in lumen diameter and a decrease in media thickness (Heeneman *et al.*, 1995). Most of these previous studies to investigate remodelling in heart failure have concentrated on using wire

or pressure myography to determine gross morphology i.e. total wall thickess, lumen diameter and wall cross-sectional area. Confocal microscopy was used to reveal more subtle alterations in the cerebral vasculature of rabbits and the mesenteric vasculature of rats after 8 weeks CAL.

The results demonstrate that 8 weeks CAL is able to induce vascular remodelling in anterior cerebral arteries. The increase in lumen diameter in these arteries along with the increase in wall thickness can be defined using Mulvany's classification as outward hypertrophic remodelling (Mulvany *et al.*, 1996, 1999). From the confocal results it is clear that hypertrophy affected both the adventitial and medial layers by significantly increasing the volume of each layer. These increases were accompanied by increases in cell number in all layers of the arteries although the SMC density was actually decreased. There is therefore evidence for cellular hyperplasia in both the adventitia and media. In the media the decrease in the cell density implies either hypertrophy of individual cells and/or an increase in the extracellular space. In the adventitia there was no change in cell density but it is possible that cell hypertrophy could be taken up within the more open cellular structure.

Remodelling in mesenteric arteries in CAL rats was mild with only small changes in vessel dimensions. In these vessels a decrease in lumen diameter was observed although no difference was seen in the wall thickness between control and ligated animals. From this we can initially say that according to Mulvany's classification of remodelling third order mesenteric arteries from a rat model of coronary artery ligation undergo inward eutrophic remodelling. A decrease in the lumen diameter was observed but this may have been due to an increase in the thickness of the intimal layer. Using LSCM we could further investigate the 'micro' remodelling of these arteries in terms of cell numbers. We found

that there was no difference in the number of endothelial cells in this model thus suggesting that this may be due to an increase in underlying connective tissues. Other studies have shown that in the mesenteric arteries from rats with CAL the amount of elastin and collagen did not change (Mulder *et al.*, 1996). A reduced number of smooth muscle cells in ligated animals was observed despite there being no difference in the medial cross-sectional area. With no net change in the volume but a remodelling of the medial layer we can say that mesenteric arteries from this model of CAL undergo eutrophic remodelling (Mulvany *et al.*, 1996).

Mulder *et al.*, (1996) and Stassen *et al.*, (1997) report that in rats after CAL there are no differences in the structure of mesenteric resistance arteries. They found that the lumen diameter, wall-to-lumen ratio and media CSA remain the same between control and ligated animals. Only Buss *et al.*, (1999) and Heeneman *et al.*, (1995) have shown remodelling of the third order mesenteric artery in rats with CAL. Buss *et al.* describe arteries which remodel around a larger lumen with no increase in wall CSA - outward eutrophic remodelling, whereas, Heeneman *et al.* show outward hypertrophic remodelling - remodelling around a larger lumen with an increase in CSA. Changes in blood flow may cause these changes since flow induced hypertrophy was observed in the study by Heeneman.

All of these studies do not investigate changes at the cellular level within the rat model used, therefore these investigators would not be aware of the decrease in smooth muscle cell density in the ligated animals observed when using LSCM and our method of investigation. Knowing that resistance arteries display decreased amounts of SMC may be important when considering functionality of the artery. Stassen *et al.*, (1997a, 1997b) show that there is a hyporeactivity to most vasoconstrictors in mesenteric arteries from rats

5 weeks after CAL. Their findings show that with no decrease in the media mass the reason may be due to an impairment of agonist induced calcium influx. We could now speculate that in rats post-CAL the loss in abilility to constrict to the same extent as control arteries may be simply due to a reduced number of smooth muscle cells. Apoptosis of SMC may be thought to be responsible for the reduction in the number of SMC in the ligated animals in CAL. Stassen *et al.*, (1997) have investigated the effect of circulating vasoactive substances such as nitric oxide, TNF-α and atrial natriuretic peptide (ANP) on the vasculature and have shown that these substances do have a growth inhibitory effect. However we can not extrapolate this to the circumstance of heart failure as the evidence to support this has not been provided yet.

7.1.2 Remodelling in the Mesenteric Artery in the Vasodilator Study in Genetic Hypertensive Rats

From tail cuff plethysmography we can see that treatment with a combination of hydralazine and hydrochlorothiazide or with irbesartan results in a decrease in systolic blood pressure. Irbesartan and H+H were found to be equipotent in preventing the rise in systolic blood pressure associated with genetic hypertension. No differences were seen in the lumen diameter of control and experimental animals although a smaller CSA was found in both the Irbesartan and H+H groups. Again as with heart failure the resistance vasculature in hypertension remodels as a result of increased systolic and peripheral pressure. In control SHRSP rats the vessel wall was significantly thicker than those treated with either treatment. According to Mulvany's classification remodelling within these vessels can be described as Eutrophic remodelling. Increases in the wall thickness may be due to hyperplasia within the arterial wall rather than hypertrophy since there was no difference in the number of cells between groups. Hypertrophy may be accredited to either an increase in the amount of connective tissues, therefore increasing the space between the

cells or a general increase in the size of the cells themselves. Since we have only used the nuclear dye Propidium Iodide to stain the cell nucleus we are not able to answer the question of cell size.

The medial hypertrophy observed in this model is similar to other models of hypertension – mesenteric arteries from renal hypertensive WKY rats have increased SMC volume but not number (Korsgaard *et al.*, 1988). Since we know that angiotensin II is strongly linked to the process of vascular remodelling it is important to note that treatment with irbesartan and H+H were equally effective at lowering systolic blood pressure and therefore preventing medial hypertrophy. Although from other results not shown in this study irbesartan is better than H+H at preventing the increase in left ventricular mass normaly seen with hypertension. It also lowered the expression of ANP and BNP (inhibitors of growth within the wall). This may indicate that AT_1 receptor blockade may have a greater beneficial effect on hypertension than treatment with calcium antagonists and diuretics.

7.1.3 Remodelling in the Mesenteric Artery in the Controlled Inducible Hypertension Study

Typical characteristics of remodelling in various vascular beds are seen in the early onset of hypertension within this model. With continuous induction of indole-3 carbinol hypertension developed within 1 week of initial administration resulting in a rise in systolic blood pressure to around 200 mmHg, whereas normotensive animals did not display any rise in pressure. Within 3rd order mesenteric arteries there was no difference in the lumen diameter or wall CSA between the control and hypertensive animals by 14 days of induction of malignant hypertension. If by using previous methods to study vascular structure this was the only information avaliable, we could say that hypertensive animals- according to Mulvany's classification- undergo eutrophic remodelling. When LSCM is

used it is possible to show more discreet changes in the vascular wall. In the hypertensive rats the medial thickness was increased whereas the adventitial thickness was not. Although an increase was observed in the medial thickness this did not alter the total vascular wall thickness since when coupled to the reduction in the adventitial layer no difference was found between control normotensive and hypertensives rats. With the medial thickness increase there was a significantly greater media/lumen ratio. Although there was no differences seen in the total wall thickness, using LSCM allows us to show that there was an increase in the total number of adventitial cells but not in the number of smooth muscle or endothelial cells. With an observed increase in the media thickness but not a corresponding increase in the number of SMC we report that a decrease was seen in the SMC density in mesenteric arteries. Similarly, with an increase in the number of adventitial cells but with no change in the adventitial thickness we can report an increase in the adventital cell density These results along with no change in the lumen diameter confirm that mesenteric arteries from the controlled inducible hypertension study undergo eutrophic remodelling.

Although it is widely known that increases in systolic blood pressure may lead to vascular remodelling we have to consider an alternative hypothesis that remodelling within the mesenteric arteries may occur independently or jointly with rises in blood pressure. Induction of hypertension within these rats leads to an activation of the renin angiotensin system (RAS). From the results obtained by collegues at the University of Edinburgh regarding the neurohormonal levels within these rats, we see that hypertensive rats display significantly higher levels of plasma angiotensin II and also plasma aldosterone. Angiotensin II may have an inhibitor effect on growth within the vascular wall and may also lead to greater production of aldosterone by the adrenal gland.

All of the above changes are consistent with the characteristics observed in mesenteric arteries from the genetic spontaneously hypertensive stroke prone (SHRSP) rat (Arribas *et al.*, 1997) and also in the basilar arteries of L-nitro arginine methyl ester (L-NAME) induced hypertension in Wistar Kyoto rats (Arribas *et al.*, 1997b). The similarities observed include an increase in number and density of adventitial cells and a reduction in the density of SMC in the media within hypertensives although we must bear in mind that different arteries were examined in each study.

7.2 Problems with Measuring an arc in an artery

One of the disadvantages of this method which I have found is the error which can occur when examining blood vessels with various internal and external diameters and wall thicknesses. The accurate examination of component wall thicknesses within an area of $102\mu m^2$ is dependent on the extent to which the arterial wall arcs. Since total wall thickness is calculated as the sum of all three tunica from one single Z series point, the curvature on the blood vessel itself should be considered when calculating total thickness within a small area. The error in wall thickness seems to be greater when we look at the tunica intima since this layer is prone to greater curvature as it runs along the internal surface of the arc of the vessel. When looking at the tunicas adventitia and media the error is not as apparent since these layers are not under the same degree of curvature because they occupy a larger area within the image examined.

If by using the examples in Figure 7.1 we consider panel II to be our control artery then we can see that in the case of panel III where we have a greater lumen diamter the distance between the first and last endothelial cell is greater. The cause of this is the larger

curvature on the artery thus resulting in the inner distance and therefore the endothelial cells of the artery being further apart.

This provides the evidence that curvature within the vessel wall is an important consideration when looking at wall thickness.

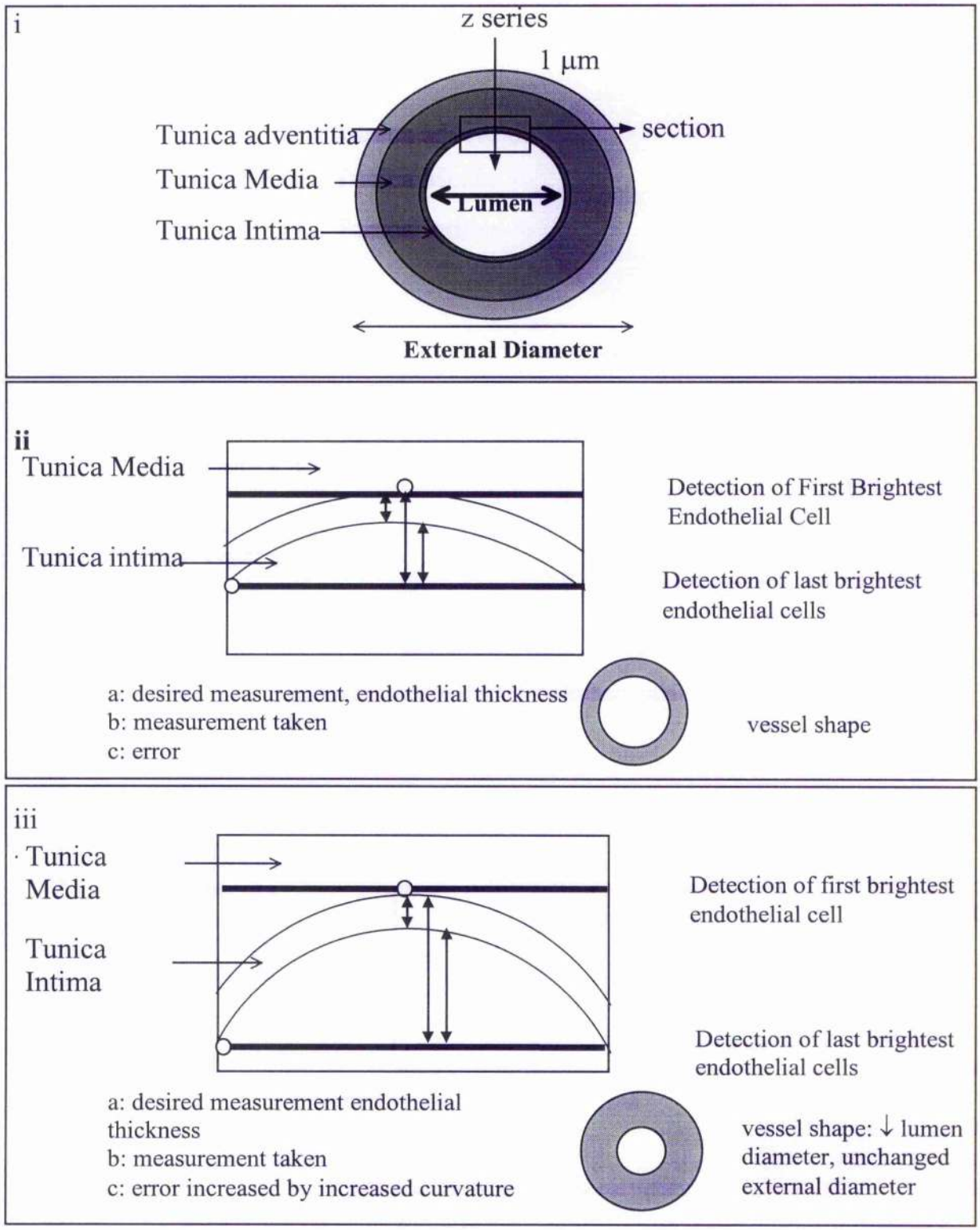

Figure 7.1 :- Schematic representation of the error found using our method.
Panel I: The section taken is only part of the $102\mu m^2$ image used for measurements.
Panel II: Representative of the normal curvature on the vessel wall. The error C is the maximum possible error that could occur in this vessel.
Panel III: Represents a blood vessel with a large curvature. The error is much larger that in a normal vessel.

7.3 Collagen content within Carotid Arteries from the rabbit model of CAL

Within this model of heart failure there were no observed differences in the amount of collagen in the wall of carotid arteries. This may be due to either the rabbit model not having severe enough myocardial infarction or the levels of neurohormones not changing between control and ligated animals.

Levels of circulating agents such as ANP, BNP and angiotensin II have been shown to increase the amount of collagen within the blood vessel wall. Heeneman *et al.*, (2003) describe the situation during myocardial infarction where increased levels of cytokines such as interlukins 1 and 4 and TNF-α along with increased levels of aldosterone and angiotensin II lead to collagen deposition. It is believed that during heart failure collagen is laid down in both the infarct in the heart and within the arterial wall to lessen the stress put out upon them and strengthen the damaged areas. Increased amounts of collagen within larger arteries such as the carotids leads to a reduction in distensibility which in turn leads to increased pressure being exerted on the heart. Normally these larger arteries would expand in line with increases in pressure so as to dissipate any increase in pressure therefore decreasing the chances of further damage to the heart and other organs. Decreased distensibility has a feedback mechanism on the heart in that the stiffening of these arteries ultimately causes the heart to work more to keep blood flowing. An increase in the work done by the heart when damaged, leads to increased collagen production in the infarct and therefore causing a degradation in the cardiac output.

7.4 Recommendations for the Effective Study of Vascular Remodelling Using Confocal Microscopy

Using the method developed by Arribas *et al.*, a group of researchers from several European labs including our own, VASCAN 2000 – EC FP5 Project (QLG1-CT-1999-00084), have further developed this technique to improve the quality and reproduciblity of images taken using LSCM. Several of these recommendations are simple and easy to use with the maximum effect being achieved in image quality.

They include:

1. Using an immersion fluid between the objective lens and coverslip which has similar properties to the mountant in which the vessel is bathed in on the slide. This reduces the difference in the shift in light, known as the refractive index (RI), when the microscope stage is moved. Not only should the RI between the mounting fluids be considered but also the RI of the tissue being examined. Thick samples will bend light to a greater extent than thinner tissues. As yet there has been no published information regarding the RI of blood vessels either fixed or unfixed and pressurised but this group recommend that the ideal mountant around the vessel should be a glycerol based medium for fixed tissues and a PBS based mountant for unfixed vessels.

2. When looking at blood vessel morphology it is important that we avoid squashing the vessel since this would distort the vessel wall. To avoid this it is recommended that instead of using a marked square of vacuum grease, as we have done, that the artery be placed within a 125 μm thick silicon rubber spacer which has been stuck to the glass slide. This will avoid the problem of compressing some areas and stretching others if the coverslip rests against the vessel wall.

3. VASCAN also recommend that number 1 ½ coverslips of a thickness of 170μm be used. These coverslips are routinely specified for use with most of the common objective lenses used on modern microscopes. This thickness of coverslip will reduce the dispersal of light coming from the laser to the specimen.

Visualisation of 3 dimensional volumes for the purpose of quantitative analysis within the arterial wall has also been recognised to be a problem. These researchers have also found that curvature within the vessel wall will complicate the analysis. To count all the nuclei present in a 3D volume of the total data set would introduce a bias if the nuclei are not evenly distributed throughout the vessel wall.

4. To overcome the problems represented in figure 7.1 it is recommended that a wedge shaped analysis area be employed with its apex at the centre of the vessel, instead of the traditional cuboidal area. The wedge shape would outline a volume which contains a fraction of the whole vessel thus representing the whole vessel since each concentric area would contain an equal portion of each layer. Obtaining a wedge shape analysis area would prove to be very difficult since the only way in which this could be done would be to decrease the size of the image being captured every time a sample was taken. The centre of the vessel would also have to be known so a calculation could be made as to how big the wedge should be. In practice this recommendation would not be possible.

5. Orientation of the artery under the microscope is important since any deviation from the vertical or horizontal in an XY image would result in larger measurement being made. Consider an artery with its long axis running horizontally to the bottom edge of the image. If a line was to be drawn perpendicular to the bottom edge of the image passing through the artery it should bisect the artery at an angle of 90° – figure 7.2. But consider an artery

which is not running along the horizontal to the bottom edge of the image and a line perpendicular to this edge was made again passing through the artery we would find that it would bisect the artery at an angle greater than 90°.

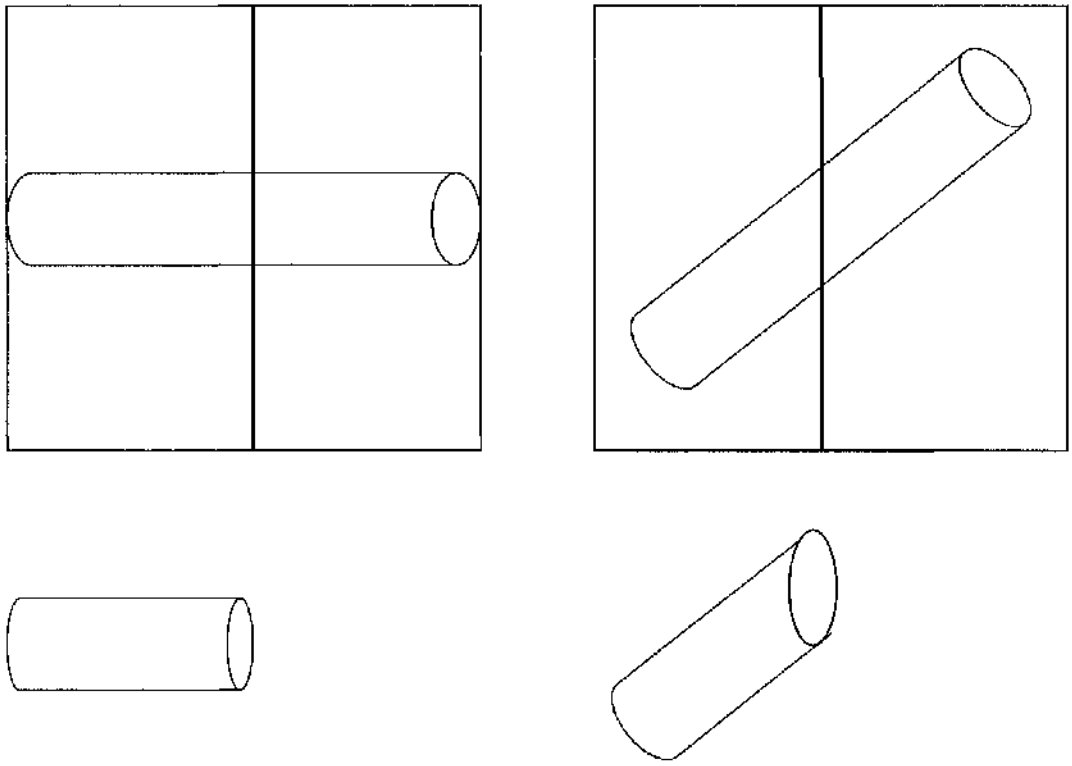

Figure 7.2 :- Representation of the error seen in misaligned blood vessels under the confocal microscope. Panel A: Correct orientation to the base of the image required for accurate wall measurements to be made. Panel B: Orientation which would result in false measurements to be made of the vessel wall.

The problem of orientation of the blood vessel is not only important when calculating lumen diameter but also when counting nuclei per unit length and volume since when the artery is bisected at an angle greater that 90° the area of the "cut" is greater. The number of nuclei per unit volume and the number of nuclei per unit length would increase since the thickness of each stack would be used when calculating the length of the vessel.

Bibliography

Bibliography

Akishita M, Yamada H, Dzau VJ, Horiuchi M. Increased vasoconstrictor response of the mouse lacking angiotensin II type 2 receptor. Biochemical and Biophysical Research Communications 1999; 261(2):345-349.

Arribas SM, Hillier C, Gonzalez C, McGrory S, Dominiczak AF, McGrath JC. Cellular aspects of vascular remodeling in hypertension revealed by confocal microscopy. Hypertension 1997; 30(6):1455-1464.

Baandrup U, Gundersen HJG, Mulvany MJ. It is Possible to Solve the Problem: Hypertrophy/Hyperplasia of Smooth Muscle Cells in the Vessel Wall of Hypertensive Subjects? Progress in Applied Microcirculation 1985; 8:122-128.

Baumbach GL, Heistad DD. Cerebral-Circulation in Chronic Arterial-Hypertension. Hypertension 1988; 12(2):89-95.

Baumbach GL, Heistad DD. Remodeling of Cerebral Arterioles in Chronic Hypertension. Hypertension 1989; 13(6):968-972.

Bevan JA, Dodge J, Walters CL, Wellman T, Bevan RD. As human pial arteries (internal diameter 200-1000 mu m) get smaller, their wall thickness and capacity to develop tension relative to their diameter increase. Life Sciences 1999; 65(11):1153-1161.

Boyle JJ, Lawrie G, Mcphaden AR, Richens D, Lindop GBM. Arterial Lesions Associated with Medial Disorganization and Fibrosis in Endomyocardial Biopsies from Human Cardiac Allografts. Histopathology 1995; 27(5):439-444.

Buus NH, Kahr O, Mulvany MJ. Effect of short- and long-term heart failure on small artery morphology and endothelial function in the rat. Journal of Cardiovascular Pharmacology 1999; 34(1):34-40.

Carlson EC, Burrows ME, Johnson PC. Electron-Microscopic Studies of Cat Mesenteric Arterioles - A Structure-Function Analysis. Microvascular Research 1982; 24(2):123-141.

Daly C, McGee A, Vila E, Briones A, Giraldo J, Arribas SM *et al.*. Analysing the 3D Structure of Blood Vessels using Confocal Microscopy. Microvascular Research November, 5-8. 2002.
Ref Type: Abstract

Denvir MA, MacFarlane NG, Miller DJ, Cobbe SM. Enhanced SR function in saponin-treated ventricular trabeculae from rabbits with heart failure. American Journal of Physiology-Heart and Circulatory Physiology 1996; 40(3):H850-H859.

Denvir MA, MacFarlane NG, Cobbe SM, Miller DJ. Sarcoplasmic reticulum Ca2+ loading in rabbits 8 and 15 weeks after coronary artery ligation. Pflugers Archiv-European Journal of Physiology 1998; 436(3):436-442.

Dickhout JG, Lee RMKW. Structural and functional analysis of small arteries from young spontaneously hypertensive rats. Hypertension 1997; 29(3):781-789.

Gattone VH, Miller BG, Evan AP. Microvascular Smooth-Muscle Cell Quantitation from Scanning Electron-Microscopic Preparations. Anatomical Record 1986; 216(3):443-447.

Gratton JA, Sauter A, Rudin M, Lees KR, McColl J, Reid JL *et al.*. Susceptibility to cerebral infarction in the stroke-prone spontaneously hypertensive rat is inherited as a dominant trait. Stroke 1998; 29(3):690-694.

Halpern W, Kelley M. Invitro Methodology for Resistance Arteries. Blood Vessels 1991; 28(1-3):245-251.

Heeneman S, Leenders PJA, Aarts PJJW, Smits JFM, Arends JW, Daemen MJAP. Peripheral Vascular Alterations During Experimental Heart- Failure in the Rat - do They Exist. Arteriosclerosis Thrombosis and Vascular Biology 1995; 15(9):1503-1511.

Heeneman S, Cleutjens JP, Faber BC, Creemers EE, van Suylen RJ, Lutgens E *et al.* The dynamic extracellular matrix: intervention strategies during heart failure and atherosclerosis. Journal of Pathology 2003; 200(4):516-525.

Johnson G. On Certain Points in the anatomy of Bright's Disease with Contracted Kidney. Transactions of the Royal Medical Chir Society 51, 57-58. 1868.
Ref Type: Generic

Junqueira LCU, Bignolas G, Brooker G. Picosirius Staining plus Polarization Microscopy, a Specific Method for Collagen Detection in Tissue Section. Histopathology 1979; 11:447-455.

Kantachuvesiri S, Fleming S, Peters J, Peters B, Brooker G, Lammie AG *et al.* Controlled hypertension, a transgenic toggle switch reveals differential mechanisms underlying vascular disease. Journal of Biological Chemistry 2001; 276(39):36727-36733.

Korner PI, Angus JA. Vascular remodeling. Hypertension 1997; 29(4):1065-1066.

Korsgaard N, Mulvany MJ. Cellular Hypertrophy in Mesenteric Resistance Vessels from Renal Hypertensive Rats. Hypertension 1988; 12(2):162-167.

Korsgaard N, Aalkjaer C, Heagerty AM, Izzard AS, Mulvany MJ. Histology of Subcutaneous Small Arteries from Patients with Essential-Hypertension. Hypertension 1993; 22(4):523-526.

Kvist S, Mulvany MJ. Contrasting regression of blood pressure and cardiovascular structure in declipped renovascular hypertensive rats. Hypertension 2003; 41(3):540-545.

Langille BL. Remodeling of Developing and Mature Arteries - Endothelium, Smooth-Muscle, and Matrix. Journal of Cardiovascular Pharmacology 1993; 21:S11-S17.

Lee RMKW, Forrest JB, Garfield RE, Daniel EE. Ultrastructural-Changes in Mesenteric-Arteries from Spontaneously Hypertensive Rats - A Morphometric Study. Blood Vessels 1983; 20(2):72-91.

Lew MJ, Angus JA. Wall Thickness to Lumen Diameter Ratios of Arteries from Shr and Wky - Comparison of Pressurized and Wire-Mounted Preparations. Journal of Vascular Research 1992; 29(6):435-442.

Miller BG, Connors BA, Bohlen HG, Evan AP. Cell and Wall Morphology of Intestinal Arterioles from 4-Week- Old to 6-Week-Old and 17-Week-Old to 19-Week-Old Wistar-Kyoto and Spontaneously Hypertensive Rats. Hypertension 1987; 9(1):59-68.

Mulder P, Elfertak L, Richard V, Compagnon P, Devaux B, Henry JP *et al.* Peripheral artery structure and endothelial function in heart failure: Effect of ACE inhibition. American Journal of Physiology-Heart and Circulatory Physiology 1996; 40(2):H469-H477.

Mulder P, Compagnon P, Devaux B, Richard V, Henry JP, Elfertak L *et al.* Response of large and small vessels to alpha and beta adrenoceptor stimulation in heart failure: Effect of angiotensin converting enzyme inhibition. Fundamental & Clinical Pharmacology 1997; 11(3):221-230.

Mulvany MJ, Halpern W. Contractile Properties of Small Arterial Resistance Vessels in Spontaneously Hypertensive and Normotensvie Rats. Circulation Research 41[1], 19-26. 1977.
Ref Type: Abstract

Mulvany MJ, Baandrup U, Gundersen HJG. Evidence for Hyperplasia in Mesenteric Resistance Vessels of Spontaneously Hypertensive Rats Using A 3-Dimensional Disector. Circulation Research 1985; 57(5):794-800.

Mulvany MJ, Aalkjaer C. Structure and Function of Small Arteries. Physiological Reviews 1990; 70(4):921-961.

Mulvany MJ, Baumbach GL, Aalkjaer C, Heagerty AM, Korsgaard N, Schiffrin EL *et al.* Vascular remodeling. Hypertension 1996; 28(3):505-506.

Ng GA, Cobbe SM, Smith GL. Non-uniform prolongation of intracellular Ca2+ transients recorded from the epicardial surface of isolated hearts from rabbits with heart failure. Cardiovascular Research 1998; 37(2):489-502.

Okamoto K, Yamori Y, Nagaoka A. Establishment of the Stroke-Prone Spontaneously Hypertensive Rat (SHR). Circulation Research 1974; 23:I-143-I-152.

Osol G, Halpern W. Myogenic Properties of Cerebral Blood-Vessels from Normotensive and Hypertensive Rats. American Journal of Physiology 1985; 249(5):H914-H921.

Osol G, Halpern W. Spontaneous Vasomotion in Pressurized Cerebral-Arteries from Genetically Hypertensive Rats. American Journal of Physiology 1988; 254(1):H28-H33.

Pye MP, Black M, Cobbe SM. Comparison of in vivo and in vitro haemodynamic function in experimental heart failure: Use of echocardiography. Cardiovascular Research 1996; 31(6):873-881.

Stassen FRM, Fazzi GE, Leenders PJA, Smits JFM, Demey JGR. Coronary arterial hyperreactivity and mesenteric arterial hyporeactivity after myocardial infarction in the rat. Journal of Cardiovascular Pharmacology 1997; 29(6):780-788.

Stassen FRM, Willemsen MJJM, Janssen GMJ, Fazzi GE, Schiffers PMH, Smits JFM *et al.* Reduced responsiveness of rat mesenteric resistance artery smooth muscle to phenylephrine and calcium following myocardial infarction. British Journal of Pharmacology 1997; 120(8):1505-1512.

Sterio DC. The Unbiased Estimation of Number and Sizes of Arbitrary Particles Using the Disscctor. Journal of Microscopy-Oxford 1984; 134(MAY):127-136.

Takakura S, Furuichi Y, Yamamoto T, Ogawa T, Satoh H, Mori J. Effect of Nilvadipine on the Development of Neurological Deficits in Stroke-Prone Spontaneously Hypertensive Rats. Stroke 1994; 25(3):677-682.

Tanaka M, Tsuchida S, Imai T, Fujii N, Miyazaki H, Ichiki T *et al.* Vascular response to angiotensin II is exaggerated through an upregulation of AT1 receptor in AT2 knockout mice. Biochemical and Biophysical Research Communications 1999; 258(1):194-198.

Thybo NK, Stephens N, Cooper A, Aalkjaer C, Heagerty AM, Mulvany MJ. Effect of Antihypertensive Treatment on Small Arteries of Patients with Previously Untreated Essential-Hypertension. Hypertension 1995; 25(4):474-481.

Walmsley JG, Gore RW, Dacey RG, Damon DN, Duling BR. Quantitative Morphology of Arterioles from the Hamster-Cheek Pouch Related to Mechanical Analysis. Microvascular Research 1982; 24(3):249-271.

Walmsley JG, Owen MP, Bevan JA. Medial Morphometry and Mechanics of Sequential Rabbit Ear Arteries and Myograph Ring Segments. American Journal of Physiology 1983; 245(5):H840-H848.

Winquist RJ, Bohr DF. Structural and Functional-Changes in Cerebral-Arteries from Spontaneously Hypertensive Rats. Hypertension 1983; 5(3):292-297.

Zervoudaki AI, Toutouzas PK. Remodeling of Resistance Vessels in Essential Hypertension. Hellenic Journal of Cardiology 44, 116-124. 2003.

Appendix

AP 1: Raw data of the ACA in the Rabbit Model of Coronary Artery Ligation

	Control ACA (n=9)		Ligated ACA (n=8)		Student t-test	
	MEAN	SEM	MEAN	SEM	Cont v Ligated	
area of image(mm2)	10485.00	0.00	10485.00	0.00		
EF (%)	75.89	1.75	45.50	0.98		
Fixation pressure (mmHg)	55.00	0.83	60.00	0.63		
Wall thickness (µm)	25.22	1.22	36.38	4.11	0.015	*
Adv thickness (µm)	5.78	0.55	7.63	1.02	0.119	
Media thickness (µm)	12.72	1.13	20.19	2.62	0.016	*
Intimal thickness (µm)	6.83	0.85	8.81	1.67	0.291	
Number of Adv Cells/Stack	13.94	1.31	16.06	2.48	0.448	
Number of SMC/Stack	52.06	3.41	56.56	3.38	0.365	
Number of Endo Cells / mm2	1950.91	105.48	1692.58	152.22	0.176	
No. Adv Cells / Adv volume (Density) (cells / mm3)	231785.29	22994.22	241712.32	75534.14	0.896	
No. SMC / Media volume (Density) (cells / mm3)	415258.48	48345.96	285366.36	25086.17	0.037	*
Lumen Diameter (µm)	343.15	33.08	445.99	25.44	0.029	*
Wall/lumen Ratio (%)	7.98	0.87	8.33	0.97	0.792	
Media/lumen Ratio (%)	3.96	0.44	4.57	0.56	0.397	
Wall CSA (mm2)	29032.51	2772.96	55545.13	8093.75	0.005	**
Adv. CSA (mm2)	6841.55	773.79	11518.77	1441.00	0.010	**
Media CSA (mm2)	14985.34	2256.52	31380.56	5496.05	0.011	*
Intima CSA (mm2)	7205.62	843.95	12645.80	2781.55	0.068	
Total cell number (No Cells / 1 mm length)	9556.75	1241.74	13001.33	1150.24	0.062	

* $p<0.05$, ** $p<0.005$, *** $p<0.001$

AP 2: Raw data of the 3rd Order Mesenteric in the Rat Model of Coronary Artery Ligation

	Control Mesenteric (n=7)			Ligated Mesenteric (n=9)			Student t-test	
	MEAN	SEM		MEAN	SEM		Cont v Ligated	
area of image(mm2)	10485.00	0.00		10485.00	0.00			
EF	#DIV/0!	#DIV/0!		#DIV/0!	#DIV/0!			
Fixation pressure (mmHg)	50.00	0.00		50.00	0.00			
thickness	45.79	3.39		55.19	2.97		0.055	
A.thickness	15.43	1.49		18.44	2.22		0.308	
M.thickness	21.86	1.60		22.64	1.21		0.698	
I. thickness	8.93	1.48		14.67	2.35		0.075	
n AC	20.96	3.24		18.36	1.89		0.476	
n SMC	45.43	3.39		37.11	3.41		0.111	
Number of EC/mm2	1273.54	122.26		1082.93	167.22		0.399	
n AC/volume A DENSITY	131037.54	33220.85		106447.06	27255.58		0.573	
n SMC/volume M DENSITY	205357.37	12150.84		157057.33	8946.58		0.005	**
Lumen Diameter (µm)	200.39	22.72		176.88	9.88		0.320	
Wall/lumen Ratio(%)	25.15	3.67		32.33	2.96		0.146	
Media/lumen Ratio (%)	11.85	1.55		13.14	1.11		0.495	
Wall CSA (mm2)	34778.70	2965.66		40363.77	3149.93		0.228	
Adv. CSA (mm2)	13000.58	1321.01		15042.82	2228.96		0.477	
Media CSA (mm2)	16357.10	1659.15		16328.45	1320.79		0.989	
Intima CSA (mm2)	5421.02	594.79		8992.50	1649.73		0.089	
Total cell number	5714.13	618.55		4489.74	428.29		0.115	

* p<0.05, ** p<0.005, ***p<0.001

AP 3: Raw data of the 3rd Order Mesenteric in the Rat Vasodilator Hypertensive Study

	SHRSP Control (n= 8)		H+H (n=6)		Irb (n=7)		Student T-Test				
	MEAN	SEM	MEAN	SEM	MEAN	SEM	Cont V H+H		Cont V Irbe		H+H V Irbe
Area of image(mm2)	10485.00	0.00	10485.00	0.00	10485.00	0.00					
Fixation pressure (mmHg)	82.92	2.22	62.08	1.88	59.92	3.47					
thickness	53.19	2.32	44.38	2.37	42.71	2.87	0.019	*	0.013	*	0.699
Adv thickness (µm)	13.75	1.37	13.56	1.21	12.21	1.17	0.920		0.418		0.561
Media thickness (µm)	26.81	2.05	20.63	1.26	20.00	1.18	0.022	*	0.016	*	0.631
Intimal thickness (µm)	13.44	0.96	10.06	1.12	10.71	1.42	0.038	*	0.128		0.741
Number of Adv Cells/Stack	19.50	1.52	15.38	0.88	17.64	1.67	0.034	*	0.425		0.124
Number of SMC/Stack	49.13	2.83	49.50	1.73	44.50	2.24	0.912		0.232		0.221
Number of Endo Cells/mm2	1583.47	208.84	1492.91	117.90	1718.44	216.14	0.711		0.662		0.233
No. Adv Cells / Adv Volume (Density) (Cells / mm3)	126559.72	10627.51	98415.68	10863.52	135109.35	25080.23	0.085		0.747		0.180
No. SMC / Media volume (Density) (cells / mm3)	179857.64	14340.70	238920.85	13831.63	218632.17	18696.30	0.010	*	0.119		0.667
Lumen Diameter (µm)	181.24	13.32	160.00	15.14	184.85	10.76	0.310		0.840		0.317
Wall/lumen Ratio (%)	30.99	3.64	29.40	2.95	23.81	2.41	0.740		0.135		0.251
Media/lumen Ratio (%)	15.98	2.76	13.57	1.29	11.15	1.12	0.444		0.149		0.223
Wall CSA (mm2)	39146.13	2635.11	28728.58	3023.29	30444.14	2297.21	0.021	*	0.029	*	0.830
Adv. CSA (mm2)	11194.21	1177.56	9886.84	747.77	9753.29	1063.07	0.365		0.386		0.900
Media CSA (mm2)	19518.67	1251.28	13185.79	1576.43	14161.71	902.71	0.007	**	0.005	**	0.871
Intima CSA (mm2)	8433.26	1010.44	5655.95	1085.72	6529.14	843.58	0.082		0.179		0.635
Total Cells number (No Cells / 1 mm length)	5737.08	485.82	4728.83	391.93	5223.93	322.77	0.129		0.409		0.334

* p<0.05, ** p<0.005, ***p<0.001

AP 4: Raw data of the 3rd Order Mesenteric in the Rat Inducible Hypertensive Study

	Fischer Controls		Inducible Hyperten'		Student t-test	
	MEAN	SEM	MEAN	SEM	Con v Hypertensive	
area of image(mm2)	10485.00	0.00	10485.00	0.00		
Systolic Blood Pressure (mmHg)	110.94	1.09	200.63	0.59	0.000	***
Fixation Pressure (mmHg)	50.00	0.00	50.00	0.00		
Wall thickness (µm)	46.50	2.87	52.92	2.75	0.117	
Adv thickness (µm)	16.47	1.69	18.82	1.29	0.270	
Media thickness (µm)	19.47	1.42	24.95	1.89	0.031	*
Intimal thickness (µm)	10.84	0.82	9.16	0.87	0.173	
Number of Adv Cells/Stack	18.38	2.49	32.82	2.33	0.000	***
Number of SMC/Stack	46.56	2.72	48.26	2.99	0.681	
Number of Endo Cell/mm2	1234.11	72.51	1199.27	47.45	0.682	
No of Adv Cells / Adv volume (Density) (Cells / mm3)	102662.61	11853.37	155451.42	11005.55	0.003	**
No of SMC / Media volume (Density) (Cells / mm3)	246599.36	18582.04	199339.83	10722.60	0.029	*
Lumen Diameter (µm)	280.31	13.55	292.64	13.07	0.519	
Wall/lumen Ratio (%)	17.17	1.35	18.97	1.44	0.372	
Media/lumen Ratio (%)	7.00	0.45	8.81	0.70	0.045	*
Wall CSA (mm2)	48217.35	4012.34	57403.64	3684.37	0.101	
Adv. CSA (mm2)	18210.37	2099.60	22346.03	1622.20	0.123	
Media CSA (mm2)	20234.88	2140.88	26629.11	2573.13	0.071	
Intima CSA (mm2)	9772.10	801.97	8428.50	756.84	0.233	
Total Number Adv cells per 1mm3	1787.67	242.94	3425.83	289.60	0.000	***
Total number SMC / 1mm3	4659.45	423.90	4994.16	369.78	0.554	
Total cell number (No of cells / 1 mm length)	7520.11	563.08	9518.48	652.54	0.030	*

* p<0.05, ** p<0.005, ***p<0.001

Figure AP 5: Confocal image of the lumen diameter of a WKY 3rd order mesenteric artery stained with Propidium Iodide. Arrow indicated the inner surface from which the lumen diameter is measured

Figure AP 6: 3 Dimensional XYZ reconstruction of a 3rd order rat mesenteric artery Indicating the location of nuclei of adventitial, smooth muscle and endothelial cells which have been stained with Propidium Iodide.

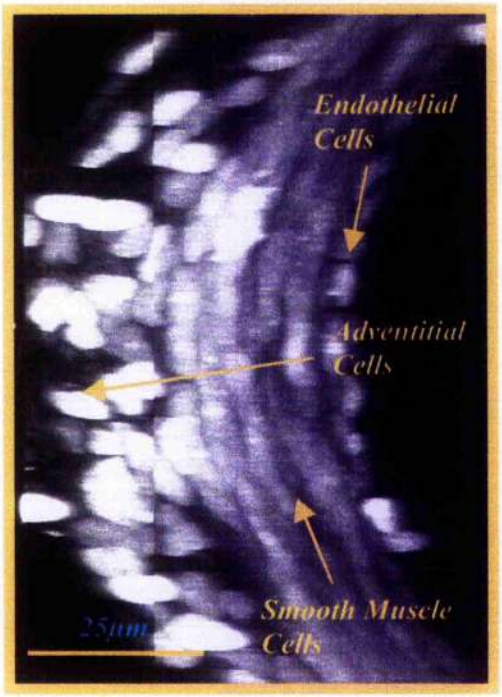

Figure AP 7: 3 Dimensional XY reconstruction of a 3rd order rat mesenteric artery indicating the location of nuclei of adventitial, smooth muscle and endothelial cells which have been stained with Propidium Iodide. This plane demonstrates the curvature of the pressurised fixed blood vessel and the relationship of the various cell types to each other.

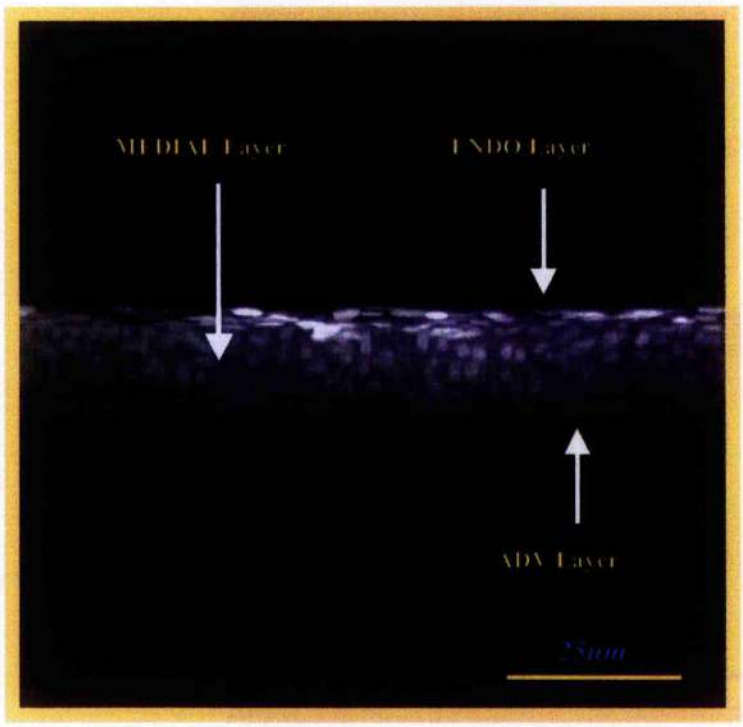

Figure AP 8: 3 Dimensional XZ reconstruction of a 3rd order rat mesenteric artery indicating the location of nuclei of adventitial, smooth muscle and endothelial cells which have been stained with Propidium Iodide.

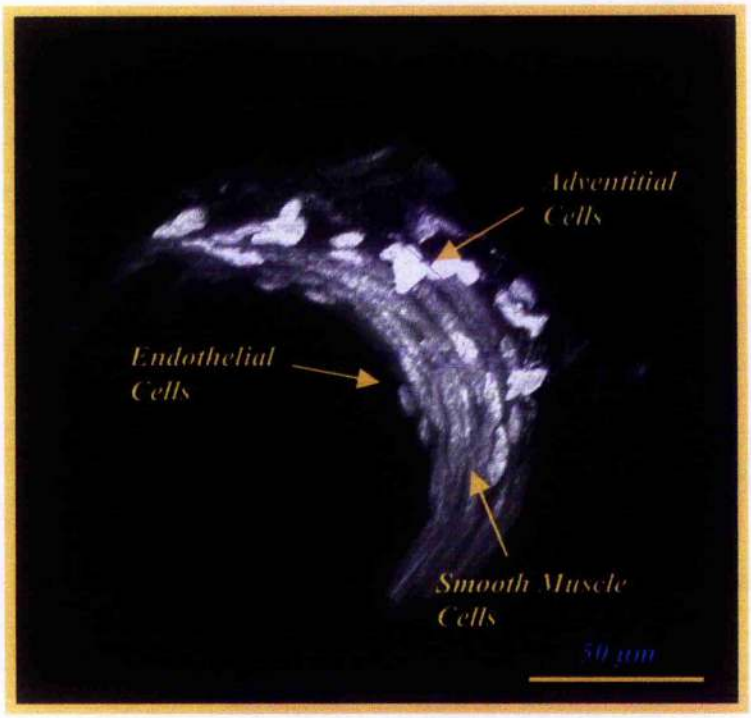

Figure AP 9: 3 Dimensional XYZ reconstruction of a 3rd order rat mesenteric artery rotated using image analysis software indicating the location of nuclei of adventitial, smooth muscle and endothelial cells which have been stained with Propidium Iodide. This plane demonstrates the curvature of the pressurised fixed blood vessel and the relationship of the various cell types to each other.

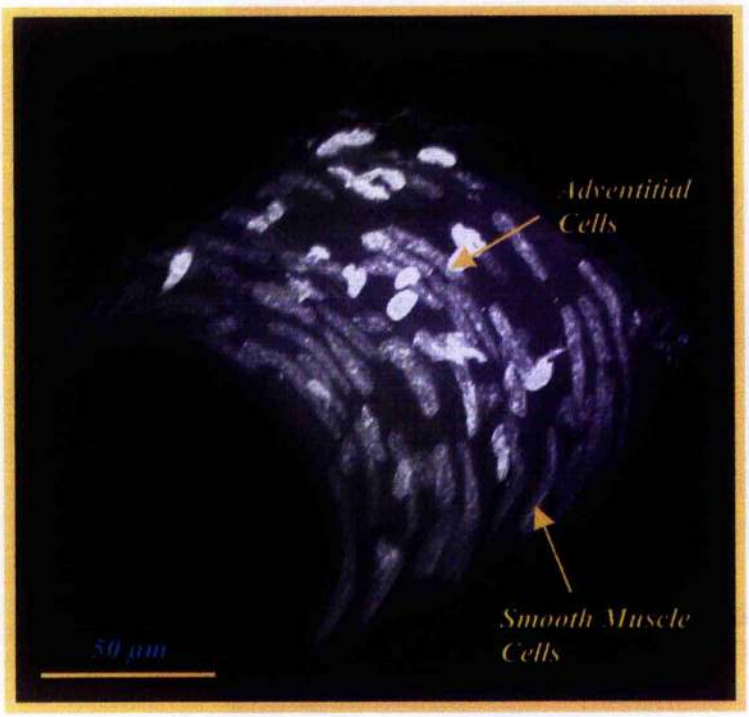

Figure AP 10: 3 Dimensional XYZ reconstruction of a 3rd order rat mesenteric artery rotated using image analysis software indicating the location of nuclei of adventitial, smooth muscle and endothelial cells which have been stained with Propidium Iodide. This plane demonstrates the curvature of the pressurised fixed blood vessel and the relationship of the various cell types to each other.

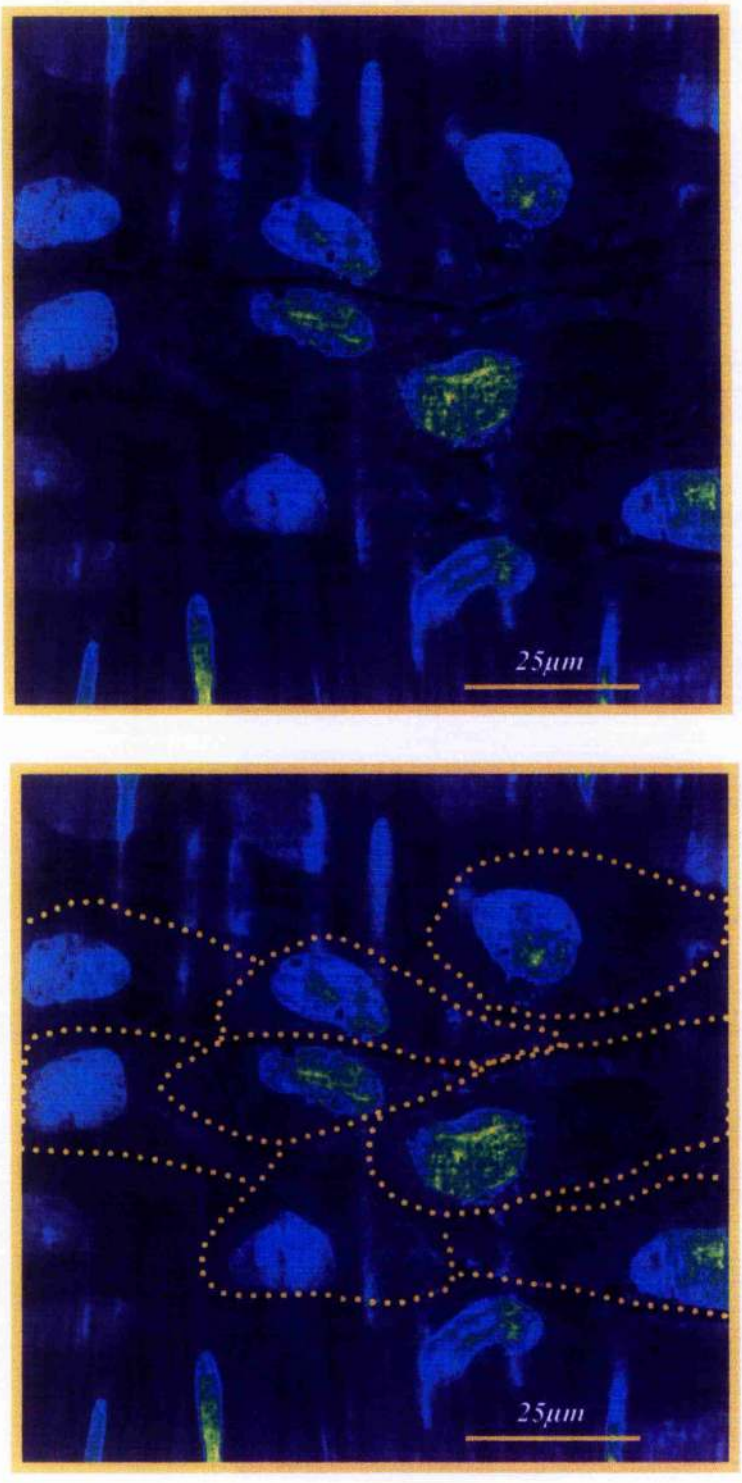

Figure AP 11: **Panel A**: 3 Dimensional XYZ reconstruction of a 3rd order rat mesenteric artery endothelial layer showing both the outline of the cells and the nucleus. **Panel B**: Indicates the rough outline of the endothelial cells.